

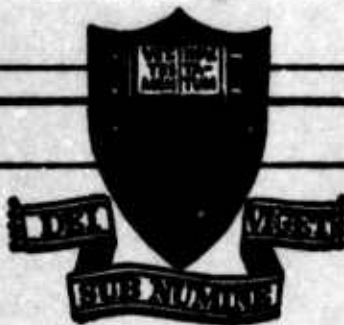
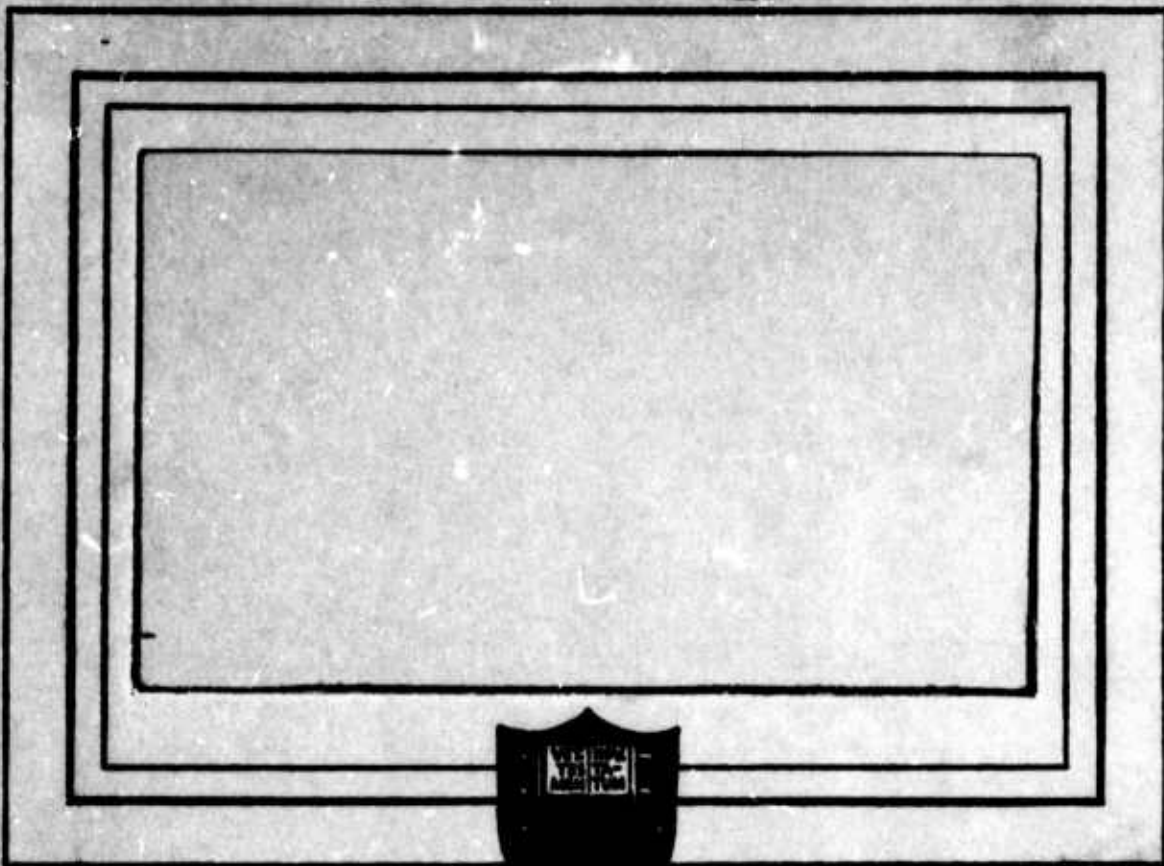
RESEARCH SPONSORED BY THE AIR FORCE OFFICE OF SCIENTIFIC  
RESEARCH, OFFICE OF AEROSPACE RESEARCH, UNITED STATES  
AIR FORCE.

AFOSR SCIENTIFIC REPORT NO. 66-2728



*[Handwritten signature]*  
U55-10

AD649860



DDC  
RECORDED  
APR 12 1967  
*[Handwritten initials]*

PRINCETON UNIVERSITY  
DEPARTMENT OF  
AEROSPACE AND MECHANICAL SCIENCES

ARCHIVE COPY

QUALIFIED REQUESTORS MAY OBTAIN ADDITIONAL COPIES FROM  
THE AEROSPACE DOCUMENTATION CENTER. ALL OTHERS SHOULD  
CONTACT THE CLEARINGHOUSE FOR FEDERAL SCIENTIFIC AND  
TECHNOLOGICAL INFORMATION.

**Best  
Available  
Copy**

AIR FORCE OFFICE OF SCIENTIFIC RESEARCH

AFOSR REPORT NO. 66-2725

EXPERIMENTAL INVESTIGATION OF HIGH-FREQUENCY  
LONGITUDINAL COMBUSTION INSTABILITY IN  
GASEOUS PROPELLANT ROCKET MOTORS

BY

CRAIG THOMAS BOWMAN

AFOSR Contract AF49(638)1268

Project-Task 9711-01

January 1967

Approved by:

*James M. Hausel*  
*for*

Irvin Glassman  
Professor of Aeronautical  
Engineering  
Principal Investigator

Qualified requestors may obtain additional copies from the Defense Documentation Center. All others should apply to the Clearinghouse for Federal Scientific and Technical Information.

Reproduction, translation, publication, use and disposal in whole or in part by or for the United States Government is permitted.

Guggenheim Laboratories for the Aerospace Propulsion Sciences  
Department of Aerospace and Mechanical Sciences

Technical Report 784

Princeton University  
Princeton, New Jersey

A dissertation submitted to the Department of  
Aerospace and Mechanical Sciences of Princeton  
University in partial fulfillment of require-  
ments for the degree of Doctor of Philosophy.

Guggenheim Laboratories for the Aerospace Propulsion Sciences  
Department of Aerospace and Mechanical Sciences  
Princeton University  
Princeton, New Jersey  
1966

ABSTRACT

The properties of the longitudinal mode of high-frequency combustion instability in a rocket motor burning premixed gaseous propellants have been determined experimentally. The experimental observations have been compared with the results of a non-linear instability theory (23) based on a chemical kinetic driving mechanism. It has been shown that the theory gives the correct waveform for longitudinal instability. In addition the theory gives the correct qualitative dependence of the stability limits on the mean combustion temperature and activation energy. The theory also gives the correct qualitative dependence of the instability strength on the mean combustion temperature and mean Mach number of the combustion gases. Harmonic mode longitudinal instabilities have been observed, and a criterion for their appearance, consistent with a chemical kinetic driving mechanism, has been suggested. The dependence of the stability limits and instability strength on the mean combustion pressure, combustion chamber length, injector and exhaust nozzle have been determined experimentally. These effects are not included in the instability theory. Plausible explanations for the above effects, consistent with the theoretical model, have been suggested. Based on the general agreement between the experimental observations and theoretical results it is concluded that the appropriate driving mechanism for high-frequency longitudinal gas-phase combustion instability is chemical kinetics.

ACKNOWLEDGEMENTS

The author wishes to thank his advisor, Professor Irvin Glassman, for his advice, assistance and encouragement throughout the course of this investigation. Thanks are due also to Professors L. Crocco and R. Eichorn for their many helpful suggestions.

The technical assistance of Messrs. A. Bozowski, S. Marquardt, H. Pannell and J. Sivo was greatly appreciated.

The author also wishes to thank Mr. D. Hardesty, who assisted in the final phases of the experimental work.

The financial assistance of the Daniel and Florence Guggenheim Foundation and the Air Force Office of Scientific Research, under Contract No. AF 49(638)-1268, has made this investigation possible.

TABLE OF CONTENTS

	<u>PAGE</u>
TITLE PAGE	1
ABSTRACT	11
ACKNOWLEDGEMENTS	111
TABLE OF CONTENTS	iv
LIST OF SYMBOLS	vi
LIST OF FIGURES	x
CHAPTER 1. INTRODUCTION	1
CHAPTER 2. EXPERIMENTAL APPARATUS	5
A. Gas Rocket System	5
B. Instrumentation	12
CHAPTER 3. THEORETICAL CONSIDERATIONS	15
A. Historical Background	15
B. The Sirignano-Crocco Instability Model	20
C. Theoretical Results	23
D. Discussion of the Assumptions	25
E. Discussion of Theoretical Results and Some Critical Experiments	31
CHAPTER 4. EXPERIMENTAL CONSIDERATIONS	38
A. General Comments on the Operation of the Gas Rocket	38

	<u>PAGE</u>
B. Waveform of Longitudinal Combustion Instability	38
C. Dependence of Stability Limits on $E/\bar{P}\bar{T}$	40
D. Dependence of Instability Strength on $\bar{T}$	65
E. Dependence of Instability Strength on $\bar{M}$	68
F. Harmonic Mode and Transverse Mode Instabilities	70
G. Effect of Mean Combustion Pressure on the Instability	77
H. Effect of Combustion Chamber Length on the Instability	84
I. Injector Experiments	89
J. Effect of Nozzle Geometry on the Instability	93
K. Measurement of Axial Temperature Profiles	96
CHAPTER 5. CONCLUSIONS	100
A. Mechanism for High-Frequency Longitudinal Gas-Phase Combustion Instability	100
B. Possible Applications of Gas Rocket Instability Data	101
APPENDIX A. CALIBRATION PROCEDURES	
APPENDIX B. EXPERIMENTAL UNCERTAINTIES	
APPENDIX C. SOME RESULTS OF THE SIRIGNANO-CROCCO THEORY	
APPENDIX D. GAS DATA	
REFERENCES	
FIGURES	

LIST OF SYMBOLS

- $\bar{v}$  = mean sound speed (cm/sec)  
 A = area (cm<sup>2</sup>)  
 b = pre-exponential factor  
 B = pre-exponential factor- see equation (3-1)  
 c,d = parameters defined by equation (4-19)  
 C<sub>D</sub> = discharge coefficient- see equation (A-2)  
 c<sub>p</sub> = specific heat at constant pressure (cal/gm-°K)  
 D = diameter of combustion chamber (cm)  
 E = an activation energy (kcal/mole)- see equation (3-1)  
 E<sub>act</sub> = chemical activation energy (kcal/mole)  
 f = frequency of oscillation (cps)  
 $g(\gamma, m) = \left\{ \frac{\gamma m}{R} \cdot \left[ \frac{2}{\gamma + 1} \right]^{\gamma + 1 / \gamma - 1} \right\}^{1/2}$   
 h = convective heat transfer coefficient (cal/cm<sup>2</sup>-sec-°K)  
 k = specific rate constant- see equation (4-18)  
 L = combustion chamber length (cm)  
 $\dot{m}$  = mass flow rate (gm/sec)  
 $\bar{M}$  = mean Mach number of combustion gases  
 $m$  = molecular mass (gm/mole)  
 n<sub>1</sub> = order of reaction with respect to reactant 1  
 P = combustion pressure (atm)  
 $\bar{P}$  = mean combustion pressure

- $P'$  = perturbation in combustion pressure  
 $\Delta P$  = pressure change across the shock wave  
 $q$  = heat of reaction  
 $Q$  = heat transfer rate/unit area (cal/sec-cm<sup>2</sup>)  
 $r$  = energy release rate  
 $\bar{r}$  = mean value of  $r$   
 $r'$  = perturbation in  $r$   
 $\hat{r}$  = chemical reaction rate  
 $R$  = universal gas constant = 1.986 cal/mole-°K  
 $S$  = flame speed (cm/sec)  
 $t$  = time co-ordinate (sec)  
 $T$  = combustion temperature (°K)  
 $\bar{T}$  = mean combustion temperature  
 $\bar{T}_{crit}$  = critical value for the mean combustion temperature  
 $u$  = velocity of combustion gases relative to laboratory (cm/sec)  
 $\Delta u$  = change in gas velocity across the shock wave  
 $V$  = shock velocity relative to laboratory  
 $x$  = axial distance co-ordinate (cm)  
 $x_i$  = mole fraction of  $i^{th}$  species  
 $\beta$  = compressibility factor- see equation (A-2)

$$Z = \frac{16}{\gamma + 1} \cdot \frac{1}{(1 - \nu^2) \left[ \frac{1 - M}{1 + M} \cdot \frac{1 + \nu}{1 - \nu} + \frac{1 + M}{1 - M} \right]}$$

see Appendix C

- $\alpha$  = thermal diffusivity =  $\frac{\kappa}{\rho C_p}$   
 $\beta$  = eddy diffusivity  
 $\gamma$  = ratio of specific heats =  $c_p / c_v$   
 $\delta$  = reaction zone thickness (cm)  
 $\epsilon$  = shock strength parameter- see equation (3-2)  
 $\Theta$  = apparent period of oscillation (sec)  
 $\kappa$  = thermal conductivity (cal/°K-sec-cm)  
 $\lambda$  = wave shape parameter- see equation (3-3)  
 $\mu$  = gas viscosity (gm/cm-sec)  
 $\nu$  =  $\frac{\gamma-1}{2} \bar{M}$   
 $\rho$  = gas density (gm/cm<sup>3</sup>)  
 $\tau$  = gas residence time (sec)  
 $\Phi$  = equivalence ratio =  $\frac{\dot{m}_O/\dot{m}_F}{(\dot{m}_O/\dot{m}_F)_{\text{stoic.}}}$

Subscripts:

AB = downstream moving shock wave

BC = upstream moving shock wave

t = turbulent flame

l = laminar flame

o,f = oxidizer, fuel

limit = at the stability limit

LIST OF FIGURES

1. Flow Schematic of Propellant Feed System.
2. Typical Critical Flow Orifice.
3. Schematic of Gas Rocket (Converging-Diverging Nozzle).
4. Photograph of Gas Rocket Mounted on Test Stand.
5. Mixing Chamber Section.
6. Ratio of the Equivalence Ratio Measured Downstream from the Mixing Chamber ( $\Phi$  output) to the Equivalence Ratio Supplied to the Mixing Chamber ( $\Phi$  input) for Several Values of  $\Phi$  input: No Injector.
7. Flashback Shutdown System (Wiring Schematic).
8. Photographs of Porous Plug and Showerhead Injectors.
9. Schematic of 10-Hole Showerhead Injector.
10. Schematic of Impinging Injector.
11. Typical Combustion Chamber Section.
12. Water-Cooled Converging-Diverging Exhaust Nozzle.
13. Photograph and Schematic of Plug Nozzle.
14. Theoretical Dependence of Shock Strength on  $E/\bar{RT}$  for Constant  $\bar{M}$ .
15. Theoretical Dependence of Shock Strength on  $\bar{M}$  for Constant  $E/\bar{RT}$ .
16.
  - a. Typical Theoretical Pressure-Time History (Reference 23).
  - b. Typical Experimental Pressure-Time History: Fundamental Mode.
17. Regions of Unstable Combustion in the  $\Phi$ -L Plane for  $H_2$ -Air and  $H_2$ -Dilute Air:  $\bar{P} = 7.8$  atm.
18. Mean Combustion Temperature at the Stability Limits for Hydrogen-Air and Hydrogen-Dilute Air:  $\bar{P} = 7.8$  atm, 31-Hole Showerhead Injector.

19. Regions of Unstable Combustion in the  $\Phi$  -L Plane for  $\text{CH}_4$ -Dilute Oxygen and  $\text{CH}_4$ -Air:  $\bar{P} = 7.8$  atm.
20. Mean Combustion Temperature at the Stability Limits for Methane-Dilute Oxygen and Methane-Air:  $\bar{P} = 7.8$  atm, 49-Hole Showerhead Injector.
21. Comparison of  $E_{\text{limit}}$  with  $E_{\text{act}}$  for Various Propellant Combinations.
22. a. Stability Limits for  $\text{CO}(\text{H}_2\text{O})$ -Air and  $\text{CO}(\text{H}_2\text{O})$ -Air- $\text{H}_2$  for  $\bar{P} = 7.8$  atm,  $L = 104$  cm, 49-Hole Showerhead<sup>2</sup> Injector.<sup>2</sup>  
 b. Comparison of Results of the Sirignano-Crocco Theory with Chemical Kinetics Data.
23. Variation of  $\Delta P/\bar{P}$  with Combustion Temperature for  $\text{H}_2$ -Air.
24. Variation of  $\Delta P/\bar{P}$  with Combustion Temperature for  $\text{CH}_4$ - $0.4 \text{ O}_2 + 0.6 \text{ N}_2$ : Data from Reference 27.
25. Variation of  $\Delta P/\bar{P}$  with Combustion Temperature for  $\text{H}_2$ -Air and Two Values of  $\bar{M}$ .
26. Variation of Theoretical and Experimental  $\rho$  with Combustion Temperature for  $\text{H}_2$ -Air.
27. Pressure-Time History and  $X - t$  Diagram for One Shock Wave ( $n=1$ ).
28. Pressure-Time History and  $X - t$  Diagram for Two Shock Waves ( $n=2$ ).
29. Pressure-Time History and  $X - t$  Diagram for Three Shock Waves ( $n=3$ ).
30. Regions of Harmonic Mode Instability in the  $\Phi$  -L Plane for  $\text{H}_2$ -Air:  $\bar{P} = 7.8$  atm, 31-Hole Showerhead Injector.
31. Pressure-Time History Showing Superposition of First Tangential and Longitudinal Modes.
32. Regions of Unstable Combustion in the  $\Phi$  - $\bar{P}$  Plane for  $\text{H}_2$ -Air,  $L = 38$  cm.
33. Regions of Unstable Combustion in the  $\Phi$  - $\bar{P}$  Plane for  $\text{H}_2$ -Air,  $L = 104$  cm.

34. Regions of Unstable Combustion in the  $\Phi$  - $\bar{P}$  Plane for  $\text{CH}_4$ -Air: Chamber Length Not Specified (Data from Reference 31).
35. Variation of  $\Delta P/\bar{P}$  with Combustion Temperature for  $\text{H}_2$ -Air and Two Combustion Pressures.
36. Variation of  $\Delta P/\bar{P}$  with Combustion Temperature for  $\text{H}_2$ -Air and Two Chamber Lengths.
37. Regions of Unstable Combustion in the  $\Phi$  -L Plane for  $\text{H}_2$ -Air:  $\bar{P} = 7.8$  atm, 10-Hole Showerhead Injector.
38. Regions of Unstable Combustion in the  $\Phi$  -L Plane for  $\text{H}_2$ -Air:  $\bar{P} = 7.8$  atm, 49-Hole Showerhead Injector.
39. Regions of Unstable Combustion in the  $\Phi$  -L Plane for  $\text{H}_2$ -Air:  $\bar{P} = 7.8$  atm, Impinging Injector.
40. Regions of Unstable Combustion in the  $\Phi$  -L Plane for  $\text{H}_2$ -Air and Various Exhaust Nozzles:  $\bar{P} = 4.4$  atm.
41. Typical Pressure-Time Histories for Various Exhaust Nozzles: Second Harmonic.
42. Typical Pressure-Time Histories for Various Exhaust Nozzles: Second Harmonic.
43. Typical Axial Temperature Profiles for Various Injectors:  $\text{H}_2$ -Air,  $\bar{P} = 7.8$  atm.

CHAPTER 1. INTRODUCTION

The phenomenon of combustion instability in rocket motors is characterized by periodic oscillations in the combustion pressure. These pressure oscillations generally result in erratic operation, and frequently cause a catastrophic failure of the rocket motor. It is desirable, therefore, to understand the nature of the instability phenomenon and to derive design criteria for preventing unstable combustion.

In general three basically different types of combustion instability are recognized. The first of these is termed "low-frequency instability" or "chugging", and is characterized by oscillation frequencies in the range of 20 to 200 cps. Low-frequency instability results from an interaction between the combustion process and the propellant feed system. Studies by various investigators (1-12)\* have resulted in a satisfactory understanding of low-frequency instability, and have provided reasonably accurate guidelines for preventing its occurrence.

The second type of instability is termed "intermediate-

---

\*Numbers in parentheses indicate references listed in the references section.

frequency instability", and is characterized by oscillation frequencies in the range of 200 to 600 cps. Intermediate-frequency instability results from the production of entropy waves in the combustion chamber and the interaction of these waves with the exhaust nozzle. Several studies of the intermediate-frequency instability phenomenon have been made (10,13). Intermediate-frequency instability is seldom observed in practice.

The third type of instability is termed "high-frequency instability" or "screaming", and is characterized by oscillation frequencies generally in excess of 600 cps. High-frequency instability results from an interaction between the combustion process and the acoustic properties of the combustion chamber, and exists in several forms which depend on the acoustic mode of the chamber excited by the combustion process. Thus a distinction is made between longitudinal and transverse mode instabilities. High-frequency combustion instability has received a great deal of attention in recent years. Experimental studies by various investigators (9-12, 14-17) have helped to define the nature of the phenomenon. Theoretical studies based on various simplified models have been made by Crocco (5, 8, 17-19), Priem and Guentert (20), Culick (21), Hart and McClure (22) and others. These studies have provided a partial understanding of the phenomenon together with suggestions on how to improve the stability characteristics of a rocket motor. The fact that a complete theory of high-frequency combustion

instability in solid and liquid propellant motors is not yet available is largely due to uncertainties in the details of the unsteady multi-phase burning process.

From a theoretical standpoint it is desirable to separate the complex multi-phase burning process into a series of simpler processes (eg. atomization, vaporization, mixing, reaction). The contribution that each individual process makes to the overall instability phenomenon then can be determined. If it were possible to couple the contributions of the individual processes an overall instability theory could be obtained. Such a coupling may not be possible but, the investigation of the individual processes may provide certain stability parameters which would not be available from a simplified combustion model.

The present work is directed toward understanding the contribution of the gas phase to high-frequency combustion instability. The investigation employs a rocket using premixed gaseous propellants. This "gas rocket" eliminates those phenomena peculiar to solid and liquid propellant motors, and any instability encountered can be attributed to phenomena in the gas phase. By its very simplicity the gas rocket readily lends itself as a model for the theoretical treatment of the problem.

Simplicity is only one reason for investigating gas-phase

combustion instability. Experimental studies (14, 17, 24) have shown that there are certain similarities between high-frequency instability in gas rockets and high-frequency instability in solid and liquid propellant motors (eg. pressure waveform). In addition it is possible that the gas phase plays an important role in the initiation of high-frequency oscillations in solid and liquid propellant motors. Hence an understanding of gas-phase instability may provide some insight into the more complicated instability phenomena observed in solid and liquid propellant motors.

In this thesis the experimentally observed properties of the longitudinal mode of high-frequency combustion instability in a gas rocket are presented. A comparison of the experimental observations with the results of an instability theory (23) based on a model closely approximating conditions in a gas rocket is made. From this comparison some conclusions concerning the driving mechanism for high-frequency instability in gas rockets are drawn, and some comments on the role of the gas phase in high-frequency instability in solid and liquid propellant motors are made.

## CHAPTER 2. EXPERIMENTAL APPARATUS

### A. Gas Rocket System

From experimental studies of high-frequency combustion instability in liquid propellant rocket motors (10-12, 14-17) it is known that the longitudinal mode is strongly dependent on the length of the combustion chamber, the mixture ratio, the propellant combination and also to a lesser extent on the injector and the nozzle. The gas rocket system was designed so that these five parameters could be changed easily. Two basic sub-systems make up the gas rocket system - the propellant feed system and the rocket motor (consisting of a mixing chamber, injector, combustion chamber and exhaust nozzle).

#### 1. Propellant Feed System

The purpose of the propellant feed system (Figure 1) is to supply the desired propellant flow rates to the rocket motor. The feed system is capable of simultaneously supplying as many as three different gases to the motor (The need for this capability will be discussed in Chapter 4). Flow metering is accomplished using critical flow orifices of the type shown in Figure 2. A total of ten orifices with different throat diameters are available so that a wide range of flow rates can be obtained. The critical flow orifices were calibrated using a water displacement technique (Appendix A).

## 2. Rocket Motor

The rocket motor sub-system consists of a mixing chamber, an injector, a combustion chamber and an exhaust nozzle. A schematic of the rocket motor is shown in Figure 3, and a photograph of the motor mounted on the test stand is shown in Figure 4. The individual components of the rocket motor are described below.

### Mixing Chamber

The mixing chamber (Figure 5) provides for the mixing of the gaseous propellants prior to their injection into the combustion chamber. Primary mixing of the fuel and oxidizer is provided by the impingement injector. Provision is made for introducing a third gas just downstream from the impingement injector through a radial-type showerhead injector. Final mixing is obtained by passing the crudely mixed gases through a tightly packed bed of stainless steel balls.

Experiments performed by Zucrow (24) using premixed and unmixed gaseous propellants show that the degree of mixing can influence the instability phenomenon. It is of interest, therefore, to consider the extent to which the propellant gases are mixed by the mixing chamber. To this end an experiment was carried out in which given flow rates of an oxidizer ( $O_2$ ) and a fuel ( $H_2$ ) were supplied to the mixing chamber.

Samples of the gas mixture at a station just downstream from the mixing chamber were obtained. These samples were analyzed using a gas chromatograph to determine the relative amounts of  $O_2$  and  $H_2$  (ie. mixture ratio). This mixture ratio was then compared to the input mixture ratio (determined from the known flow rates of  $O_2$  and  $H_2$ ) to obtain an indication of the degree of mixing. In the experiment three different mixture ratios were used; five samples were taken for each mixture ratio. The results of this experiment are shown in Figure 6. The scatter in the data, as indicated by the vertical bars, is approximately  $\pm 4\%$ . This is of the same order as the uncertainty in the known flow rates (Appendix B). It is concluded, therefore, that the mixing chamber provides for complete mixing of the gaseous propellants.

Since the propellants are premixed before injection into the combustion chamber there exists the possibility that combustion (which normally occurs in the combustion chamber) can propagate upstream through the injector and occur in the mixing chamber itself. The tendency for such a "flash-back" of combustion can be considerably reduced by a correct choice of injector and starting procedure. Unfortunately even with these precautions flash-back does occur on occasion (particularly when operating with a propellant combination for the first time). To prevent damage to the mixing chamber by

flash-back two safety devices were incorporated in the chamber design. The first device is a burst diaphragm, designed to relieve the over-pressure associated with combustion in the mixing chamber. The second device is an electro-mechanical system (Figure 7) which automatically shuts off the oxidizer flow when flash-back occurs (25). The system consists of a sensing circuit which actuates a solenoid valve which in turn controls a pressure-actuated valve in the oxidizer line upstream from the mixing chamber. The sensing elements are photoelectric cells mounted in the wall of the mixing chamber, and sense the combustion generated light through plexiglas windows. After a shutdown due to flash-back fuel continues to flow to prevent any remaining oxidizer from reacting with the metal components of the mixing chamber.

The mixing chamber is also fitted with a pressure tap so that the static pressure of the gases in the chamber can be monitored continuously.

### Injectors

After being thoroughly mixed in the mixing chamber, the gaseous propellants flow through an injector into the combustion chamber. The injector is essentially a circular metal plate, with some arrangement of injection orifices, fitted in the downstream end of the mixing chamber (Figures 3 and 5). To determine the effect of

the injection pattern on the instability phenomenon experiments were carried out using three different types of injectors. The first type of injector is a "porous" plug composed of sintered stainless steel powder with a mean pore size of five microns (Figure 8). The porous plug injector provides nearly one-dimensional injection of the propellants into the combustion chamber and hence should provide experimental data which can be correlated with one-dimensional instability theories.

To determine the effect of deviations from one-dimensional injection on the instability phenomenon two types of injectors which produce combustion zone recirculation were used. The first type, termed a "showerhead" injector, is a copper plug with injection orifices parallel to the longitudinal axis of the combustion chamber. Showerhead injectors characteristically produce weak recirculation patterns; hence, slight deviations from one-dimensional injection are to be expected. Three different showerhead injectors were used in the instability studies- 10 holes, 31 holes and 49 holes (Figures 8 and 9). The second type of "recirculating" injector is a copper plug with two sets of impinging triplets (Figure 10). Impinging injectors produce strong recirculation patterns; hence, fairly significant deviations from one-dimensional injection are to be expected. The total flow areas for the three showerhead injectors and the impinging injector were approximately equal, and were chosen so that the injection flow was choked under all conditions

of operation. Therefore any instability encountered using these injectors cannot be attributed to variations in the propellant injection rate. It was not possible to obtain choked injection flow using the porous plug injector.

#### Combustion Chamber

The cylindrical combustion chamber has an internal diameter of 3.8 cm. This diameter was chosen so as to discourage the occurrence of the transverse modes of combustion instability (As will be seen in Chapter 4 transverse modes do occur on occasion near stability limits). The length of the combustion chamber can be varied from 10 cm to 200 cm by using various combinations of nine 12.5 cm sections and two 50 cm sections together with one of three nozzle assemblies (described in the following section). A typical combustion chamber section is shown in Figure 11. The design of the chamber sections took into consideration the large heat transfer rates associated with unstable combustion and the requirement of extended run times (30 seconds or more). The sections have thick copper walls which serve as a heat sink and stainless steel liners to reduce heat transfer to the walls. In addition the exterior wall of the combustion chamber was spray-cooled using water.

The first chamber section (ie. the one just downstream from the mixing chamber) was modified to accept a high-frequency pressure trans-

ducer, a spark plug (used for igniting the propellants), a steady-state pressure transducer and five thermocouples (used to obtain temperature distributions in the combustion zone). Two other chamber sections were each modified to accept a single high-frequency pressure transducer; hence, data from as many as three high-frequency pressure transducers can be obtained during a given run.

#### Exhaust Nozzles

Theoretical studies of the longitudinal mode of high-frequency combustion instability (8, 21, 23) indicate that the instability phenomenon depends on the mean flow velocity of the combustion gases and on the geometry of the exhaust nozzle (eg. the length of the convergent section). To investigate these effects experimentally two different sets of exhaust nozzles were designed. In experiments to determine the effect of the mean flow velocity on the instability phenomenon two water-cooled converging-diverging nozzles were used (Figure 12). These nozzles have identical convergence angles ( $60^\circ$ ) and different contraction ratios- the contraction ratio ( $C_R = A_{\text{chamber}}/A_{\text{throat}}$ ) for one nozzle is approximately 23 and for the other nozzle approximately 46. In the experiments the exhaust flow from the nozzles was choked under all conditions of operation; hence, the mean flow velocities for the two nozzles varied inversely with the contraction ratios. To study the effect of the length of the convergent section of

the exhaust nozzle on the instability phenomenon experiments were carried out using the smaller converging-diverging nozzle and an un-cooled tungsten "plug" nozzle (Figure 13). These two nozzles have approximately the same flow area , but have converging sections of different length (The plug nozzle approximates the "zero-length" nozzles employed in some theoretical instability models- see, for example, Reference 23).

#### B. Instrumentation

The instrumentation used with the gas rocket system can be divided roughly into two groups- feed system instrumentation and combustion chamber instrumentation.

##### 1. Feed System Instrumentation (Figure 1)

The desired propellant flow rates were obtained using calibrated critical flow orifices. For such orifices the flow rate is determined by the stagnation pressure and temperature upstream from the orifice. Stagnation pressures were measured using steady-state pressure transducers (Statham PG 731); stagnation temperatures were measured using copper-copper+constantan thermocouples. The output signals from the pressure transducers and thermocouples were recorded on Leeds and Northrup recording potentiometers. To assure that the orifice flow was choked during a given run the pressure downstream from the orifice was monitored. The

pressure in the mixing chamber was also monitored to determine if the injector flow was choked.

## 2. Combustion Chamber Instrumentation

### Steady-State Instrumentation

The steady-state or mean combustion pressure was measured by a Flader PSHD pressure transducer. Mean gas temperatures in the combustion zone were measured using five uncoated platinum-platinum+10% rhodium thermocouples with platinum-6% rhodium shields installed in the first combustion chamber section. Thermocouples of this type were required because of the high-temperature oxidizing environment which existed under certain conditions of operation of the gas rocket. Because of this environment the thermocouples were not equipped with radiation shields. The output signals from the five thermocouples and the Flader transducer were recorded on Leeds and Northrup recording potentiometers.

### Transient Instrumentation

The amplitude and frequency of the pressure oscillations associated with unstable combustion were measured by one or more water-cooled, strain gage type, high-frequency pressure transducers (Dynisco PT 49) mounted in the wall of the combustion chamber so that the pressure-

sensitive diaphragms were flush with the interior wall. The output signals from the Dynisco transducers were recorded on a seven-track magnetic tape recorder (Ampex S-3561). For the purposes of data reduction the recorded signals were displayed on a visicorder (Minneapolis-Honeywell 1108). The only filtering of the transducer output is that inherent in the transient pressure recording system. The effect of this inherent filtering on the transient pressure data is discussed in Appendix B.

### CHAPTER 3. THEORETICAL CONSIDERATIONS

#### A. Historical Background

One of the initial works to appear on high-frequency combustion instability in gas rockets was due to Zucrow and Osborn (31). They reported the results of an experimental study of the longitudinal mode of combustion instability and suggested a driving mechanism based on a coupling of the pressure oscillations with the chemical reaction rate. In this driving mechanism a small localized pressure disturbance (perhaps due to turbulence) propagates longitudinally in the combustion chamber. When this pressure disturbance traverses the reaction zone it increases the burning rate (due to the increased pressure and temperature associated with the disturbance). The increased burning rate, in turn, reinforces the disturbance. If the energy supplied to the disturbance (by the increased burning rate) is greater than the energy lost due to dissipation and reflection from the nozzle, the disturbance will be amplified during each succeeding oscillation until dissipative phenomena within the wave limit further amplification. If the energy supplied by combustion is less than the energy lost the disturbance will decay in time. To account for the experimentally observed minimum chamber length for instability (for chamber lengths less than the minimum the combustion is stable) Zucrow and Osborn postulated that the net energy supplied to the disturbance depends on the period of the oscillation and hence on the chamber length.

For short chambers the period of the oscillation is small, hence only a small amount of propellant will be injected during each cycle. Thus as the chamber length decreases the energy released per cycle decreases, and for some minimum chamber length the energy addition will not be sufficient to amplify a disturbance (Implicit in this argument is the assumption that the energy lost per cycle, due to dissipation, flow work and mean nozzle flow, is essentially independent of the period of the oscillation).

The instability mechanism suggested by Zucrow and Osborn was reviewed by Crocco (32). Crocco pointed out that the energy lost per cycle is not independent of the period of the oscillation, but, in fact, decreases with decreasing period. Thus the balance between the energy supplied and the energy lost per cycle is relatively insensitive to the period of the oscillation. In addition Crocco pointed out that if the Zucrow-Osborn argument were carried to its logical conclusion there would be no upper length limit for stability- ie. no maximum length above which the combustion would be stable. Crocco noted that although this conclusion seemed to agree with available gas rocket data it was inconsistent with accepted "time-lag" theories of combustion instability. If, as Zucrow and Osborn postulated, the driving mechanism is a chemical kinetic one then the relevant time-lag should be the chemical reaction time- ie. the time required to convert gaseous reactants into gaseous products. For combustion instability to occur there must be a coupling of the pressure

oscillations and the combustion process. For this coupling to occur the ratio of the chemical reaction time and the period of the oscillation must lie in certain ranges. Since the period of the oscillation depends on the chamber length it follows that there must be a lower and an upper critical length for each mode of longitudinal oscillation. Below or above these critical lengths combustion will be stable with respect to a particular mode (Although it may still be unstable for other modes). In view of the above results Crocco concluded that the instability mechanism suggested by Zucrow and Osborn was incorrect.

Since it appeared that the driving mechanism for gas-phase instability was not related to chemical kinetics, a different driving mechanism, based on a coupling between oscillations in the chamber and the heat transfer to the injector, was suggested by Bortzmeyer and Crocco (26). In this driving mechanism it is assumed that the gaseous propellants are in thermal equilibrium with the injector- ie. the injection temperature of the gases is equal to the temperature of the face of the injector. If a small disturbance occurs near the injector face the heat transfer to the injector will increase (due to the increased gas temperature associated with the disturbance). At some later time (determined by the "inertia" of the transfer processes) the temperature of the injector face (and thus the injection temperature of the gases) will increase. Due to the increased injection temperature (and after a

proper time-lag) the temperature of the burned gases increases. Note that as the temperature of the injector face increases the heat transfer to the injector decreases (since the difference between gas temperature and injector temperature decreases). Bortzmeyer and Crocco argued that if the time-lags associated with the transfer processes were properly related to the period of the oscillation, unstable combustion would occur. Using this driving mechanism Bortzmeyer and Crocco carried out a theoretical analysis to obtain the stability limits for the longitudinal mode of gas-phase combustion instability. The results of this analysis agreed in some respects with the experimental data obtained by Zucrow and Osborn (31) and Pelmas (27). The analysis predicted a minimum chamber length for instability and no upper length limit for stability. It also predicted that combustion in the gas rocket tends to be stable around the stoichiometric mixture ratio. This prediction agreed with the results of Pelmas but not with the results of Zucrow and Osborn (who found unstable combustion around the stoichiometric mixture ratio). The stability limits obtained from the analysis are strongly dependent on two heat transfer parameters- the heat transfer coefficient of the combustion gases and the thermal conductivity of the injector. An experiment in which the heat transfer coefficient of the combustion gases (for a given fuel and oxidizer) was altered was carried out by Schob (29). This experiment showed effectively no dependence of the stability limits

on the heat transfer coefficient. Experiments using geometrically similar injectors with and without insulating coatings (28) showed no dependence of the stability limits on the thermal conductivity of the injector. Thus experiments indicated that heat transfer to the injector has little or no effect on gas-phase combustion instability.

Sirignano and Crocco (23) then carried out a theoretical analysis of the longitudinal mode of high-frequency combustion instability in which the driving mechanism is based on chemical kinetics. The mechanism is somewhat similar to the one used by Zucrow and Osborn (31) to qualitatively explain their experimental results in that instability is produced by a coupling of the pressure oscillation with the chemical reaction. The theory assumes that the response time of the combustion process is negligible compared to the period of the oscillation. Hence, no phase or time-lag exists between energy addition from combustion and pressure. The analysis provides information both on the stability limits and on the instability waveform. The theory is discussed in some detail in the following sections since it seems particularly relevant to gas-phase combustion instability and forms the basis for much of the experimental work discussed in Chapter 4.

The explanation for some of the experimentally observed properties of the longitudinal mode of gas-phase instability (in particular the existence of harmonic modes) cannot be found in the Sirignano-Crocco

model. In an effort to account for the presence of harmonics Crocco has recently advanced a theory, based on a chemical kinetics driving mechanism, which assumes a combustion zone of finite thickness (33). Analytical and experimental studies based on this new model are currently in progress at Princeton.

Culick has carried out a theoretical investigation of high-frequency combustion instability for the general case of a three-dimensional flow field with distributed combustion (21). A solution of the linearized equations gives an expression for the stability limits in which the effects of combustion, nozzle and mean flow are separated. Under suitable simplifications it should be possible to reduce the equation for the stability limits to a form which is applicable to the longitudinal mode of gas-phase instability. Since the Culick analysis provides less information about the instability phenomenon (stability limits only) than the Sirignano-Crocco analysis, no attempt was made in the present study to correlate Culick's results with experimental observations.

Some comments on the results of the various studies discussed in this section are given in Chapter 5.

#### B. The Sirignano-Crocco Instability Model

Sirignano and Crocco (23) have carried out a theoretical in-

vestigation of the longitudinal mode of high-frequency combustion instability based on a chemical kinetics driving mechanism. The driving mechanism assumes that instability is produced by a coupling of the pressure oscillation with the chemical reaction and that there is no time-lag between energy addition from combustion and pressure. The model on which the analysis is based closely approximates the conditions in a rocket burning premixed gaseous propellants. In the following sections a brief discussion of the theory is presented to serve as a background for the experimental work discussed in Chapter 4. Details of the theoretical development can be found in Reference 23 and Appendix C.

The Sirignano-Crocco analysis differs from the linearized approaches to the instability problem (8, 17-19, 21) in that it seeks a solution to the non-linear equations of motion- ie. a solution which is valid inside a region of unstable combustion and not just at the stability limits. The principal assumptions on which the analysis is based are:

- (1) The response time of the combustion process is negligible compared to the period of the oscillation.
- (2) A plane shock wave propagates longitudinally in the combustion chamber with constant period, and reflects alternately from the nozzle and injector.
- (3) The combustion chamber is sufficiently long so that the

configuration may be approximated by the limiting case of a zero-length nozzle and a zero-thickness combustion zone.

- (4) There are no entropy waves in the flow field.
- (5) The flow is one-dimensional and adiabatic.
- (6) The combustion gases are calorically perfect.
- (7) The cross-sectional area of the combustion chamber is constant.

Because of the presence of shock waves in the flow field it is convenient to use a characteristic co-ordinate perturbation technique to obtain solutions. To this end the unsteady, one-dimensional equations of motion of the gas in the chamber are transformed into characteristic co-ordinates, and the dependent variables (which include  $x, t$  in the characteristic co-ordinate system) are expanded in terms of an as yet undefined amplitude parameter  $\epsilon$ . The boundary condition at the combustion zone is defined in terms of an energy release parameter  $r$ . The boundary condition at the nozzle is defined in terms of a nozzle admittance parameter. It is noted that the Sirignano-Crocco analysis differs from the standard approaches to the non-linear instability problem (20) in that it seeks a "stable" periodic solution rather than an indication of the stability of a given steady-state operation to known perturbations. Hence, the initial condition is replaced by a cyclic condition (which in effect states that the oscillation is periodic). "Stable" periodic

solutions to the equations, compatible with the boundary conditions and the cyclic condition, are obtained only after considerable labor (Phenomenologically a "stable" periodic solution exists when the energy supplied to the wave by the combustion process just balances the energy dissipated by the wave due to its reflection from the nozzle and its motion). The solutions give the strength of the shock wave (in terms of the changes in pressure and gas velocity across the wave), the wave velocity, the period of the oscillation and the time decay (for fixed location) in pressure and gas velocity behind the wave as functions of three important instability parameters-  $\epsilon$  ,  $\lambda$  ,  $r$  (Appendix C). If the functional form of the combustion law ( $r$ ) is known then it is possible to obtain  $\epsilon$  and  $\lambda$  . Knowing  $\epsilon$  ,  $\lambda$  and  $r$  the waveform of the instability can be determined. Alternatively, if the waveform of the instability is known (through experiments) then it is possible, in theory, to work backwards to obtain the appropriate functional form of the combustion law. In the following sections some theoretical results obtained for a choice of  $r$  particularly appropriate for gas rockets are presented.

### C. Theoretical Results

For any reasonable  $r$  the waveform obtained from the theory consists of shock discontinuities followed by exponential time decay in pressure and velocity. The shock wave oscillates with approximately

the fundamental acoustic frequency of the combustion chamber.

In order to determine some explicit information about the instability waveform Sirignano and Crocco assumed a simplified combustion law of the Arrhenius type

$$r = B \exp \left\{ -\frac{E}{RT} \right\} \quad (3-1)$$

where E= an activation energy, T= combustion temperature, B= pre-exponential factor (independent of T) and R= universal gas constant. Admittedly this expression may be too simple to be realistic, but it does contain some of the essential features of gas-phase kinetics and provides theoretical results which are readily compared with the experimental data. With this choice for r the functional forms of  $\epsilon$  and  $\lambda$  are (23)

$$\epsilon = \bar{M} \left\{ (\gamma-1) \frac{E}{RT} - \frac{\gamma(\gamma-1)}{2} \right\} \quad (3-2)$$

$$\lambda = \frac{16\bar{M} \left\{ \left( \frac{\gamma-1}{2} \right) \frac{1}{1-\nu} \right\}^2 \left\{ 2 \left( \frac{E}{RT} \right)^2 - 3 \left( \frac{E}{RT} \right) - \frac{\gamma(\gamma-1)}{(\gamma-1)^2} \right\}}{(\gamma+1)(1+\nu) \left\{ \frac{1-\bar{M}}{1+\bar{M}} \left( \frac{1+\nu}{1-\nu} \right) + \frac{1+\bar{M}}{1-\bar{M}} \right\}} \quad (3-3)$$

The parameter  $\epsilon$  can be considered an amplitude parameter, roughly pro-

portional to the strength of the instability (Appendix C). The parameter  $\lambda$  can be considered a shape parameter giving the nature of the exponential decay in pressure and velocity behind the wave (Appendix C).

#### D. Discussion of the Assumptions

In this section some of the assumptions on which the theory is based are reviewed, with particular emphasis being placed on a comparison of the assumptions with conditions in the gas rocket.

Assumption 1. The response time of the combustion process is negligible compared to the period of the oscillation.

The response time of the combustion process is the time required for the reaction rate to adjust to a change in conditions (pressure, temperature)-

$$t_{\text{response}} \sim \frac{1}{\text{reaction rate}} = \frac{1}{K \prod_{i=1}^m [\text{reactant } i]^{n_i}}$$

where  $k$  = specific rate constant,  $[\text{reactant } i]$  = concentration of reactant  $i$  and  $n_i$  = order of the reaction with respect to reactant  $i$ . For the conditions existing in the gas rocket typical values for  $t_{\text{response}}$  are of the order of  $10^{-5}$  seconds. Typical values for the period of the oscillation are  $10^{-2}$  to  $10^{-3}$  seconds. Thus for rocket motors burning premixed gaseous propellants the assumption of no time-lag between energy addition by

combustion and the oscillation is a valid one (This is not true for liquid propellant motors where energy addition depends on factors other than gas-phase kinetics).

Assumption 2. A plane shock wave propagates longitudinally in the combustion chamber.

Experimental studies of the longitudinal mode of high-frequency combustion instability in liquid propellant rockets (9-12, 14) and in gas rockets (27, 29-31, 34) have shown that the instability frequently appears as a shock wave propagating longitudinally in the combustion chamber. This observation is confirmed by the present experimental study (Chapter 4).

Assumption 3. The nozzle length and combustion zone thickness are negligible compared to the combustion chamber length.

The combustion zone thickness and nozzle length in the gas rocket are generally very much less than the length of the combustion chamber (See Chapter 4). Hence, Assumption 3 (which is necessary to make the problem mathematically tenable) is valid, to a first approximation, for the gas rocket.

In general a combustion zone and nozzle of finite size have a stabilizing effect on the combustion process. The stabilizing effect of a finite combustion zone results from the non-optimum addition of energy

to the combustion oscillation- ie. energy addition over a finite length rather than at a pressure antinode. It is conceivable that for sufficiently short chambers (ie. for pressure oscillations with small wave length) the combustion oscillations would not be amplified. In fact this argument is frequently offered as an explanation for the experimentally observed minimum chamber length for longitudinal instability (32). As the length of the combustion chamber increases the energy addition approaches the optimum and the stabilizing effect decreases.

Any stabilizing effect of the nozzle results from variations in the amplitude and phase of pressure and velocity produced by the interaction of the oscillation with the nozzle. In general these amplitude and phase variations decrease with decreasing frequency (longer chambers); hence, as the chamber length increases the stabilizing effect of the nozzle decreases. An experimental study of the effects of the combustion zone and nozzle on the instability phenomenon is discussed in Chapter 4.

Assumption 4. No entropy waves exist in the flow field.

In a rocket motor burning premixed gaseous propellants entropy waves can be produced by localized pressure variations (such as accompany unstable combustion) in the combustion zone. Adjacent propellant elements will have different entropies; the mean downstream motion of these

elements is termed an entropy wave. An entropy wave can have two possible effects on the instability phenomenon. The first effect is the appearance of intermediate-frequency instability (discussed in Chapter 1). The second effect results from the interaction of the entropy wave with the pressure waves associated with high-frequency instability. Due to the highly turbulent flow in the combustion chamber of the gas rocket it is reasonable to assume that entropy waves are "erased" due to turbulent mixing. If this is true then the effects of the entropy wave can be neglected. In the experiments of Chapter 4 no effects attributable to entropy waves were observed.

Assumption 5. The flow is one-dimensional and adiabatic.

Due to the high turbulence level downstream from the combustion zone it is reasonable to assume that the mean flow properties are constant over a given cross-section. The nature of the flow immediately downstream from the injector and in the combustion zone depends on the injection pattern. The effects of non-uniform flow in the combustion zone on the instability phenomenon are not known a priori. Hence, an experimental study of the effects of the injection pattern on the instability has been made (Chapter 4).

The flow in the gas rocket is definitely non-adiabatic. Heat transfer to the walls of the combustion chamber is relatively large for

stable combustion, and when the combustion is unstable the heat transfer increases significantly. Heat transfer has a stabilizing effect on the combustion process (as do all dissipative phenomena).

Assumptions in Equation (3-1).

Two important assumptions are embodied in the energy release law (3-1). First, the energy release rate is assumed to be independent of pressure or species concentration. A more rigorous expression for the energy release rate would be

$$r = q \hat{r}$$

where  $q$  is a heat of reaction and  $\hat{r}$  is the chemical reaction rate and is written

$$\hat{r} = b(T) \prod_{i=1}^m [\text{reactant } i]^{n_i} \exp \left\{ -\frac{E}{RT} \right\}$$

where  $b(T)$  = a temperature dependent pre-exponential factor. Expressing the concentration of the  $i^{\text{th}}$  reactant in terms of the mole fraction ( $x_i$ ) and the total pressure the energy release law becomes

$$r = q b(T) \left[ \frac{P}{RT} \right]^{\sum n_i} \prod_{i=1}^m x_i^{n_i} \exp \left\{ -\frac{E}{RT} \right\}$$

In employing an energy release law of this type Sirignano and Crocco found that for reasonable values of  $\sum_1 n_1$  (the overall order of the reaction) the combustion was predicted always to be unstable. This conclusion is contrary to experimental observations (Chapter 4). That the more rigorous rate expression predicts a result not in agreement with experimental data is due primarily to the fact that the isentropic assumption used to relate P and T in the analysis of the combustion zone boundary condition is not valid. The constant entropy assumption is violated due to the energy release and diffusion in the combustion zone. Hence to obtain non-trivial theoretical results it is necessary to assume that the combustion process in the gas rocket is approximated sufficiently well by equation (3-1). As will be seen in Chapter 4 simplified rate expressions, such as (3-1), provide theoretical results which agree in many respects with the experimental observations.

A direct result of the form of the energy release law (3-1) is that the mean energy release rate ( $\bar{r}$ ) can increase without limitation as the mean combustion temperature ( $\bar{T}$ ) increases. In the gas rocket the mean energy release rate is the product of the propellant injection rate ( $\dot{m}$ ) and a heat of reaction ( $q$ ),

$$\bar{r} = \dot{m} q$$

During a given run  $\dot{m}$  and the mixture ratio (and hence  $q$ ) are constant. It follows that the mean energy release rate is constant (and essentially independent of the mean combustion temperature). If the mean combustion temperature were increased (eg. by heat addition through the walls of the combustion chamber) equation (3-1) would predict a corresponding increase in the mean energy release rate. In the gas rocket the increased combustion temperature would produce a temporary increase in the instantaneous energy release rate- ie. an increase in the propellant consumption rate. Since the propellant consumption rate is now greater than the propellant injection rate the increased energy release rate cannot persist. After some time the energy release rate must decrease so that in the mean the propellant consumption rate is equal to the propellant injection rate. Thus it is seen that equation (3-1) neglects the fact that the gas rocket is an energy-limited system- ie. that the energy release rate is limited by the propellant injection rate.

A further discussion of the effects of deviations from the assumptions on the instability phenomenon is presented in Chapter 4.

#### E. Discussion of Theoretical Results and Some Critical Experiments

A careful study of the results of the Sirignano-Crocco analysis (Section C and Appendix C) suggests several experiments which can be

used to test the validity of the proposed instability driving mechanism and combustion law.

The theory predicts that the instability exists as a plane shock wave oscillating longitudinally in the combustion chamber with approximately the fundamental acoustic frequency of the chamber. According to the theory the time-decay in pressure behind the wave (at fixed location) is exponential and depends on the functional form of the combustion law. To obtain data on the instability waveform an experiment can be performed in which pressure-time histograms are obtained during unstable combustion at various locations in the chamber (Chapter 4).

From equations (3-2), (3-3), (C-3) and (C-4) it is seen that the equation for the stability limits (a stability limit is defined by  $\Delta P/P = 0$ ) is obtained by setting  $\epsilon = 0$  in equation (3-2).

$$\left(\frac{E}{RT}\right)_{\text{limi}} = \frac{(3\gamma - 1)}{2(\gamma - 1)} \quad (3-4)$$

Thus the stability limits are defined in terms of a critical value for the rate parameter  $E/RT$ . For a given propellant combination (and over a moderate range of mixture ratios) it is reasonable to assume that  $E$  is constant. Thus the stability limits are defined in terms of a critical

combustion temperature,  $\bar{T}_{crit}$ . From equation (3-2) it is seen that whenever  $\bar{T} < \bar{T}_{crit}$  the amplitude parameter  $\epsilon > 0$ ; hence, from equations (C-3) and (C-4),  $\Delta P/\bar{P} > 0$  - ie. the combustion is unstable. Whenever  $\bar{T} > \bar{T}_{crit}$ ,  $\epsilon < 0$  and  $\Delta P/\bar{P} < 0$  - ie. the combustion is stable. The important conclusion to be drawn from this discussion is that the tendency for instability is greater at lower combustion temperatures. It is noted that the combustion temperature depends on the equivalence ratio ( $\Phi$ ), is a maximum at stoichiometric ( $\Phi = 1$ ) and decreases as the values for  $\Phi$  vary from  $\Phi = 1$ . If the maximum combustion temperature for the propellant combination is greater than  $\bar{T}_{crit}$  then two values for  $\Phi_{limit}$  exist-  $\Phi_{limit}^{(1)} < 1$  and  $\Phi_{limit}^{(2)} > 1$ . This is interpreted to mean that in the  $\Phi - L$  or  $\Phi - \bar{P}$  plane two regions of unstable combustion will be found, one on either side of stoichiometric. According to the theory once a stability limit has been crossed (proceeding away from  $\Phi = 1$ ) unstable combustion persists until the combustion limit is reached. When the maximum combustion temperature is less than  $\bar{T}_{crit}$  unstable combustion will occur over the entire range of combustible equivalence ratios. From the above considerations it is seen that the theory provides a criterion for the number and location of unstable regions.

From equation (3-4) it is seen that for propellant combinations characterized by two unstable regions ( $\bar{T}_{max} > \bar{T}_{crit}$ ) it is possible to

collapse the two regions into a single region if the overall range of combustion temperatures can be reduced without altering  $E$  (eg. by the addition of an inert diluent). The two unstable regions should just coalesce into a single region when  $\bar{T}_{\max} = \bar{T}_{\text{crit}}$ .

To test the concept of a critical value for  $E/R\bar{T}$  at the stability limits two experiments can be carried out. In the first experiment the regions of unstable combustion for several propellant combinations are located in the  $\Phi - L$  and  $\Phi - \bar{P}$  planes. For those combinations which exhibit two unstable regions a comparison is made between the experimental values for  $(E/R\bar{T})_{\text{limit}}$  and the values given by equation (3-4). For those propellant combinations which exhibit one unstable region the theoretical criterion  $(E/R\bar{T})_{\text{limit}} < (E/R\bar{T})_{\text{stoic}}$  is tested.

The second experiment involves one of the propellant combinations which exhibits two unstable regions. In this experiment the overall range of combustion temperatures is reduced (without altering  $E$ ) through the addition of an inert diluent, and the stability limits for various diluent concentrations obtained. According to equation (3-4),  $(E/R\bar{T})_{\text{limit}}$  should remain essentially constant (a slight variation in  $\gamma$  is produced by the addition of a diluent). Since the combustion temperatures are lower the theory indicates a shift in the stability

limits toward  $\Phi = 1$  (and relatively higher combustion temperatures) as the amount of diluent is increased.

From equation (3-4) it is seen that the stability limits depend on an overall activation energy characteristic of the propellant combination. To determine the dependence of the stability limits on E an experiment involving a propellant combination which exhibits two unstable regions can be performed. In this experiment E, but not  $\bar{T}$ , is altered by the addition of trace amounts of a catalyzing species. In accordance with equation (3-4), a shift in stability limits should be observed with the addition of the catalyzing species.

Equations (3-2), (3-3), (C-3) and (C-4) give the dependence of the strength of the instability ( $\Delta P/\bar{P}$ ) on the rate parameter ( $E/R\bar{T}$ ) and the mean Mach number of the combustion gases ( $\bar{M}$ ). A typical plot of the theoretical variation of  $\Delta P/\bar{P}$  with  $E/R\bar{T}$  for constant  $\bar{M}$  is shown in Figure 14. It is noted that  $\Delta P/\bar{P}$  is a monotonically increasing function of  $E/R\bar{T}$ . For a given propellant combination E is approximately constant, hence  $\Delta P/\bar{P}$  is a monotonically decreasing function of  $\bar{T}$ . Recalling the dependence of  $\bar{T}$  on  $\Phi$ , it is seen that  $\Delta P/\bar{P}$  increases as  $\Phi$  varies away from stoichiometric. Thus for propellant combinations which exhibit two unstable regions it is to be expected that the instability strength increases as an equivalence ratio traverse is made

across an unstable region (from the stability limit to the combustion limit); the strength is a maximum at the combustion limits. For propellant combinations which exhibit one unstable region it is to be expected that the strength is a minimum at stoichiometric and a maximum at the combustion limits. To determine the dependence of  $\Delta P/\bar{P}$  on  $E/R\bar{T}$  for constant  $\bar{M}$  an experiment can be carried out in which  $\Delta P/\bar{P}$  is measured as equivalence ratio traverses are made across regions of unstable combustion.

A typical plot of the theoretical variation of  $\Delta P/\bar{P}$  with  $\bar{M}$  for constant  $E/R\bar{T}$  is shown in Figure 15. It is seen that  $\Delta P/\bar{P}$  is a monotonically increasing function of  $\bar{M}$ . It is noted that for given propellants  $\bar{M}$  depends primarily on the throat area of the exhaust nozzle (for choked nozzle flow). To determine the dependence of  $\Delta P/\bar{P}$  on  $\bar{M}$  for constant  $E/R\bar{T}$  an experiment can be performed in which  $\Delta P/\bar{P}$  is measured for fixed  $E/R\bar{T}$  (ie. for fixed  $\bullet$ ) using exhaust nozzles with different throat areas.

As noted in Section D the instability phenomenon depends to a certain extent on the injection pattern, nozzle geometry and combustion chamber length. An experimental study of these effects has been carried out and is discussed in Chapter 4.

A detailed description of the experiments outlined in this

section together with a comparison of the experimental results with the theory is presented in Chapter 4.

CHAPTER 4. EXPERIMENTAL CONSIDERATIONS

A. General Comments on the Operation of the Gas Rocket

A typical gas rocket run consists of three distinct phases-starting, steady-state and data recording. During the starting phase combustion is established with reduced propellant flow rates. This procedure serves to reduce the severity of flashback (should it occur) and to prevent a "hard" start. The details of the starting procedure depend on the individual experiment and will be discussed in the sections describing the experiments. Steady-state operation is achieved by gradually increasing the propellant flow rates to their steady-state values (determined by mixture ratio and combustion pressure requirements). Steady-state operation is characterized by constant propellant flow rates and constant mean combustion pressure. The duration of steady-state operation is on the order of 20 to 30 seconds so that transients associated with starting and with transition to steady-state operation have sufficient time to decay. Instability data are recorded during the final 10 to 15 seconds of the steady-state period.

B. Waveform of Longitudinal Combustion Instability

The instability waveform obtained from the Sirignano-Crocco analysis consists of shock discontinuities followed by exponential

decay in time (for fixed location) of pressure and velocity. The shock wave oscillates with approximately the fundamental longitudinal acoustic frequency of the combustion chamber. A typical theoretical pressure-time history is shown in Figure 16a. The results are for an observer located at  $x/L = 0.16$  (ie. near the injector).

In the present study pressure-time histories during unstable combustion were recorded at several stations in the combustion chamber of the gas rocket. Figure 16b is a typical pressure-time history during unstable combustion at a station just downstream from the injector. The first pressure rise corresponds to a wave traveling upstream toward the injector. The second pressure rise corresponds to the wave after reflection from the injector (traveling downstream toward the nozzle). A comparison of the theoretical and experimental pressure-time histories shows that they are qualitatively the same. From pressure-time histories such as Figure 16b it has been determined that the instability occurs as a plane shock wave oscillating with approximately the fundamental longitudinal acoustic frequency of the combustion chamber with exponential time-decay of pressure behind the wave. For certain conditions of operation other forms of combustion oscillations have been observed. These are discussed in Section F. Waveform of the type shown in Figure 16b have been observed in other studies of combustion instability in gas rockets (27, 29, 31, 34).

### C. Dependence of Stability Limits on $E/R\bar{T}$

In Chapter 3 (Section E) it was noted that the stability limits are defined in terms of a critical value for the rate parameter ( $E/R\bar{T}$ ). Several experiments which serve to test this conclusion were discussed. In each of these experiments the dependence of the stability limits on one of the two variables in the rate parameter ( $E$  and  $\bar{T}$ ) is determined holding the other variable constant.

#### 1. Dependence of Stability Limits on $\bar{T}$ ( $E = \text{constant}$ )

To determine the dependence of the stability limits on  $\bar{T}$  the regions of unstable combustion for two propellant combinations with various concentrations of an inert diluent were located in the  $\Phi$  -L plane. The two propellant combinations used in this experiment were hydrogen-air and methane-oxygen. The inert diluent was nitrogen. The addition of nitrogen to a given propellant combination reduces the overall range of combustion temperatures but has little or no effect on the overall activation energy (35). Thus the temperature dependence of the stability limits can be obtained by determining the dependence of the limits on diluent concentration. Quantitative information on  $\bar{T}$  at a stability limit was derived from the axial distribution of mean gas temperature in the combustion zone at the stability limit.

It is noted that the diluent was supplied to the rocket motor separately from the fuel and oxidizer (In the flow schematic of Figure 1 the diluent is the X gas). During the starting phase combustion was established using the fuel and oxidizer alone (no diluent). Steady-state operation was then established by increasing the flow rates of the fuel, oxidizer and diluent to their steady-state values. This technique is somewhat different from the one used in previous investigations of gas-phase instability (27-29). In these studies the desired diluent concentrations were obtained using gas cylinders in which the diluent and oxidizer were premixed to specification by the supplier. The principal advantage of adding the diluent separately is that instability data can be obtained for diluent concentrations which could not have been ignited (using a spark ignition system) had the diluent and oxidizer been premixed. In addition the use of separate diluent and oxidizer systems increases the flexibility of the propellant feed system in that variations in diluent concentration are easily obtained. In using this technique it was found that diluent concentrations were reproducible to within  $\pm 3\%$  of a nominal value.

The regions of unstable combustion in the  $\Phi$  -L plane for hydrogen-air and hydrogen-dilute air are shown in Figure 17. In this figure the diluent concentration is defined by

$$\% \text{ dilution} = \frac{\text{diluent mass flow rate}}{\text{diluent mass flow rate} + \text{air mass flow rate}} \times 100.$$

The unstable regions in the  $\Phi$  -L plane for methane-dilute oxygen are shown in Figure 19. The data of Figures 17 and 19 were obtained for  $\bar{P} = 7.8 \pm 0.3$  atm using the 31-hole showerhead injector and the plug nozzle. Unstable combustion (characterized by periodic oscillations of the combustion pressure) occurs inside the shaded regions.

From Figure 17 it is seen that for a given diluent concentration two regions of unstable combustion exist, one on either side of the stoichiometric mixture ratio. As the diluent concentration is increased the unstable regions shift toward stoichiometric. The upper stability limits of the oxygen-rich ( $\Phi > 1$ ) unstable regions are not clearly defined- ie. there is no sharp transition from unstable combustion to stable combustion. For clarity only the upper limit for H<sub>2</sub>-air is shown. The overall extent of the oxygen-rich unstable regions is only slightly dependent on the diluent concentration since as the diluent concentration increases both the upper and lower stability limits shift toward stoichiometric. The lower stability limits for the fuel-rich ( $\Phi < 1$ ) unstable regions are in reality the fuel-rich combustion limits. For clarity only the lower limit for H<sub>2</sub>-air is shown. The

overall extent of the fuel-rich unstable regions is only slightly dependent on the diluent concentration. The results of Figure 17 for  $H_2$ -air are in general agreement with the observations of Pelmas (27), Bertrand (28) and Schob (29). Bertrand (28) has observed a shift in the stability limits with increasing diluent concentration.

From Figure 19 it is seen that for  $CH_4-(0.4O_2+0.6N_2)$  two regions of unstable combustion exist, one on either side of stoichiometric. The upper limit of the oxygen-rich unstable region and the lower limit of the fuel-rich unstable region are combustion limits. As the diluent concentration is increased the unstable regions shift toward stoichiometric. For  $CH_4$ -air the fuel-rich and oxidizer-rich unstable regions have coalesced to form a single unstable region located around stoichiometric. The upper and lower boundaries of this region are combustion limits. The results of Figure 19 for  $CH_4$ -air are in general agreement with the observations of Zucrow and Osborn (24). The results for  $CH_4-(0.4O_2+0.6N_2)$  are in general agreement with the observations of Pelmas (27).

A quantitative measure of  $\bar{T}_{limit}$  was obtained from the axial distribution of mean gas temperature in the combustion zone at the stability limits (See Figure 43). The details of the measurement of gas temperatures are presented in Section K. The gas temperature (and

thus the reaction rate) varies throughout the combustion zone. For the purpose of correlating the experimental data with the theoretical results an average value for  $\bar{T}_{\text{limit}}$  was defined by

$$\exp\left\{-\frac{E}{R\bar{T}_{\text{AV}}}\right\} \equiv \frac{1}{\delta} \int_0^{\delta} \exp\left\{-\frac{E}{R\bar{T}(x)}\right\} dx \quad (4-1)$$

In this definition  $\bar{T}_{\text{av}}$  is that temperature which would give an average energy release rate equal to the local energy release rate integrated over the combustion zone. Two experimental inputs are required in (4-1)- the thickness of the combustion zone ( $\delta$ ) and the temperature profile in the combustion zone,  $\bar{T}(x)$ . The thickness of the combustion zone is taken as the distance from the injector face to the peak combustion temperature. Since temperature data could not be obtained near the injector (See Section K) an accurate determination of  $\bar{T}(x)$  could not be made. For the purpose of evaluating  $\bar{T}_{\text{av}}$  a linear temperature profile was assumed-

$$\bar{T}(x) = \bar{T}_{\text{inj}} + (\bar{T}_{\text{peak}} - \bar{T}_{\text{inj}}) \frac{x}{\delta}$$

where  $\bar{T}_{\text{inj}}$  = mean injection temperature and  $\bar{T}_{\text{peak}}$  = mean peak combustion temperature. Using this profile the average combustion temperatures

at the stability limits for  $H_2$ -air and  $H_2$ -dilute air were calculated for several choices of  $\bar{T}_{inj}$ . It was found that  $\bar{T}_{av}$  was approximately equal to  $\bar{T}_{peak}$  and nearly independent of the choice of  $\bar{T}_{inj}$ . The results of this calculation together with the stoichiometric adiabatic combustion temperatures ( $\bar{T}_{ad}$ ) for the various diluent concentrations are tabulated in Figure 18. For a given chamber length the measured combustion temperatures at the stability limits nearest stoichiometric ( $\bar{T}_{av}$ ) are approximately the same. For  $L = 104$  cm  $\bar{T}_{av} = 1405 \pm 25^\circ K$  for all diluent concentrations. For  $L = 53$  cm  $\bar{T}_{av} = 1435 \pm 40^\circ K$ . The scatter in the temperature data can be explained in terms of the experimental uncertainties in the equivalence ratio, diluent concentration and thermocouple measurement (See Appendix B). It is noted that for all diluent concentrations  $\bar{T}_{av} < \bar{T}_{ad}$ , and that as  $\bar{T}_{av}$  approaches  $\bar{T}_{ad}$  the stability limits shift toward stoichiometric.

In Figure 20 similar temperature data are presented for  $CH_4$ -dilute oxygen and  $CH_4$ -air. The  $\bar{T}_{av}$  given for  $CH_4$ -air is the temperature at stoichiometric. For  $CH_4-(0.4O_2+0.6N_2)$  and a given chamber length the measured combustion temperatures at the stability limits are approximately the same. For  $L = 76$  cm  $\bar{T}_{av} = 2050 \pm 35^\circ K$ , and for  $L = 53$  cm  $\bar{T}_{av} = 2060 \pm 20^\circ K$ . For  $CH_4-(0.4O_2+0.6N_2)$   $\bar{T}_{av} < \bar{T}_{ad}$ . For  $CH_4$ -air the measured combustion temperature at stoichiometric is somewhat less than the adiabatic combustion temperature, but approximately the same

as  $\bar{T}_{av}$  for  $CH_4-(0.4O_2+0.6N_2)$ .

To facilitate the comparison of the experimental and theoretical results a brief summary of some important conclusions obtained from the Sirignano-Crocco analysis is made. For a given propellant combination the longitudinal stability limits are defined by  $\bar{T} = \bar{T}_{crit}$ , where  $\bar{T}_{crit}$  is the solution of equation (3-4). Whenever  $\bar{T}_{crit} < \bar{T}_{max}$  two regions of unstable combustion will exist, one on either side of stoichiometric. Each of these regions is bounded by a stability limit and a combustion limit. Whenever  $\bar{T}_{crit} \geq \bar{T}_{max}$  unstable combustion occurs over the entire range of combustible equivalence ratios. Thus the theory provides a criterion for the number and location of unstable regions.

The nearly constant value for  $\bar{T}_{av}$  (for a given propellant combination) in Figures 18 and 20 strongly supports the concept of a critical combustion temperature at the stability limits. The slight dependence of  $\bar{T}_{av}$  on  $L$  is discussed in Section H. The theoretical criterion for the number and location of unstable regions is also supported by experiment. From Figures 18 and 20 it is noted that whenever  $\bar{T}_{av} < \bar{T}_{ad}$  two unstable regions exist, one on either side of stoichiometric- viz.  $H_2$ -air,  $H_2$ -dilute air and  $CH_4-(0.4O_2+0.6N_2)$ . For  $CH_4$ -air the measured combustion temperature at stoichiometric is approximately the same as  $\bar{T}_{av}$  for  $CH_4-(0.4O_2+0.6N_2)$ , and one unstable

region (located around stoichiometric) is observed.

The upper stability limits of the oxygen-rich unstable regions for  $H_2$ -air and  $H_2$ -dilute air are not predicted by the Sirignano-Crocco analysis. The probable explanation of these "additional" stability limits is given in Section D.

Combining the stability limit data of Figures 17 and 19 with the  $\gamma$ 's for the two propellant combinations it is possible to calculate  $(E/RT)_{\text{limit}}$  from equation (3-4). Using these values for  $(E/RT)_{\text{limit}}$  and the values for  $\bar{T}_{\text{av}}$  from Figures 18 and 20 it is possible to evaluate  $E_{\text{limit}}$ . These results together with overall activation energies for the two propellant combinations taken from the chemical kinetics literature are tabulated in Figure 21. The results are based on a chamber length of 53 cm. It is noted that the values for  $E_{\text{limit}}$  for  $H_2$ -air and  $H_2$ -dilute air are approximately the same. This result supports the earlier contention that nitrogen has little effect on the activation energy. The values for  $E_{\text{limit}}$  obtained from (3-4) are approximately half the corresponding activation energies obtained from the literature.

$$\frac{E_{\text{limit}}(H_2)}{E_{\text{act}}(H_2)} = 0.38$$

$$\frac{E_{\text{limit}}(CH_4)}{E_{\text{act}}(CH_4)} = 0.52$$

However, the ratio of the  $E_{\text{limit}}$  for the two reactions compares favorably with the ratio of the activation energies.

$$\frac{E_{\text{limit}}(\text{H}_2)}{E_{\text{limit}}(\text{CH}_4)} = 0.37$$

$$\frac{E_{\text{act}}(\text{H}_2)}{E_{\text{act}}(\text{CH}_4)} = 0.51$$

If the  $E_{\text{act}}$  were used with the tabulated values of  $(E/RT)_{\text{limit}}$  to calculate  $\bar{T}_{\text{crit}}$  it is found that  $\bar{T}_{\text{crit}} > \bar{T}_{\text{max}}$  for both propellant combinations. In this calculation it is necessary to correct the tabulated  $(E/RT)_{\text{limit}}$  for the temperature dependence of  $\gamma$ . From the theory whenever  $\bar{T}_{\text{crit}} > \bar{T}_{\text{max}}$  unstable combustion will exist over the entire range of combustible mixture ratios.

There are several possible explanations for the discrepancy between the magnitudes of  $E_{\text{limit}}$  and  $E_{\text{act}}$ . First it is noted that the presence of stabilizing effects in the gas rocket (heat transfer, friction, finite combustion zone) are not included in the Sirignano-Crocco analysis. When stabilizing effects are present the perturbation in the energy release rate required to support an oscillation of given strength will be greater than when no stabilizing effects are present.

Expressing the perturbation in the energy release rate in terms of the pressure perturbation (assuming an isentropic wave)

$$\frac{r'}{\bar{r}} = \frac{E}{R\bar{T}} \left( \frac{\gamma-1}{\gamma} \right) \left( \frac{P'}{\bar{P}} \right) \quad (4-2)$$

From equation (4-2) it is seen that for a given pressure perturbation to achieve an increase in the rate perturbation (for a given propellant combination) a decrease in  $\bar{T}$  is required. Thus the net effect of stabilizing influences is a shift in the stability limits toward lower combustion temperatures. In later sections it will be seen that stabilizing effects are not sufficient to account for the discrepancy between  $E_{\text{limit}}$  and  $E_{\text{act}}$ .

An examination of the combustion zone analysis employed in the Sirignano-Crocco theory provides a possible explanation for the discrepancy between  $E_{\text{limit}}$  and  $E_{\text{act}}$ . In the Sirignano-Crocco analysis it is assumed that the combustion process in the gas rocket is effectively a premixed turbulent flame in which the local energy release rate is given by equation (3-1). The total energy release rate ( $r_{\text{total}}$ ) is obtained by integrating the local energy release rate over the volume of the combustion zone. For one-dimensional flow

$$r_{\text{total}} = \int_0^{\delta} r(x) A dx$$

where  $r(x)$  = local energy release rate,  $\delta$  = combustion zone thickness and

A = cross-sectional area of the combustion chamber. In the Sirignano-Crocco theory it is assumed that  $\delta$  is independent of time and that  $r(x)$  can be replaced by a space-mean energy release rate,  $r_{av}$ , which is a function of time. Hence

$$r_{total} \sim r_{AV} \cdot$$

Expressing the space-mean energy release rate in terms of equation (3-1),

$$r_{total} \sim \exp \left\{ -\frac{E}{RT_{AV}} \right\} \quad (4-3)$$

In reality the combustion zone thickness is a function of time so that

$$r_{total} \sim \delta(t) \exp \left\{ -\frac{E}{RT_{AV}} \right\} \quad (4-4)$$

For a premixed turbulent flame the combustion zone thickness may be written

(45)

$$\delta \approx \sqrt{\frac{\rho \beta}{\hat{r}_T}}$$

where  $\rho$  = density of the unburned propellant,  $\beta$  = eddy diffusivity and  $\hat{r}_T$  = space-mean turbulent reaction rate. The eddy diffusivity may be

written

$$\beta \sim uD$$

where  $u$  = gas velocity and  $D$  = diameter of the combustion chamber. The density may be written

$$\rho \sim \frac{\dot{m}}{u}$$

where  $\dot{m}$  is the mass injection rate (a constant). Hence

$$\delta \sim \sqrt{\frac{l}{\rho_T}}$$

If it is assumed that the turbulent reaction rate can be expressed as

$$\hat{r}_T = b \rho^n \exp \left\{ -\frac{E}{RT_{AV}} \right\}$$

then equation (4-4) may be written

$$r_{total} \sim \rho^{-\frac{n}{2}} \exp \left\{ -\frac{E}{2RT_{AV}} \right\}.$$

Following the earlier approximation of Sirignano and Crocco  $n$  is set equal to zero

$$r_{total} \sim \exp \left\{ -\frac{E}{2RT_{AV}} \right\}. \quad (4-5)$$

For the energy release law (4-5) the defining equation for the stability limits is

$$\left(\frac{E}{RT}\right)_{\text{limit}} = \frac{3\gamma-1}{\gamma-1} \quad (4-6)$$

An alternate model for the gas rocket combustion process has been suggested by Sirignano. In this model it is assumed that each injection orifice produces a conical-type premixed turbulent flame and that the combustion zone consists of a "sheet" of these individual flames. For this model the total energy release rate is given by

$$r_{\text{total}} = \rho q s_T A_f$$

where  $\rho$  = density of the unburned propellant,  $q$  = heat of reaction/unit mass,  $s_t$  = turbulent flame speed and  $A_f$  = area of the flame front. The turbulent flame speed is a function of time. It follows that the flame area is a function of time. If, as a first approximation, it is assumed that the density and velocity of the approach flow are constant and that variations in flame area (due to variations in flame speed) are negligible then

$$r_{\text{total}} \sim s_T$$

For a premixed turbulent flame the flame speed may be written (45)

$$s_T \sim \sqrt{\beta \bar{r}_T} .$$

Proceeding as on page 51 it is found that

$$r_{\text{total}} \sim \exp \left\{ \frac{E}{2RT_{AV}} \right\} \quad (4-5)$$

and that

$$\left( \frac{E}{RT} \right)_{\text{limit}} = \frac{3\gamma-1}{\gamma-1} . \quad (4-6)$$

Thus both combustion models lead to similar results. Based on present knowledge it is not possible to determine the appropriate model for the gas rocket combustion process. A logical extension of the present study would include experiments designed to define more precisely the nature of the combustion process in the gas rocket.

The  $E_{\text{limit}}$  obtained from equation (4-6) are tabulated in Figure 21 for the various propellant combinations. It is seen that equation (4-6) provides  $E_{\text{limit}}$  which are in relatively good agreement with  $E_{\text{act}}$ .

## 2. Dependence of Stability Limits on $E$ ( $\bar{T} = \text{constant}$ )

Kaskan and Browne (37), Friedman and Nugent (38) and Lewis and von Elbe (39) have reported a substantial increase in the rate of the  $\text{CO-O}_2$

reaction by the addition of trace amounts of  $H_2$ . This reaction was employed in an experiment designed to provide information on the dependence of the stability limits on the reaction kinetics (in particular, on the overall activation energy). In the experiment the regions of unstable combustion for CO-air were located in the  $\Phi$ -L plane with and without the presence of the  $H_2$  catalyst. The shift in the stability limits produced by the addition of the  $H_2$  was correlated with the Sirignano-Crocco theory and available rate data. Air was used as the oxidizer primarily because it was found that for CO- $O_2$  stable combustion existed over the entire range of combustible mixture ratios- ie. the stability limits fell outside the combustion limits. Thus it would not have been possible to obtain the required data using CO- $O_2$ . For CO-air (with correspondingly lower combustion temperatures) the stability limits shifted toward stoichiometric and fell inside the combustion limits. An additional reason for using CO-air was the severe flashback problem encountered with CO- $O_2$ .

It was found that it was difficult to contain the reaction inside the combustion chamber when using dry CO-air (due to the relatively low flame speed). To decrease the probability of blow-off the flame speed was increased by the addition of trace amounts of water vapor to the CO (41).

It was also found that it was not possible to ignite CO( $H_2O$ )-air mixtures using the spark ignition system. To circumvent this problem a run procedure was employed in which combustion was initiated using  $H_2$  and air. Once combustion had been established the CO and air flow rates were set to their steady-state values (determined by mixture ratio and combustion pressure

requirements). The  $H_2$  flow used to initiate combustion was set so that when steady-state operation was obtained the  $H_2$  flow rate was that required to accelerate the reaction ( $\sim 2.5\%$  molar of the total flow rate). Thus the stability of the combustion with and without the  $H_2$  was determined simply by turning the  $H_2$  flow on and off. By repeating this procedure for various mixture ratios and a fixed combustion chamber length it was possible to determine the shift in stability limits produced by the addition of  $H_2$ .

The results of this experiment for a chamber length of 104 cm and a mean combustion pressure of 7.8 atm are shown in Figure 22a. The stability limit for  $CO(H_2O)$ -air is  $\Phi_{\text{limit}} = 2.35 \pm 0.05$ . This corresponds to an adiabatic combustion temperature at the stability limit of  $\bar{T}_{\text{crit}} = 1173 \pm 20^\circ K$ . The stability limit for  $CO(H_2O)$ -air- $H_2$  is  $\Phi_{\text{limit}} = 2.90 \pm 0.05$ . This corresponds to a  $\bar{T}_{\text{crit}} = 1012 \pm 13^\circ K$ .

As a first step in the interpretation of the experimental results the effect of  $H_2$ -addition on the combustion temperature of the  $CO(H_2O)$ -air reaction was determined. As noted earlier the  $H_2$  flow rate was  $2.5 \pm 1.0\%$  (molar) of the total flow rate. Theoretical calculations indicate that this amount of  $H_2$  will increase the adiabatic combustion temperature by less than  $12^\circ K$  over the range of equivalence ratios 0.5 to 4.0. This conclusion is supported by combustion pressure records during stable combustion- no change in  $\bar{P}$  was observed with the addition of the  $H_2$ . Both the increased mass flow and the increased combustion temperature which occur with the addition of  $H_2$  serve to increase the combustion pressure. If either or both the mass addition or temperature effects were significant a change in  $P$  would be observed.

Combining the stability limit data of Figure 22a with the  $\gamma$ 's of the combustion products it is possible to evaluate  $E_{\text{limit}}$  for  $\text{CO}(\text{H}_2\text{O})$ -air and  $\text{CO}(\text{H}_2\text{O})$ -air- $\text{H}_2$ . The  $E_{\text{limit}}$  obtained from combustion laws (3-1) and (4-5) and the overall activation energies for the  $\text{CO}(\text{H}_2\text{O})$ - $\text{O}_2$  reaction taken from the literature are tabulated in Figure 22a. As was true for both  $\text{H}_2$ -air and  $\text{CH}_4$ - $\text{O}_2$  the value for  $E_{\text{limit}}$  for  $\text{CO}(\text{H}_2\text{O})$ -air using combustion law (3-1) is approximately half the activation energy obtained from the literature.

$$\frac{E_{\text{limit}}(\text{CO})}{E_{\text{act}}(\text{CO})} = 0.56 .$$

The  $E_{\text{limit}}$  obtained using combustion law (4-5) is in good agreement with the literature values for  $E_{\text{act}}$ . From Figure 22a it is seen that  $E_{\text{limit}}$  for the  $\text{CO}(\text{H}_2\text{O})$ -air reaction is substantially reduced by the addition of trace amounts of  $\text{H}_2$ .

$$\frac{E_{\text{limit}}(\text{with } \text{H}_2)}{E_{\text{limit}}(\text{without } \text{H}_2)} = 0.85 \pm 0.02$$

The results of the Sirignano-Crocco analysis will now be expressed in a form which permits comparison with kinetics data. The mean energy release rate ( $\bar{r}$ ) can be expressed in two ways depending on the

combustion law used to describe the gas rocket combustion process-  
equation (3-1) or (4-5). In terms of equation (3-1)

$$\bar{r} = \text{constant} \exp \left\{ -\frac{E}{RT} \right\}$$

and in terms of equation (4-5)

$$\bar{r} = \text{constant} \exp \left\{ -\frac{E}{2RT} \right\} .$$

The mean energy release rate is related to the mean reaction rate ( $\bar{r}$ ) by

$$\dot{r} = \bar{r}q \quad (4-7)$$

Equation (4-7) can be used to compare the rates of the CO(H<sub>2</sub>O)-air  
reaction (subscript 1) and the CO(H<sub>2</sub>O)-air-H<sub>2</sub> reaction (subscript 2),

$$\frac{\dot{r}_1}{\dot{r}_2} = \frac{\bar{r}_1}{\bar{r}_2} \cdot \frac{q_2}{q_1} .$$

Substituting for  $\bar{r}$  from equation (3-1)

$$\frac{\dot{r}_1}{\dot{r}_2} = \frac{q_2}{q_1} \exp \left\{ \frac{E_2}{RT_2} - \frac{E_1}{RT_1} \right\} \quad (4-8a)$$

and substituting for  $\bar{r}$  from equation (4-5)

$$\frac{\bar{r}_1}{\bar{r}_2} = \frac{q_2}{q_1} \exp \left\{ \frac{E_2}{2R\bar{T}_2} - \frac{E_1}{2R\bar{T}_1} \right\}. \quad (4-8b)$$

To determine the effect of  $H_2$  addition on the rate of the  $CO(H_2O)$ -air reaction equations (4-8) are specialized to the case of  $\Phi = \text{constant}$ . In view of the earlier discussion of the effect of  $H_2$  addition on the combustion temperature of the  $CO(H_2O)$ -air reaction it is reasonable to assume (for constant  $\Phi$ ) that  $q_1 \approx q_2$  and  $\bar{T}_1 \approx \bar{T}_2$ . Hence equations (4-8) reduce to

$$\frac{\bar{r}_1}{\bar{r}_2} = \exp \left\{ \frac{E_2 - E_1}{RT} \right\}. \quad (4-9a)$$

$$\frac{\bar{r}_1}{\bar{r}_2} = \exp \left\{ \frac{E_2 - E_1}{2R\bar{T}} \right\}. \quad (4-9b)$$

In equations (4-9) the values for  $E_1$  and  $E_2$  are taken to be the  $E_{\text{limit}}$  for  $CO(H_2O)$ -air and  $CO(H_2O)$ -air- $H_2$  respectively. Since the values for  $E$  in equation (4-9a) are half those for  $E$  in equation (4-9b) it is seen

that equations (4-9a) and (4-9b) are the same. Substituting for  $E_1$ ,  $E_2$  and  $R$  in equations (4-9)

$$\frac{\bar{r}_1}{\bar{r}_2} = \exp \left\{ -\frac{870 \pm 160}{\bar{T}} \right\} \quad (4-10)$$

By inserting a value for  $\bar{T}$  in equation (4-10)  $\bar{r}_1/\bar{r}_2$  is determined. The  $\bar{r}_1/\bar{r}_2$  from equation (4-10) for  $\bar{T} = 1732^\circ\text{K}$  is tabulated in Figure 22b. It is emphasized that the  $\bar{r}_1/\bar{r}_2$  obtained from (4-10) is the ratio of the mean reaction rates derived from the Sirignano-Crocco analysis and the experimentally observed shift in the stability limits.

It is of interest to compare the  $\bar{r}_1/\bar{r}_2$  obtained from equation (4-10) with available kinetics data for the CO-air reaction. Two sources of kinetics data are the laminar flame speed data of Jahn (39) and the laminar flame structure studies of Friedman and Nugent (38). The flow in the gas rocket is highly turbulent hence the combustion process in the gas rocket is essentially a premixed turbulent flame. To compare the results of equation (4-10) with the kinetics data (38, 39) it is necessary to infer turbulent reaction rates from laminar flame data.

There are two basically different models for premixed turbulent

flames. The first of these, termed the wrinkled flame model, assumes that a turbulent flame is simply a laminar flame front which has been "wrinkled" due to local variations in the flow velocity (42, 43). The wrinkled flame model is generally applied to flows with low intensity, large scale turbulence. The second model, termed the distributed reaction zone model, describes a turbulent flame as a "zone of reaction distributed in depth," making no direct reference to laminar flames (44). The distributed reaction zone theory is generally applied to flows with high intensity, small scale turbulence.

Considering the intensity and scale of the turbulence in the gas rocket it is felt that the distributed reaction zone model best describes the gas rocket combustion process. The distributed reaction zone model assumes that the propagation of a premixed turbulent flame is analogous to the propagation of a premixed laminar flame (44, 45). Hence

$$\bar{S}_T \sim \sqrt{\beta \bar{r}_T} \quad (4-11)$$

The differential equation describing the turbulent flame is similar to the equation describing a laminar flame, with the laminar transport properties being replaced by turbulent transport properties. The solution of this differential equation provides a relationship between the turbulent

flame speed ( $\bar{S}_t$ ) and the laminar flame speed ( $\bar{S}_l$ ).

$$\frac{\bar{S}_t \delta_T}{\beta} = \frac{\bar{S}_l \delta_L}{a} \quad (4-12)$$

where  $a$  = thermal diffusivity,  $\delta_t$  = thickness of the turbulent flame, and  $\delta_l$  = thickness of the laminar flame. Combining equations (4-11) and (4-12) an expression for the turbulent reaction rate is obtained.

$$\bar{r}_T \sim \left(\frac{\beta}{a^2}\right) \left(\frac{\delta_L}{\delta_T}\right)^2 \bar{S}_L^2 \quad (4-13)$$

From the theory of the propagation of premixed laminar flames (45)

$$\bar{S}_L \sim \sqrt{a \bar{r}_L} \quad (4-14)$$

where  $\bar{r}_l$  = mean laminar reaction rate. Combining equations (4-13) and (4-14),

$$\bar{r}_T \sim \left(\frac{\beta}{a}\right) \left(\frac{\delta_L}{\delta_T}\right)^2 \bar{r}_L \quad (4-15)$$

Equation (4-13) or (4-15) can be used with the kinetics data (38, 39) to obtain a ratio of reaction rates for the CO-air (subscript 1) and CO-air-H<sub>2</sub> (subscript 2) reactions.

$$\frac{\bar{r}_{T1}}{\bar{r}_{T2}} = \left\{ \begin{array}{l} \left( \frac{\beta_1}{\beta_2} \right) \left( \frac{a_2}{a_1} \right)^2 \left[ \frac{\left( \frac{\delta T}{\delta L} \right)_1}{\left( \frac{\delta T}{\delta L} \right)_2} \right]^2 \left( \frac{\bar{S}_{L1}}{\bar{S}_{L2}} \right)^2 \quad (a) \\ \left( \frac{\beta_1}{\beta_2} \right) \left( \frac{a_2}{a_1} \right)^2 \left[ \frac{\left( \frac{\delta T}{\delta L} \right)_1}{\left( \frac{\delta T}{\delta L} \right)_2} \right]^2 \left( \frac{\bar{r}_{L1}}{\bar{r}_{L2}} \right) \quad (b) \end{array} \right. \quad (4-16)$$

The addition of trace amounts of H<sub>2</sub> to the CO-air reaction produces only slight variations in the combustion temperature and in the density and composition of the reactants and products. Thus the H<sub>2</sub> addition should have only a slight effect on the eddy and thermal diffusivities- ie.

$$\beta_1 \approx \beta_2$$

$$a_1 \approx a_2$$

Since the addition of trace amounts of  $H_2$  accelerates the CO-air reaction it is to be expected that the thickness of both the laminar flame and the turbulent flame will decrease. It is felt, however, that the ratio

$\delta_l / \delta_t$  will be only slightly affected by the addition of  $H_2$ . Hence, as a first approximation equation (4-16) can be written

$$\frac{\bar{r}_{T1}}{\bar{r}_{T2}} \approx \left\{ \begin{array}{l} \left( \frac{\bar{S}_{L1}}{\bar{S}_{L2}} \right)^2 \quad (a) \\ \left( \frac{\bar{r}_{L1}}{\bar{r}_{L2}} \right) \quad (b) \end{array} \right. \quad (4-17)$$

Jahn (39) has measured the effect of  $H_2$  addition on the laminar flame speed in premixed CO( $H_2O$ )-air at atmospheric pressure. Jahn's data are used with equation (4-17a) to estimate  $\bar{r}_{t1}/\bar{r}_{t2}$  for the CO( $H_2O$ )-air reaction at a temperature of 1732°K ( $\Phi = 1.49$ ). The result is tabulated in Figure 22b.

Friedman and Nugent (38) have studied the effect of the addition of trace amounts of  $H_2$  and water vapor on the CO- $O_2$  reaction. Overall specific rate constants were inferred from temperature and concentration traverses through premixed laminar flames. They also measured the effect of  $H_2$  and  $H_2O$  addition on the laminar flame speed. The studies were

performed for a pressure of 30 mm Hg. Friedman and Nugent found that the CO-O<sub>2</sub> reaction was first order with respect to the concentration of CO.

$$\bar{r}_L = \frac{d[CO]}{dt} = -k[CO] \quad (4-18)$$

The factor  $k$  in equation (4-18) is the overall specific rate constant measured by Friedman and Nugent. Using equation (4-18) and the rate constant data (referred to a temperature of 1732°K)  $\bar{r}_{11}/\bar{r}_{12}$  is calculated. This value of  $\bar{r}_{11}/\bar{r}_{12}$  is substituted into equation (4-17b) to obtain  $\bar{r}_{t1}/\bar{r}_{t2}$ . Since the value of the specific rate constant was different as determined from temperature traverse data and composition traverse data two values of  $\bar{r}_{t1}/\bar{r}_{t2}$  are tabulated in Figure 22b. Using equation (4-17a) and the flame speed data (referred to a temperature of 1732°K)  $\bar{r}_{t1}/\bar{r}_{t2}$  was calculated. This  $\bar{r}_{t1}/\bar{r}_{t2}$  is tabulated in Figure 22b.

The data of Figure 22b allow a comparison to be made between the rate ratio obtained from the Sirignano-Crocco theory and instability data and the ratio obtained from kinetics data and a model for the gas rocket combustion process. In making this comparison it is important to understand some of the limitations of the results of Figure 22b. The equations used to relate the turbulent reaction rate to the laminar reaction rate

and the laminar flame speed are order of magnitude approximations. In addition the studies of Friedman and Nugent (38) have shown that the laminar flame speed and rate constant depend on the concentration of water vapor. Since the water vapor content in the instability experiments and in the various kinetics experiments (38, 39) were not the same differences in the reaction rates are to be expected. Furthermore, the data of References 38 and 39 were obtained at pressures which were significantly smaller than the combustion pressure in the gas rocket. There are no data available on the effect of pressure on the relatively complex  $\text{CO-O}_2$  reaction. Water vapor and pressure effects should not have a strong effect on the results of Figure 22b due to the fact that ratios of reaction rates are used (and such effects would tend to cancel). Considering these and other limitations it is possible that the relatively good agreement between the results of the Sirignano-Crocco theory and kinetics data is fortuitous. However, several important conclusions can be drawn from the data of Figure 22b. The Sirignano-Crocco theory (using instability data) and chemical kinetics studies both show an increase in the rate of the  $\text{CO-O}_2$  reaction with the addition of trace amounts of  $\text{H}_2$ . The magnitude of the rate increase obtained from the kinetics studies is of the same order as that given by the Sirignano-Crocco theory using instability data.

In summary it is emphasized that the experiments described in

this section afford a critical test of a chemical kinetic instability driving mechanism. The two important kinetic parameters, temperature and activation energy, have been varied independently in instability experiments, and the observed changes in the stability limits have been shown to correlate well with an instability theory based on a chemical kinetics driving mechanism.

#### D. Dependence of Instability Strength on $\bar{T}$

For a given  $\bar{M}$  the Sirignano-Crocco analysis gives the strength of the instability ( $\Delta P/\bar{P}$ ) as a function of  $E/R\bar{T}$  and  $\gamma$ . For a given propellant combination  $E$  is approximately constant and  $\gamma$  is a function only of  $\bar{T}$ .<sup>\*</sup> Hence for given propellants  $\Delta P/\bar{P}$  is a function only of  $\bar{T}$ .

To determine the temperature dependence of  $\Delta P/\bar{P}$  an experiment was carried out in which  $\Delta P/\bar{P}$  was measured as a function of  $\Phi$  for a given propellant combination (holding  $L$ ,  $\bar{P}$  and  $\bar{M}$  constant). For a given combustion pressure  $\bar{T}$  is a function of  $\Phi$  only, hence the experiment provides  $\Delta P/\bar{P}$  as a function of  $\bar{T}$ .

The results of a typical experiment using  $H_2$ -air are presented in Figure 23 (in which  $\Delta P/\bar{P}$  is plotted as a function of the mean adiabatic combustion temperature). The data were obtained for  $L = 38$  cm,  $\bar{P} = 7.8 \pm 0.3$  atm,  $\bar{M} = 0.015 \pm 0.002$ , the 31-hole showerhead injector and

---

\* Over the range of pressures of interest  $\gamma$  is independent of pressure.

the oxidizer-rich unstable region. The fuel-rich unstable region was too narrow to permit satisfactory measurement of shock strength. The mean Mach number of the combustion gases was calculated using known mass flow rates and average values for the combustion temperatures. The heavy vertical bar gives the variation in shock strength during a given run (due to non-periodic fluctuations).

From Figure 23 it is seen that as  $\bar{T}$  decreases  $\Delta P/\bar{P}$  increases to a maximum and then decreases. For sufficiently low  $\bar{T}$  the shock strength decreases to zero producing the upper stability limits observed for the oxidizer-rich unstable regions for  $H_2$ -air and  $H_2$ -dilute air mixtures (Figure 17). The fact that the upper stability limit is not clearly defined is due to the relatively slow decrease in shock strength with  $\bar{T}$ . For relatively weak shock waves it is difficult to distinguish the combustion oscillations from the random fluctuations of turbulence. Hence when the shock strength decreases slowly precise location of the stability limits is not possible.

The results of an experiment performed by Pelmas (27) using  $CH_4-(0.4O_2+0.6N_2)$  are presented in Figure 24. These data were obtained for  $L = 79$  cm,  $\bar{P} = 7.8$  atm, a porous plug injector and the fuel-rich unstable region. Since  $\bar{M}$  was not specified in Reference 27 its value was calculated using estimated flow rates, the known  $\bar{P}$  and the adiabatic

combustion temperature. From this calculation  $\bar{M}$  was estimated to be 0.015. The results of Figure 24 agree qualitatively with the results of Figure 23 in that as  $\bar{T}$  decreases  $\Delta P/\bar{P}$  increases to a maximum and then decreases.

In contrast to the experimental results the Sirignano-Crocco analysis predicts that  $\Delta P/\bar{P}$  increases monotonically with decreasing  $\bar{T}$  (See Figure 14). The difference between experimental and analytical results can be explained as follows. As the strength of the instability increases the losses in the wave increase, and hence the energy supplied to the oscillation by the combustion process must increase. At lower combustion temperatures the mass fraction of combustibles in the reactant mixture decreases, and hence the energy which can be supplied by the combustion process (for constant mass injection rate) decreases. It is argued that below some  $\bar{T}$  the energy supplied by the combustion process is not sufficient to support an oscillation of the strength required by the theory. Further since the energy supplied by combustion decreases with the combustion temperature it follows that the strength of the instability must decrease as  $\bar{T}$  decreases below the above value.

The theoretical variation of  $\Delta P/\bar{P}$  with  $\bar{T}$  (based on combustion law 3-1) is plotted in Figure 23 for  $H_2$ -air with  $\bar{M} = 0.015$  and

$E = 15.1$  kcal/mole (the value for  $E_{\text{limit}}$  obtained from experiment) and 37.8 kcal/mole (the activation energy). A similar curve is plotted in Figure 24 for  $\text{CH}_4-(0.4\text{O}_2+0.6\text{N}_2)$  with  $\bar{M} = 0.015$  and  $E = E_{\text{limit}} = 23.6$  kcal/mole. The theoretical curves based on combustion law (4-5) correspond to the  $E = 15.1$  kcal/mole curve (Figure 23) and the  $E = 23.6$  kcal/mole curve (Figure 24). The slopes of the theoretical curves are significantly smaller than the initial slopes of the experimental curves. From Figure 23 it is seen that this result cannot be attributed to uncertainties in the value for  $E$ . Furthermore, the slight uncertainties in  $\bar{M}$  are not sufficient to account for the discrepancies between experimental and theoretical results. It is probable that the discrepancies are the result of the simplifications inherent in the combustion zone analysis and energy release law (See Chapter 3).

#### E. Dependence of Instability Strength on $\bar{M}$

For a given propellant combination and combustion temperature the Sirignano-Crocco analysis gives the instability strength as a function of the mean Mach number of the combustion gases. To determine the dependence of the instability strength on  $\bar{M}$  an experiment was carried out in which  $\Delta P/\bar{P}$  was measured as a function of  $\Phi$  (ie.  $\bar{T}$ ) for two values of  $\bar{M}$  (for given  $L$ ,  $\bar{P}$  and propellant combination). The variation in  $\bar{M}$  was obtained by using exhaust nozzles with different flow areas. The dependence of  $\Delta P/\bar{P}$  on  $\bar{M}$  was obtained by comparing

the instability strengths for the two  $\bar{M}$  at a given combustion temperature.

The results of a typical experiment using  $H_2$ -air are presented in Figure 25. In this figure  $\Delta P/\bar{P}$  is plotted against the adiabatic combustion temperature for  $\bar{M} = 0.015$  and  $0.030$  ( $\pm 0.002$ ). The data were obtained for  $L = 38$  cm,  $\bar{P} = 4.4 \pm 0.3$  atm, the 31-hole showerhead injector and the oxidizer-rich unstable region. The curve for  $\bar{M} = 0.015$  was obtained using the converging-diverging nozzle with  $C_R = 46$ . The curve for  $\bar{M} = 0.030$  was obtained using the converging-diverging nozzle with  $C_R = 23$ . The  $\bar{M}$  were calculated using the known mass flow rates and average values for the combustion temperatures. The heavy vertical bars indicate a non-periodic variation in the shock strength during a given run. The variation in shock strength is larger for the larger value of  $\bar{M}$ . This result is to be expected since the intensity of the turbulent fluctuations increases as the mean flow velocity (ie.  $\bar{M}$ ) increases. Qualitatively the  $\Delta P/\bar{P}$  curves are the same as in Figures 23 and 24- ie. with decreasing  $\bar{T}$  the instability strength increases to a maximum and then decreases. The shift in the stability limit for the  $C_R = 23$  nozzle is discussed in Section J.

In Figure 26 the experimental and theoretical shock strength ratio

$$P = \frac{\frac{\Delta P}{\bar{P}}}{\frac{\Delta P}{P}} \left| \begin{array}{l} \bar{M}=0.030 \\ M=0.015 \end{array} \right.$$

is plotted as a function of the adiabatic combustion temperature. The experimental shock strength ratio is obtained from the data of Figure 25. The theoretical shock strength ratio is obtained from the Sirignano-Crocco analysis using  $E = E_{\text{limit}}$  and the  $\gamma$ 's for the equilibrium composition of combustion products. Since the stability limits are different for the two  $\bar{M}$  the  $E_{\text{limit}}$  are different for the two  $\bar{M}$  :

$E_{\text{limit}} \Big|_{\bar{M}=0.015} = 14.2 \text{ kcal/mole}$  and  $E_{\text{limit}} \Big|_{\bar{M}=0.030} = 13.6 \text{ kcal/mole}$ .

The results of Figure 26 are also applicable for the combustion law (4-5). Considering the uncertainties in the instability strength it is seen that there is good agreement between theory and experiment even for the range of  $\bar{T}$  where the shock strength decreases with the combustion temperature. This result is to be expected since  $\bar{M}$  enters into the analysis independent of the combustion zone analysis or the form of the energy release law.

#### F. Harmonic Mode and Transverse Mode Instabilities

In the course of the experimentation it was found that longitudinal combustion oscillations could occur in a form other than a

single shock wave propagating in the combustion chamber. Two other forms of longitudinal oscillations have been observed- one in which two shock waves simultaneously propagate in the chamber and another in which three shock waves simultaneously propagate in the chamber. Pressure-time histories and x-t diagrams for the three forms of longitudinal oscillations are presented in Figures 27, 28 and 29. The pressure-time histories were obtained at a station approximately 16 cm downstream from the injector using  $H_2$ -air with  $L = 122$  cm and  $\bar{P} = 7.8$  atm. Figure 27 is the pressure-time history and x-t diagram for a single shock wave oscillating with a frequency of 260 cps ( $\Phi = 3.25$ ). Figure 28 is the pressure-time history and x-t diagram for two shock waves ( $\Phi = 2.75$ ). Note that the two waves travel in opposite directions, one wave reflecting from the nozzle, the other from the injector. The apparent oscillation frequency is 520 cps. Figure 29 is the pressure-time history and x-t diagram for three shock waves ( $\Phi = 2.50$ ). Note that the pressure-time history shows a combination of the two shock wave and three shock wave instability forms. The apparent oscillation frequency for three shock waves is 750 cps. From Figures 27 through 29 it is seen that the apparent oscillation frequencies for the various forms of longitudinal instabilities are approximately integral multiples of the oscillation frequency of the single shock wave.

$$f_n \approx n f_1$$

where  $f_n$  = apparent oscillation frequency of the  $n^{\text{th}}$  mode,  $f_1$  = oscillation frequency of a single shock wave and  $n$  = an integer = 1, 2 or 3. The various forms of longitudinal oscillations will be classified according to frequency and termed the fundamental mode ( $n = 1$ ), second harmonic ( $n = 2$ ) and third harmonic ( $n = 3$ ) by analogy with acoustic oscillations. Harmonic mode longitudinal oscillations of the type shown in Figures 27 through 29 have been observed in gas rockets by several investigators. Pelmas (27) reported the existence of harmonics in the vicinity of the stability limits for  $\text{H}_2$ -air and  $\text{CH}_4$ -(0.40 $\text{O}_2$ +0.6 $\text{N}_2$ ). Tsuji and Takeno (34) reported the existence of harmonics for natural gas- air.

In Figure 30 the regions of the various harmonic mode instabilities are located in the  $\Phi$  -L plane for  $\text{H}_2$ -air,  $\bar{P} = 7.8$  atm, the 31-hole showerhead injector and the  $C_R = 46$  converging-diverging nozzle. In the region designated "fundamental" only the fundamental mode oscillation ( $n = 1$ ) occurs. In the region designated "second harmonic" only the second harmonic mode ( $n = 2$ ) oscillation occurs. There is some overlap of these two regions (solid cross-hatching), and in this overlap region both the fundamental and second harmonic modes are observed.

For a given equivalence ratio there is a maximum chamber length for the appearance of the fundamental mode- ie. above a certain chamber length the combustion is stable with respect to the fundamental mode. The appearance of the third harmonic mode in the vicinity of the stability limit for  $L > 100$  cm indicates that there is probably an upper length limit for the appearance of the second harmonic as well. Furthermore for a given equivalence ratio the order of the harmonic modes (ie.  $n$ ) increases as the chamber length increases- ie. longer chambers favor the higher harmonics. For a given chamber length the order of the harmonics increases as the equivalence ratio approaches stoichiometric- ie. the higher harmonics lie closer to stoichiometric. The observations concerning the ordering of the harmonics are in agreement with the results of Pelmas (27) and Tsuji and Takeno (34).

In Figure 33 the regions of the various harmonic mode instabilities are located in the  $\Phi - \bar{P}$  plane for  $H_2$ -air,  $L = 104$  cm, the 31-hole showerhead injector and the  $C_R = 46$  converging-diverging nozzle. As in Figure 30 there is a region of fundamental mode oscillations and a region of second harmonic mode oscillations (with some overlap of the two regions). For a given equivalence ratio there is a maximum  $\bar{P}$  for the appearance of the fundamental mode- ie. above a certain mean combustion pressure the combustion is stable with respect to the fundamental mode. The appearance of the third harmonic mode in the vicinity of the stability limit for

$\bar{P} > 7.8$  atm indicates that there is probably an upper pressure limit for the appearance of the second harmonic mode as well. In addition for a given equivalence ratio the order of the harmonic mode increases as  $\bar{P}$  increases- ie. higher pressures favor higher harmonics. As before the order of the harmonics increases as the equivalence ratio approaches stoichiometric. These observations are in agreement with the results of Tsuji and Takeno (34).

The Sirignano-Crocco analysis, by assumption, considers only the fundamental mode of longitudinal instability. In principle their analysis could be modified to include harmonic modes. This modification would involve altering Assumption 2 (Chapter 3) to allow for more than one shock wave, and obtaining a solution subject to this new assumption. Such a modification, if possible, would provide little additional information about the instability phenomenon. In particular since the mode of the oscillation enters the analysis by assumption it would not be possible to obtain a criterion for the occurrence of the harmonic modes.

A qualitative criterion for the occurrence of harmonic mode instabilities, based on the fact that in the gas rocket the combustion zone has a finite thickness, has been devised. For a combustion zone of finite thickness there is a finite time between the injection of a gas particle and its final conversion to burned products. If  $\tau$  is the residence time of a gas particle in the combustion zone (overall reaction

time) and  $\Theta$  is the apparent period of the oscillation then the criterion for the occurrence of harmonic mode instabilities can be expressed as

$$c < \Theta / \tau < d \quad (4-19)$$

where  $c$  and  $d$  are some critical parameters (not necessarily constants). The favored harmonic mode is the one for which  $\Theta / \tau$  is in  $(c, d)$ . Whenever  $\Theta / \tau$  exceeds  $d$  the next higher harmonic mode (smaller  $\Theta$ ) is favored. Whenever  $\Theta / \tau$  becomes less than  $c$  the next lower harmonic mode (larger  $\Theta$ ) is favored. The concept of a critical range of values for  $\Theta / \tau$  is supported by the results of Tsuji and Takeno (34)- for a given  $\bar{P}$  and  $\Phi$  they found that the boundaries between regions of harmonic mode oscillations were defined by  $\Theta = \text{constant}$ . The criterion (4-19) can be applied to explain the dependence of the boundaries separating the various harmonic regions on  $L$ ,  $\bar{P}$  and  $\Phi$ . For given  $\bar{P}$  and  $\Phi$  as  $L$  is increased  $\Theta$  increases and  $\tau$  remains approximately constant. Hence as  $L$  increases  $\Theta / \tau$  increases. If the increase in  $L$  is sufficient to cause  $\Theta / \tau$  to exceed  $d$  the next higher harmonic mode is favored. Hence (4-19) predicts that the higher harmonics are favored at longer chamber lengths. This result is in agreement with the results of Figure 30. For given  $L$  and  $\Phi$  as  $\bar{P}$  is increased  $\Theta$  remains approximately

constant and  $\tau$  decreases (reaction rate increases). Hence as  $\bar{P}$  increases  $\Theta / \tau$  increases. If the increase in  $\bar{P}$  is sufficient to cause  $\Theta / \tau$  to exceed  $d$  the next higher harmonic mode is favored. Hence (4-19) predicts that the higher harmonics are favored at higher combustion pressures. This result is in agreement with the results of Figure 33. For given  $L$  and  $\bar{P}$  as  $\Phi$  approaches stoichiometric (ie. as  $\bar{T}$  increases) both  $\Theta$  and  $\tau$  decrease (both the sound speed and reaction rate increase with increasing  $\bar{T}$ ). Since the reaction rate is a stronger function of  $\bar{T}$  than is the sound speed  $\tau$  decreases faster than  $\Theta$  as  $\bar{T}$  increases. Hence as  $\Phi$  approaches stoichiometric  $\Theta / \tau$  increases. If  $\Theta / \tau$  exceeds  $d$  the next higher harmonic mode is favored. Hence (4-19) predicts that the higher harmonics are favored closer to stoichiometric. This result is in agreement with the data of Figures 30 and 33 and with the results of Pelmas and Tsuji and Takeno.

The harmonic mode criterion given by equation (4-19) is somewhat over-simplified. However, the concept of a critical range of values for the parameter  $\Theta / \tau$  does account for the essential features of the experimental data, and indicates that to account for harmonic mode instabilities the existence of a finite combustion zone must be considered. Crocco (33) has recently advanced a theory for longitudinal gas-phase instability, assuming a combustion zone of finite thickness and employing a rate function which is somewhat more realistic than (3-1).

On occasion the first tangential transverse mode would occur simultaneously with the longitudinal mode in the vicinity of the stability limits. A typical pressure-time history is shown in Figure 31. The frequency of the longitudinal mode is 630 cps. The frequency of the first tangential mode is approximately 7500 cps.

#### G. Effect of Mean Combustion Pressure on the Instability

##### 1. Dependence of Stability Limits on $\bar{P}$

To determine the dependence of the stability limits on the mean combustion pressure ( $\bar{P}$ ) the regions of unstable combustion for  $H_2$ -air were located in the  $\Phi$ - $\bar{P}$  plane. The results for combustion chamber lengths of 38 cm and 104 cm are shown in Figures 32 and 33 respectively. These results were obtained using the 31-hole showerhead injector and  $C_R = 46$  converging-diverging nozzle. Only the oxidizer-rich unstable regions are shown since variations in the fuel-rich stability limits over the range of  $\bar{P}$  investigated were negligible. For the range of  $\Phi$  investigated (2.0 to 4.0) no upper stability limit was observed for  $L = 104$  cm. It was not possible to obtain  $\Phi > 4.0$  using available critical flow orifices. Considering the results of Figures 17 and 32 it is probable that the upper stability limit exists for some  $\Phi > 4.0$ . The present study involves only the limits separating regions of stable combustion from regions of unstable combustion. From Figures 32 and 33 it is seen that as  $\bar{P}$  is decreased the  $\Phi$ -range for

unstable combustion decreases and the values for  $\Phi_{\text{limit}}$  (at the lower stability limit) shift away from stoichiometric. Although unstable combustion was encountered over the entire range of  $\bar{P}$  investigated, the data seem to indicate that there is some minimum value for  $\bar{P}$  below which the combustion will be stable. These conclusions are in qualitative agreement with the results of other experimental studies of combustion instability in gas rockets (31, 34). In these studies a decrease in the  $\Phi$  - extent of the unstable regions with decreasing  $\bar{P}$  and a minimum  $\bar{P}$  for unstable combustion were observed. Some typical results from Reference 31 for methane-air are shown in Figure 34.

In the Sirignano-Crocco analysis the stability limits are independent of  $\bar{P}$ . To explain the differences between the experimental observations and the theoretical results the effect of  $\bar{P}$  on various combustion parameters will be examined, and the dependence of the stability limits on these parameters will be noted.

#### Effect of $\bar{P}$ on the Adiabatic Combustion Temperature

As  $\bar{P}$  decreases the overall range of adiabatic combustion temperatures decreases. This effect is due primarily to increased dissociation at the lower pressures. The maximum adiabatic combustion temperatures for  $H_2$ -air for various pressures are shown below.

$\bar{P}$ (atm)	$\bar{T}_{ad}$ (°K)	$\Phi$
4.4	2410	1.0
7.8	2422	1.0
11.2	2430	1.0

As noted earlier, a decrease in the overall range of combustion temperatures results in a shift in the stability limits toward stoichiometric. Thus a decrease in  $\bar{P}$  should produce a shift in  $\Phi_{\text{limit}}$  toward stoichiometric. This effect is opposite to the experimental observations of Figures 32 and 33. It is concluded, therefore, that the dependence of  $\bar{T}$  on  $\bar{P}$  cannot explain the observed shift in stability limits.

Effect of  $\bar{P}$  on  $\gamma$

Equation (3-4) defines the stability limits in terms of  $\gamma$ . If  $\gamma$  is a function of pressure then  $(E/R\bar{T})_{\text{limit}}$ , and hence the stability limits, is a function of pressure.  $\gamma$  has been computed for the equilibrium products of combustion of  $H_2$ -air for various  $\bar{P}$  and  $\Phi$ . Over the range of  $\bar{P}$  of interest and for  $\Phi$  in the vicinity of  $\Phi_{\text{limit}}$   $\gamma$  assumes a constant value of 1.29. It is concluded, therefore, that the shift in stability limits with  $\bar{P}$  cannot be explained in terms of the

pressure dependence of  $\gamma$  .

Effect of  $\bar{P}$  on Heat Transfer

The rate of heat transfer/unit area to the walls of the combustion chamber (Q) may be approximated by

$$Q \approx h\bar{T}_g$$

where  $h$  = convective heat transfer coefficient (defined by equation 4-20) and  $\bar{T}_g$  = mean gas temperature. The heat transfer coefficient can be expressed as (46)

$$\frac{hD}{K} = \text{constant} \left( \frac{\dot{m}}{\mu D} \right)^{0.8} \left( \frac{\mu c_p}{K} \right)^{\frac{1}{3}} \quad (4-20)$$

where  $D$  = diameter of the chamber,  $K$  = thermal conductivity of the combustion gases,  $\dot{m}$  = mass flow rate,  $\mu$  = viscosity of the gases and  $c_p$  = specific heat at constant pressure of the gases. Neglecting the pressure and temperature dependence of  $\mu$ ,  $c_p$  and  $K$ ,

$$h \approx \text{constant} \dot{m}^{0.8}.$$

Hence,

$$Q \approx \text{constant } \dot{m}^{0.8} \bar{T}_g.$$

For critical flow at the exhaust nozzle

$$\dot{m} = \text{constant } \frac{\bar{P}}{\sqrt{\bar{T}_g}}.$$

Hence,

$$Q \approx \text{constant } \bar{P}^{0.8} \bar{T}_g^{0.6}. \quad (4-21)$$

From equation (4-21) it is seen that as  $\bar{P}$  increases  $Q$  increases- ie. heat losses increase. From equation (4-3) it is seen that as heat losses increase the stability limits tend to shift to lower combustion temperatures- ie. away from stoichiometric. The decrease in gas temperature due to heat transfer is given by

$$T_{ad} - \bar{T}_g = \frac{Q}{\dot{m} \bar{c}_p}.$$

Neglecting the temperature dependence of  $\bar{c}_p$  this equation may be written

$$T_{ad} - \bar{T}_g \approx \text{constant } \frac{Q \bar{T}_g^{\frac{1}{2}}}{\bar{P}} \quad (4-22)$$

Combining equations (4-21) and (4-22),

$$\frac{T_{ad}}{\bar{T}_g} - 1 \approx \text{constant} \frac{\bar{T}_g^{0.1}}{\bar{P}^{0.2}} \quad (4-23)$$

From equation (4-23) it is seen that as  $\bar{P}$  increases the gas temperature increases. The seemingly contradictory effects of increasing heat transfer and increasing gas temperature result from the coupling of the heat transfer rate and the mass flow rate. From earlier discussions it is recalled that increasing the gas temperature produces a shift in the stability limits toward lower combustion temperatures. Hence a heat transfer argument leads to the conclusion that increasing  $\bar{P}$  produces a shift in stability limits away from stoichiometric. Since this conclusion is contrary to the experimental observations it is felt that the pressure dependence of heat transfer cannot account for the observed shift in stability limits.

#### Effect of $\bar{P}$ on Combustion Zone Analysis

In the analysis of the combustion zone boundary condition pressure and temperature were related through the isentropic equations. As noted in Chapter 3 the isentropic equations are not valid in the combustion zone due to energy release and diffusion. In employing a pressure-dependent energy release law with the results of the isentropic

combustion zone analysis Sirignano and Crocco obtained results which were not in agreement with experimental observations. To circumvent this problem they assumed that the gas rocket combustion process could be approximated by an energy release law which was independent of pressure (equation 3-1). It is not surprising, therefore, that the theoretical stability limits are independent of pressure.

In the analysis of the combustion zone boundary condition Sirignano and Crocco assumed that the combustion zone thickness ( $\delta$ ) was constant. As noted in Section C  $\delta$  is a function of time and depends on the reaction rate. If the reaction rate were pressure dependent then  $\delta$  would also depend on pressure. Thus it is seen that to properly account for pressure effects (for an Arrhenius-type rate function) it is necessary to include non-isentropic effects and a variable  $\delta$  in the combustion zone analysis.

## 2. Dependence of Instability Strength on $\bar{P}$

To determine the dependence of the instability strength ( $\Delta P/\bar{P}$ ) on the mean combustion pressure an experiment was carried out in which  $\Delta P/\bar{P}$  was measured as a function of  $\Phi$  (ie.  $\bar{T}$ ) for several different  $\bar{P}$  (for given  $L$ ,  $\bar{M}$  and propellant combination). The results of a typical experiment using  $H_2$ -air are presented in Figure 35. In this figure  $\Delta P/\bar{P}$  is plotted against the adiabatic combustion temperature for  $\bar{P} = 4.4$  and

11.2 atm. The data were obtained for  $L = 38$  cm, the 31-hole showerhead injector, the  $C_R = 46$  converging-diverging nozzle ( $\bar{M} = 0.015$ ) and the oxidizer-rich unstable region. The heavy vertical bars indicate the variation in shock strength during a given run. For a given combustion temperature the instability strength for  $\bar{P} = 4.4$  atm is significantly less than the instability strength for  $\bar{P} = 11.2$  atm.

In the Sirignano-Crocco analysis the strength of the instability is independent of  $\bar{P}$  (due to the fact that the combustion law 3-1 is independent of pressure). In Section G-1 it was noted that a pressure-independent rate law was necessary due to certain simplifications in the combustion zone analysis. The data of Figure 35 are presented as further evidence for the importance of modifying the combustion zone analysis so that a pressure-dependent rate law can be employed.

#### H. Effect of Combustion Chamber Length on the Instability

##### 1. Dependence of Stability Limits on $L$

From the instability maps of Figures 17 and 19 it is seen that for a given propellant combination, combustion pressure, injector and exhaust nozzle the value of  $\Phi_{\text{limit}}$  can depend on the combustion chamber length ( $L$ ). Experimental studies of longitudinal combustion instability in gas rockets (27, 29, 31) have shown that for a given propellant combination and combustion pressure there is a minimum value for  $L$  below

which the combustion is stable. Values for  $L_{\min}$  for some propellant combinations of interest are tabulated below.

Propellant	$L_{\min}$ (cm)	Source
H <sub>2</sub> -air	12.7	(27)
CH <sub>4</sub> -air	27.9	(31)
natural gas-air	18.0	(34)

In the Sirignano-Crocco analysis the stability limits are independent of  $L$  and no minimum length for stable combustion is predicted. The differences between the experimental observations and the theoretical results can be explained by comparing the conditions in the gas rocket with the assumptions of the theory. From the discussion of Chapter 3 it is recalled that the Sirignano-Crocco analysis assumes frictionless, adiabatic flow. The flow in the gas rocket is highly non-adiabatic (See Figure 43), and frictional effects are present. Earlier it was shown that for the energy release law used in the Sirignano-Crocco analysis losses due to heat transfer and friction tend to shift the stability limits toward lower combustion temperatures. Heat transfer and friction losses increase with increasing chamber length. Hence as  $L$  increases it is expected that the stability limits will shift toward lower combustion temperatures-*ie.* away from

stoichiometric . This shift in the stability limits is evident for the oxidizer-rich unstable regions in Figures 17 and 19. The variation in the adiabatic  $\bar{T}_{limit}$  corresponding to the observed change in  $\Phi_{limit}$  for  $H_2$ -air as L varies from 19 cm to 104 cm is approximately  $130^\circ K$ . In the vicinity of the fuel-rich unstable region for  $H_2$ -air an equivalent variation in  $\bar{T}_{limit}$  corresponds to a variation in  $\Phi_{limit}$  of 0.04. This variation in  $\Phi_{limit}$  is too small to be detected experimentally, and is the probable explanation for the apparent lack of dependence of  $\Phi_{limit}$  on L for the fuel-rich unstable regions.

The Sirignano-Crocco analysis assumes that the combustion zone thickness is significantly smaller than the chamber length-i.e. that the energy is added to the oscillation at  $x = 0$ . In the gas rocket the combustion zone thickness is of the order of 2-4 cm (See Section K). As the chamber length decreases below 40 cm the assumption of a "zero-thickness" combustion zone becomes less appropriate, and the analysis becomes subject to doubt. In addition as  $\delta$  becomes a significant fraction of L energy is added to the oscillation in a non-optimum manner. Non-optimum energy addition gives a steady-state instability strength which is less than the steady-state instability strength for energy addition at a pressure antinode (assuming the same energy release rate for both cases). As the chamber length decreases the combustion zone extends over a larger fraction of the chamber and hence the energy added to the oscillation

decreases. It is conceivable that for sufficiently short chambers (ie. for pressure oscillations with wavelengths of the same order as  $\delta$ ) the energy addition would not be sufficient to support a combustion oscillation. This conclusion is supported by the minimum length data of Reference 27 and the measurement of  $\delta$  (Section K) for  $H_2$ -air:

$$L_{\min} = 12.7 \text{ cm}$$

$$\delta \approx 4 \text{ cm}$$

for  $\bar{P} = 7.8$  atm and a 10-hole showerhead injector.

## 2. Dependence of Instability Strength on L

To determine the dependence of the instability strength ( $\Delta P/\bar{P}$ ) on the length of the combustion chamber (L) an experiment was carried out in which  $\Delta P/\bar{P}$  was measured as a function of  $\Phi$  (ie.  $\bar{T}$ ) for several values of L (for a given  $\bar{P}$ ,  $\bar{M}$  and propellant combination). The results of a typical experiment using  $H_2$ -air are presented in Figure 36. In this figure  $\Delta P/\bar{P}$  is plotted against the adiabatic combustion temperature for  $L = 38$  cm and  $76$  cm. The data were obtained for  $\bar{P} = 4.4$  atm, the 31-hole showerhead injector, the  $C_R = 46$  converging-diverging nozzle ( $\bar{M} = 0.015$ ) and the oxidizer-rich unstable region. The heavy vertical bars indicate a non-periodic variation in instability strength during a given run. For

a given combustion temperature the instability strength for  $L = 76$  cm is significantly larger than for  $L = 38$  cm. A similar length effect has been reported by Zucrow and Osborn (31) for propane-air. Some results from their study are tabulated below.

L (in)	$\Delta P$ (psi)
12.6	4
16.3	17
22.3	22
28.0	22

propane-air  
 $\Phi = 1.2$   
 $\bar{P} = 45$  psia

As  $L$  increases from 12.6 inches to 22.3 inches  $\Delta P/\bar{P}$  increases from 0.09 to 0.49.

In Section H-1 it was noted that due to non-optimum energy addition the energy added to the oscillation decreases as the chamber length decreases. It follows that as the chamber length decreases the strength of the oscillation decreases. Thus it is seen that the observed decrease in instability strength with decreasing  $L$  can be explained in terms of a finite-size combustion zone, and is directly related to the existence of a minimum  $L$  for unstable combustion.

An alternative explanation for the length dependence of the instability strength was suggested by Zucrow and Osborn (31). Their explanation is based on an assumed increase in the energy available to support an oscillation with increasing  $L$ . A critical analysis of the results of Zucrow and Osborn by Crocco (32) indicates that the energy available to support an oscillation is relatively insensitive to variations in  $L$ . Hence, the length dependence of instability strength cannot be explained by an increase in available energy with increasing  $L$ .

## I. Injector Experiments

### 1. Effect of Injector on Stability Limits

To determine the effect of the injection pattern on the stability limits an experiment was carried out in which the regions of unstable combustion for  $H_2$ -air were located in the  $\phi$ - $L$  plane for five injectors with different injection patterns. The injectors used in the experiment were: porous plug, 10-hole showerhead, 31-hole showerhead, 49-hole showerhead and double-triplet impinging. A detailed description of these injectors is presented in Chapter 2. The porous plug injector provides for nearly one-dimensional injection of propellants. The showerhead injectors produce injection patterns which deviate from one-dimensional injection. In addition the combustion zone thicknesses ( $\delta$ ) obtained with the showerhead injectors are significantly larger than the  $\delta$  obtained with the

porous plug injector (See Section K). As the number of injection orifices in the showerhead injectors decreases deviations from one-dimensional injection and the combustion zone thickness increase. The impinging injector produces a strong recirculation pattern and hence provides an injection pattern which deviates significantly from one-dimensional injection. The above combination of injectors permits an investigation of the effects of deviations from one-dimensional injection and combustion zone thickness on the stability limits.

The results of the experiment for  $\bar{P} = 7.8$  atm and the  $C_R = 46$  converging-diverging nozzle are presented in Figures 30 and 37 through 39. From Figures 30, 37 and 38 it is seen that as the number of injection orifices in the showerhead injectors increases (ie. as the injection pattern approaches one-dimensional and  $\delta$  decreases) the stability limits shift toward lower combustion temperatures. For the porous plug injector stable combustion was observed over the entire range of equivalence ratios tested (0.3 to 3.0). This result is consistent with the data of Pelmas (27) and with the data of Figures 30, 37 and 38 (since the porous plug injector is in effect a "many-hole" showerhead injector). If the trend of Figures 30, 37 and 38 is extended then the stability limits for the "many-hole" porous plug injector should fall at a lower combustion temperature than the stability limits for the 49-hole showerhead injector (and thus in all probability outside the range of  $\Phi$  tested). The results for

the impinging injector (Figure 39) are also consistent with the above observations. The impinging injector provides a non-uniform injection pattern and a diffuse combustion zone. Hence the stability limit for the impinging injector should fall at higher combustion temperatures than the stability limits for the showerhead injectors.

The important observation to be made from the above results is that the dependence of the stability limits on the injector seems contrary to what would be expected from the Sirignano-Crocco analysis. The porous plug injection closely approximates the conditions of the Sirignano-Crocco model (ie. one-dimensional flow and zero-length combustion zone) and yet the results obtained using this injector are, at best, in poor agreement with the theory. If the stability limits fall outside the range of tested, as suggested, then the value for  $E_{\text{limit}}$  would differ even more from the accepted values for the activation energy than is the case for the showerhead injectors. The discrepancies between the theoretical results and the experimental observations probably can be traced to the simplified combustion zone analysis employed in the Sirignano-Crocco theory.

## 2. Effect of Injector on the Location of Regions of Harmonic Mode Instabilities

The experiments of Section I-1 also provide information on the

effect of the injector on the location of the regions of harmonic mode instabilities. Of particular interest are the experiments using the three showerhead injectors. From Figures 30, 37 and 38 it is seen that for given  $\Phi$  the minimum critical length for the appearance of the second harmonic mode decreases as the number of injection orifices increases. This result can be explained in terms of the harmonic mode criterion (4-19). As will be seen in Section K for a given combustion pressure and equivalence ratio the thickness of the combustion zone decreases as the number of injection orifices increases-ie. the residence time of a gas particle in the combustion zone ( $\tau$ ) decreases as the number of injection orifices increases. From (4-19) the lower limit for a given harmonic mode is defined by

$$\frac{\Theta}{\tau} = c .$$

For this equation to be satisfied, as  $\tau$  decreases  $\Theta$  must decrease. In other words as the number of injection orifices increases the minimum critical length for a given harmonic mode decreases. A similar argument can be advanced to explain the minimum critical length for the second harmonic mode for the impinging injector (Figure 39). The data of Section K indicate that the impinging injector gives a diffuse combustion zone. Hence the residence time (and thus  $\Theta$ ) increases. The argument is not

as clear cut as for the showerhead injectors due to the highly non-uniform injection pattern produced by the impinging injector.

#### J. Effect of Nozzle Geometry on the Instability

##### 1. Dependence of Stability Limits on Nozzle Geometry

To determine the dependence of the stability limits on exhaust nozzle geometry the regions of unstable combustion for  $H_2$ -air were located in the  $\Phi$ -L plane for several different nozzles. The nozzles employed in this experiment were: two converging-diverging nozzles with convergence angles of  $60^\circ$  and contraction ratios of 23 and 46 (Figure 12) and a tungsten plug nozzle with an effective contraction ratio of 46 (Figure 13). The results of this experiment for  $\bar{P} = 4.4$  atm and the 31-hole showerhead injector are shown in Figure 40. Only the stability limits nearest stoichiometric for the oxidizer-rich unstable regions are shown.

The effect of the length of the convergent section of the nozzle on the stability limits is obtained by comparing the limits obtained for the smaller converging-diverging nozzle ( $C_R = 46$ ) and the plug nozzle. These two nozzles have identical contraction ratios (ie. identical flow areas) and convergent sections of different length (The plug nozzle approximates the "zero-length" nozzle assumed in the Sirignano-Crocco analysis). From Figure 40 it is seen that the stability limits for the two nozzles are the same within the error of the experiment (Appendix B).

In view of the results of Figure 40 it is concluded that the assumption of a zero-length nozzle is reasonable for nozzle lengths less than 0.05 L.

The effect of nozzle contraction ratio on the stability limits is obtained by comparing the limits for the two converging-diverging nozzles. These two nozzles have identical convergence angles and different contraction ratios. From Figure 40 it is seen that the stability limits for the two nozzles are significantly different. The stability limit for the nozzle with the larger flow area ( $C_R = 23$ ) is located at lower combustion temperatures than is the limit for the smaller nozzle. This result can be attributed to two effects- energy losses at the nozzle and increased heat transfer. The energy lost from a wave during reflection increases as the nozzle flow area increases-*ie.* the stabilizing effect of the nozzle increases as the flow area increases. Hence as the contraction ratio decreases the stability limits should shift toward lower combustion temperatures. To maintain a given  $\bar{P}$  the mean mass flow rate increases as the nozzle flow area increases. As noted earlier increasing the mass flow rate increases the heat transfer to the combustion chamber walls. Hence, as before, the stability limits should shift toward lower combustion temperatures.

## 2. Effect of Nozzle Geometry on Instability Waveform

To determine the effect of the exhaust nozzle on the instability

waveform pressure-time histories at a station just upstream from the nozzle entrance plane were obtained for three different nozzles- the tungsten plug nozzle, the  $C_R = 46$  converging-diverging nozzle and the  $C_R = 23$  converging-diverging nozzle. Four typical pressure-time histories are presented in Figures 41 and 42. These histories were obtained using  $H_2$ -air for  $L = 104$  cm,  $\bar{P} = 6.1$  atm, critical nozzle flow, the 31-hole showerhead injector and the oxidizer-rich unstable region. The pressure transducer was flush-mounted in the wall of the combustion chamber approximately 5 cm upstream from the nozzle entrance plane. The mode of the instability is the second harmonic. Figure 41a is a typical pressure-time history for the tungsten plug nozzle. The first pressure rise corresponds to a wave incident on the nozzle; the second pressure rise corresponds to the wave after reflection from the nozzle. It is seen that both the incident and reflected waves are well-defined shock waves and that no significant loss in shock strength occurs upon reflection. Figure 41b is a typical pressure-time history for the  $C_R = 46$  converging-diverging nozzle. This nozzle has the same flow area as the plug nozzle. It is seen that some distortion of the wave occurs on reflection from the nozzle but that the reflected wave remains shock-like. No significant loss in shock strength occurs upon reflection. At a given combustion temperature there is no significant difference between the shock strengths for the plug nozzle and the  $C_R = 46$  converging-diverging nozzle. Figure 42a is a typical pressure-time history for the  $C_R = 23$  converging-

diverging nozzle. This nozzle has the same convergence angle as the  $C_R = 46$  converging-diverging nozzle and twice the flow area. It is seen that the reflected wave is distorted, but still shock-like, and that there is a measurable loss in shock strength on reflection. From the results of this experiment it is concluded that for a given oscillation frequency (ie. L) the loss in shock strength on reflection depends primarily on nozzle flow area and is relatively independent of the length of the convergent section of the nozzle. A similar result was obtained by Feiler (47) in a shock tube study of the reflection of shock waves from critical flow nozzles. Although some distortion of the reflected shock front is observed with the converging-diverging nozzles the wave remains shock-like and, in fact, soon steepens into a sharp shock front. Figure 42b is a typical pressure-time history at a station 15 cm upstream from the entrance plane of the  $C_R = 46$  nozzle. Note that the distorted wave front of Figure 41b has steepened into a well-defined shock front.

#### K. Measurement of Axial Temperature Profiles

In several of the experiments described in this chapter axial distributions of mean gas temperature were obtained using a series of thermocouples located on the centerline of the combustion chamber. A detailed description of the thermocouples is presented in Chapter 2. The temperature distributions are used to determine the mean combustion

temperatures at the stability limits ( $\bar{T}_{\text{limit}}$ ) and the thickness of the combustion zone ( $\delta$ ). In addition the temperature distributions give a quantitative measure of the total heat transfer from the combustion gases (See Assumption 5, Chapter 3).

In Figure 43 typical temperature profiles are shown for the various injectors used in the experiments. The profiles shown were obtained using  $\text{H}_2$ -air with  $\bar{P} = 7.8$  atm,  $L = 104$  cm and the plug nozzle. The equivalence ratio and corresponding adiabatic combustion temperature are given for each profile.

Before considering the results of Figure 43 several details of the measurement procedure will be discussed. The thermocouples used in the experiments were not equipped with radiation shields. To obtain an estimate of radiation losses an experiment was carried out in which the gas temperature at a given location in the combustion chamber was measured simultaneously by a radiation shielded thermocouple and an unshielded thermocouple. The results of this experiment indicated that within the scatter of the temperature data ( $\pm 15^\circ\text{K}$ ) there was no difference between the two thermocouple readings. This result is in agreement with the results of a heat transfer analysis of the thermocouple system. The fact that the readings of the shielded and unshielded thermocouples are approximately the same is due to the very large convective heat transfer

coefficient of the combustion gases. Since it appears that no correction for radiation losses is necessary the temperature data of Figure 43 are direct thermocouple readings. Temperature measurements were made using uncoated platinum-platinum/rhodium thermocouples. It is well known that platinum has a catalytic effect on the hydrogen-oxygen reaction. Hence the temperature measurements made in the reaction zone itself are probably not reliable. Downstream from the reaction zone (ie. downstream from the peak temperature) the temperature data should be reliable to within  $\pm 1\%$  (the accuracy of the thermocouple). The thermocouple configuration is such that the temperature measured is a stagnation temperature. Since the mean Mach number of the combustion gases is very small ( $< 0.03$ ) the stagnation and static temperatures are for all intents and purposes the same.

From Figure 43 it is seen that for a given equivalence ratio the peak temperature is essentially independent of the injector and approximately  $40^{\circ}\text{K}$  less than the adiabatic combustion temperature. This result is not surprising since the heat losses from the relatively thin combustion zone are small. It is seen that the combustion zone thickness for the porous plug injector is significantly less than the  $\delta$ 's for the showerhead and impinging injectors. Furthermore  $\delta$  decreases as the number of injection orifices in the showerhead injectors increases. Finally it is noted that the decrease in gas temperature over the length of the combustion chamber ( $\sim 100$  cm) is considerable ( $\sim 700^{\circ}\text{K}$ ) so that

the assumption of adiabatic flow (for long motors at least) is not particularly good.

CHAPTER 5. CONCLUSIONS

A. Mechanism for High-Frequency Longitudinal Gas-Phase  
Combustion Instability

The Sirignano-Crocco combustion instability analysis is based on a gas-phase chemical kinetic driving mechanism, and employs a simplified model for the gas rocket combustor (Chapter 3). In comparing the experimental observations with the theoretical results (Chapter 4) it was found that within the limitations imposed by the analytical assumptions there is relatively good agreement between theory and experiment. The theory provides a criterion for the boundaries separating regions of stable and unstable combustion (equations 3-4 and 4-6) which was verified qualitatively by experiment. In addition the theory gives the correct dependence of instability strength on the mean Mach number of the combustion gases and the mean combustion temperature. The several areas of disagreement between theory and experiment generally can be explained in terms of differences between the conditions in the gas rocket and the theoretical model. The results of Chapter 4 indicate that the most important differences between theory and experiment can be traced to oversimplifications in the combustion zone boundary condition and the energy release law. The experimental results point up the fact that the effects of a finite combustion zone on the instability phenomenon are not fully understood. Crocco has recently advanced an instability theory (33)

which incorporates a more realistic energy release law and a combustion zone of finite thickness. Hardesty (49) is presently carrying out experiments to better understand the effect of a finite combustion zone on the instability phenomenon.

Various experimental studies of longitudinal combustion instability in gas rockets have been carried out (27-29, 31, 34). In Chapter 4 and Reference 50 the results of these studies have been shown to be consistent with the results of the present investigation. Available gas rocket data, together with the results of the Sirignano-Crocco analysis, provide strong evidence for a mechanism for high-frequency longitudinal gas-phase combustion instability based on the interaction between the combustion oscillation and the energy release rate-i.e. chemical kinetics.

#### B. Possible Applications of Gas Rocket Instability Data

The most obvious application of gas rocket instability data is to homogenous gas-phase chemical kinetics. If a theory could be developed which provides a quantitatively accurate criterion for the stability limits in terms of the chemical kinetic parameters then it would be possible to use stability limit data obtained from gas rocket experiments to determine the overall kinetics for the gas-phase reaction of a given propellant combination.

If a comparison is made between the experimentally observed properties of the longitudinal mode of high-frequency combustion instability in gaseous propellant and liquid propellant motors it is found that in a number of ways they are similar. Under certain conditions the instability waveform are identical-*ie.* shock discontinuities followed by exponential decay in pressure and velocity, with oscillation frequencies corresponding to one of the resonant frequencies of the combustion chamber. The nature and ordering of the regions of harmonic mode instabilities are the same. In spite of these similarities it is felt that due to several uncertainties in the gas-phase instability phenomenon an attempt to relate gas-phase and two-phase combustion instability would be premature.

APPENDIX A: CALIBRATION PROCEDURESCritical Flow Orifices

The mass flow rate of a perfect gas through a critical flow orifice is given by

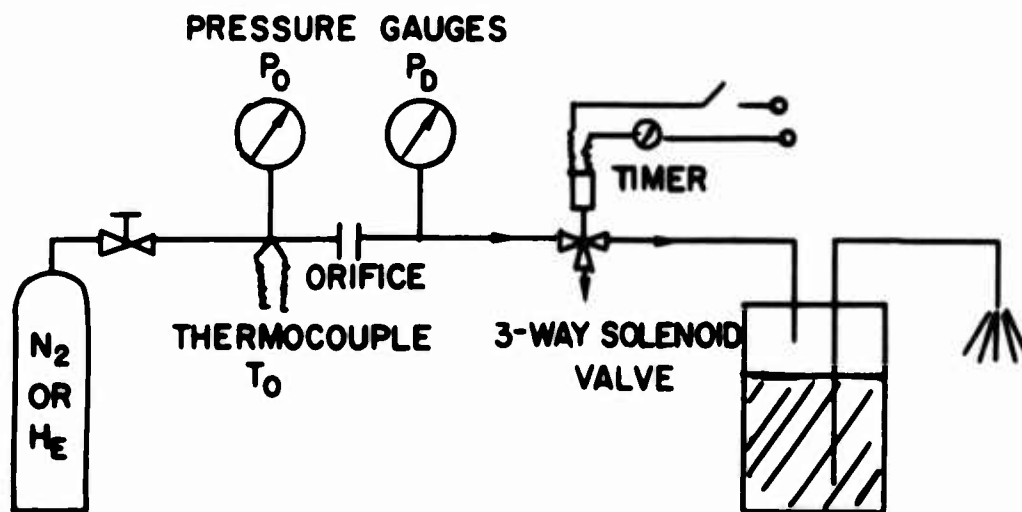
$$\dot{m} = g(\gamma, \pi) A_{\text{ORIFICE}} \frac{P_0}{\sqrt{T_0}} \quad (\text{A-1})$$

where  $\dot{m}$  = mass flow rate,  $g(\gamma, \pi)$  = function of the specific heat ratio and molecular weight,  $A_{\text{orifice}}$  = exit area of the orifice,  $P_0$  = stagnation pressure and  $T_0$  = stagnation temperature. For the flow of a real gas through a critical flow orifice equation (A-1) must be modified to include the effects of friction and compressibility- ie.

$$\dot{m} = \frac{C_D}{z} g(\gamma, \pi) A_{\text{ORIFICE}} \frac{P_0}{\sqrt{T_0}} \quad (\text{A-2})$$

where  $C_D$  = discharge coefficient  $< 1$  (a function of the Reynolds number) and  $z$  = compressibility factor. It is noted that in equation (A-1)  $\gamma$  is a constant (for a given gas) whereas in equation (A-2)  $\gamma$  is a function of  $P_0$ . The compressibility factor and  $\gamma$  are tabulated as functions of  $P_0$  for several gases in Reference 48. The discharge coefficient is not known a priori so that it is not possible to obtain solutions to equation (A-2). To determine  $\dot{m}$  as a function of  $P_0$  and  $T_0$

the critical flow orifices used in the gas rocket propellant feed system were calibrated using a water displacement technique. In this technique the mass flow rate (for known  $P_o$  and  $T_o$ ) is determined by allowing the gas to displace water from a container (see sketch). By measuring the volume of the water displaced during a known time and the pressure and temperature of the gas in the container it is possible to calculate the mass of gas which flowed into the container during the known time (ie. the mass flow rate).



SKETCH OF ORIFICE CALIBRATION RIG

By performing this measurement for several  $P_0$  and referencing the result to a fixed stagnation temperature ( $T_{0 \text{ REF}}$ ) a calibration curve for the orifice for a given gas and  $T_{0 \text{ REF}}$  is obtained. This calibration curve may be extended to other  $T_0$  by using

$$\dot{m}(T_0) \approx \dot{m}(T_{0 \text{ REF}}) \sqrt{\frac{T_0}{T_{0 \text{ REF}}}} \quad (\text{A-3})$$

Nine critical flow orifices were calibrated using  $N_2$  and/or He in the pressure range of 0-1800 psig (1-123 atm-abs). The resulting calibration curves were extended to the propellant gases using

$$\dot{m}_{\text{PROP}} = \dot{m}_{\text{CAL}} \left\{ \frac{C_{D \text{ PROP}}}{C_{D \text{ CAL}}} \right\} \left\{ \frac{\gamma_{\text{CAL}}}{\gamma_{\text{PROP}}} \right\} \left\{ \frac{g(\gamma, \mu)_{\text{PROP}}}{g(\gamma, \mu)_{\text{CAL}}} \right\} \quad (\text{A-4})$$

with tabulated values for  $\gamma$  and  $\mu$  (Reference 48) and experimental values for  $C_D$ . A discussion of experimental uncertainties in the calibration data is presented in Appendix B.

#### Pressure Transducers

At regular intervals the steady-state and transient pressure transducers were calibrated using a dead weight testor. The output from a given steady-state transducer was recorded on the chart recorder used to record the transducer output during the experiments so that the

A-4

complete pressure recording system was calibrated. The transient pressure transducers were calibrated statically, recording the transducer output on the visicorder.

APPENDIX B: EXPERIMENTAL UNCERTAINTIESOrifice Calibration Data

The major uncertainty in the orifice calibration data is introduced in extending the data from the calibration gases ( $N_2$ , He) to the propellant gases ( $H_2$ ,  $CH_4$ , CO,  $O_2$ , air). This extension requires a knowledge of the ratio of the discharge coefficients for the propellant gas and calibration gas (see equation A-4). In using equation (A-4) it was assumed that the Reynolds number dependence of  $C_D$  was the same for both the propellant gas and the calibration gas (The Reynolds number dependence of  $C_D$  for the calibration gas was obtained from the calibration data). The uncertainty in the calibration data is obtained by combining estimates of the uncertainty introduced by the  $C_D$  assumption with the uncertainty in the measured parameters of the calibration experiment. The estimated uncertainties for several sets of calibration data are tabulated below.

orifice	propellant	uncertainty (%)
7	$H_2$	$\pm 1.5$
6	CO	$\pm 0.5$
3	air	$\pm 0.5$

Equivalence and Dilution Ratios

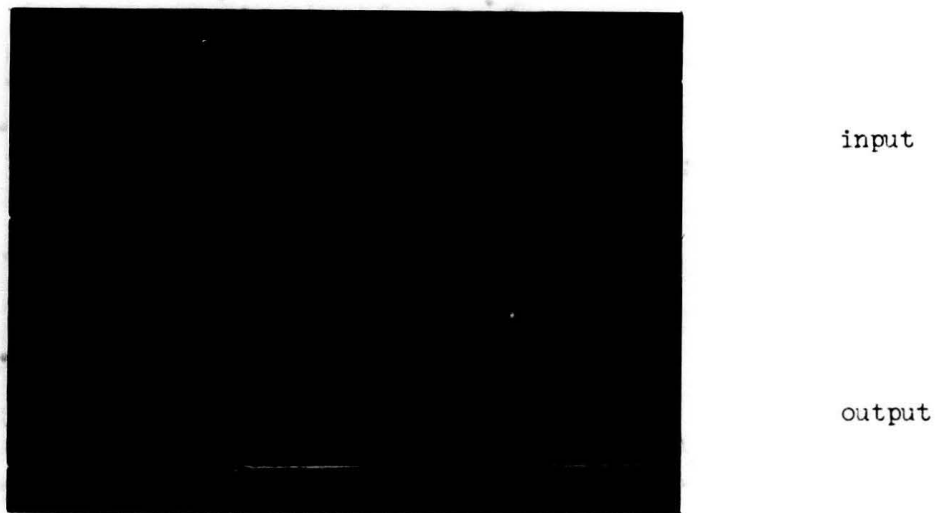
Two factors contribute to the uncertainty in the equivalence and dilution ratios. The first factor is the uncertainty in the orifice calibration data. The second factor is the uncertainty in the measurement of the experimental variables (stagnation pressure and temperature). Combining these two factors the uncertainty in the equivalence and dilution ratios for the various propellant combinations were estimated. The results are tabulated below.

propellant combination	uncertainty in $\Phi$ (%)		uncertainty in dilution ratio (%)
	$\Phi > 1$	$\Phi < 1$	
H <sub>2</sub> -air	±2.5	±1.5	-
H <sub>2</sub> -dilute air	±2.5	±1.5	±1.0
CH <sub>4</sub> -air	±2.0	±1.5	±1.0
CH <sub>4</sub> -(.4O <sub>2</sub> +.6N <sub>2</sub> )	±2.0	±1.5	±1.0
CO-air	±1.5	±1.5	-

It is noted that uncertainties in the equivalence and dilution ratios result in corresponding uncertainties in the adiabatic combustion temperature (eg. for H<sub>2</sub>-air,  $\Phi = 2.50 \pm 0.06$  gives  $T_{ad} = 1425 \pm 25$  °K).

#### Transient Pressure Data

The frequency response of the transient pressure recording system was flat to within 10% from 20 cps to 6 kc and to within 20% from 15 cps to 12 kc. To determine the effect of the inherent filtering of the recording system on the experimental data a 1 kc square wave was fed into the recording system. The output and input are shown below.



1 kc Square Wave

It is seen that there is only a very slight difference between the input waveform and the output waveform. It is concluded, therefore,

B-4

that for oscillation frequencies less than 1 kc the effect of inherent filtering on the transient pressure data is negligible.

Temperature Measurement

See Chapter 4.

APPENDIX C: SOME RESULTS OF THE SIRIGNANO-CROCCO THEORY

The strength of the shock wave instability, in terms of the changes in gas velocity and pressure across the wave, is given by (23)

$$\frac{\Delta u_{AB}}{\bar{u}} = \frac{\epsilon Z}{\lambda} \left( \frac{1+\nu}{1-\nu} \right) \frac{1 - \exp(-\lambda)}{1 + \exp(-\lambda)} + \mathcal{O}(\epsilon^2) \quad (C-1)$$

$$\frac{\Delta u_{BC}}{\bar{u}} = \frac{\epsilon Z}{\lambda} \cdot \frac{1 - \exp(-\lambda)}{1 + \exp(-\lambda)} + \mathcal{O}(\epsilon^2) \quad (C-2)$$

$$\frac{\Delta P_{AB}}{\bar{p}} = \frac{\epsilon \gamma Z}{\lambda} \left( \frac{1+\nu}{1-\nu} \right) \frac{1 - \exp(-\lambda)}{1 + \exp(-\lambda)} + \mathcal{O}(\epsilon^2) \quad (C-3)$$

$$\frac{\Delta P_{BC}}{\bar{p}} = \frac{\epsilon \gamma Z}{\lambda} \cdot \frac{1 - \exp(-\lambda)}{1 + \exp(-\lambda)} + \mathcal{O}(\epsilon^2) \quad (C-4)$$

It is noted that the strength of the instability is independent of time and is altered only by reflection from the nozzle or injector. As  $\bar{M} \rightarrow 0$ ,  $\nu \rightarrow 0$  and thus the changes in  $u$  and  $P$  across the wave are the same for both the downstream and upstream moving waves.

The velocity of the shock wave is given by (23)

$$\frac{V_{AB}}{\bar{a}} = (1+\bar{M}) + \frac{\epsilon \bar{z}}{\lambda} \left\{ \frac{3-\gamma}{4} - \frac{3-\gamma}{2} \cdot \frac{\exp[-\lambda(1+\bar{M})t]}{1+\exp(-\lambda)} \right\} + \mathcal{O}(\epsilon^2) \quad (C-5)$$

$$\frac{V_{BC}}{\bar{a}} = (\bar{M}-1) + \frac{\epsilon \bar{z}}{\lambda} \left( \frac{1+\nu}{1-\nu} \right) \left\{ \frac{\gamma-3}{4} + \frac{3-\gamma}{2} \cdot \frac{\exp[\lambda(1-\bar{M})(\frac{1}{1+\bar{M}}-t)]}{1+\exp(-\lambda)} \right\} + \mathcal{O}(\epsilon^2) \quad (C-6)$$

It is noted that the shock velocity increases in time and is altered by reflection.

The period of the oscillation is given by (23)

$$\Theta(\bar{a}) = \frac{2}{1-\bar{M}^2} + \frac{\epsilon \bar{z}}{\lambda} \left( \frac{3-\gamma}{4} \right) \left\{ \left( \frac{1+\nu}{1-\nu} \right) \left( \frac{1}{1-\bar{M}} \right)^2 + \left( \frac{1}{1+\bar{M}} \right)^2 \right\} + \mathcal{O}(\epsilon^2) \quad (C-7)$$

$$\left\{ \frac{2}{\lambda} \cdot \frac{1-\exp(-\lambda)}{1+\exp(-\lambda)} - 1 \right\} + \mathcal{O}(\epsilon^2)$$

It is noted that the period of the oscillation corresponds to the fundamental longitudinal acoustic mode of the chamber with a correction for a finite strength wave and mean flow.

The equations for the gas velocity and pressure behind the

downstream moving shock (as functions of  $x$  and  $t$ ) are (23)

$$\frac{u}{\bar{u}} = \bar{M} + \frac{\epsilon Z}{\lambda} \left\{ \frac{\exp \left[ -\lambda \left( \frac{1-\bar{M}^2}{2} \right) t \right]}{1 + \exp(-\lambda)} \cdot \left[ \left( \frac{1+\nu}{1-\nu} \right) \exp \left[ \frac{\lambda}{2} (1-\bar{M}) x \right] - \right. \right. \quad (C-8)$$

$$\left. \left. \exp \left[ -\frac{\lambda}{2} (1+\bar{M}) x \right] \right] - \frac{\nu}{1-\nu} \right\} + \sigma(\epsilon^2)$$

$$\frac{p}{\bar{p}} = 1 + \frac{\epsilon \gamma Z}{\lambda} \left\{ \frac{\exp \left[ -\lambda \left( \frac{1-\bar{M}^2}{2} \right) t \right]}{1 + \exp(-\lambda)} \cdot \left[ \left( \frac{1+\nu}{1-\nu} \right) \exp \left[ \frac{\lambda}{2} (1-\bar{M}) x \right] + \right. \quad (C-9)$$

$$\left. \exp \left[ -\frac{\lambda}{2} (1+\bar{M}) x \right] \right] - \frac{1}{1-\nu} \right\} + \sigma(\epsilon^2)$$

It is noted that both pressure and velocity decay exponentially in time behind the shock wave.

The equations for the gas velocity and pressure behind the upstream moving shock (as functions of  $x$  and  $t$ ) are (23)

$$\frac{u}{\bar{u}} = \bar{M} + \frac{\epsilon Z}{\lambda} \left\{ \frac{\exp \left[ -\lambda \left( \frac{1-\bar{M}^2}{2} \right) t \right]}{1 + \exp(-\lambda)} \cdot \left[ \left( \frac{1+\nu}{1-\nu} \right) \exp \left[ \frac{\lambda}{2} (1-\bar{M}) x \right] - \right. \quad (C-10)$$

$$\left. \exp \lambda \exp \left[ -\frac{\lambda}{2} (1+\bar{M}) x \right] \right] - \frac{\nu}{1-\nu} \right\} + \sigma(\epsilon^2)$$

$$\frac{P}{P} = i + \frac{\epsilon \gamma z}{\lambda} \left\{ \frac{\exp\left[-\lambda \frac{(1-\bar{M}^2)}{2}\right]}{1 + \exp(-\lambda)} \left[ \left(\frac{1+\nu}{1-\nu}\right) \exp\left[\frac{\lambda}{2} (1-\bar{M}) x\right] + \right. \right. \quad (C-11)$$

$$\left. \left. \exp \lambda \exp\left[-\frac{\lambda}{2} (1+\bar{M}) x\right] - \frac{1}{1-\nu} \right\} + o(\epsilon^2)$$

APPENDIX D: GAS DATA

Gas	Source	Grade	Typical Analysis	
			Gas	Concentration
H <sub>2</sub>	General Dynamics	Electrolytic	H <sub>2</sub> O <sub>2</sub> Dew point	99.9% (vol.) 0.2% not available
CH <sub>4</sub>	Matheson	Commercial	CH <sub>4</sub> C <sub>2</sub> H <sub>6</sub> C <sub>3</sub> H <sub>8</sub> CO <sub>2</sub> N <sub>2</sub>	93.6% (mole) 3.6% 1.0% 0.7% 0.5%
CO	Matheson	C. P.	CO CO <sub>2</sub> O <sub>2</sub> N <sub>2</sub> H <sub>2</sub> O	99.5% (vol.) 200 ppm 20 ppm 75 ppm 80-130 ppm
O <sub>2</sub>	Air Products	Dry	O <sub>2</sub> N <sub>2</sub> Ar Dew point	99.5% (mole) 0.05% 0.45% -76°F
N <sub>2</sub>	Air Reduction	Liquid	N <sub>2</sub> Dew point	99.95% (vol.) -80°F

REFERENCES

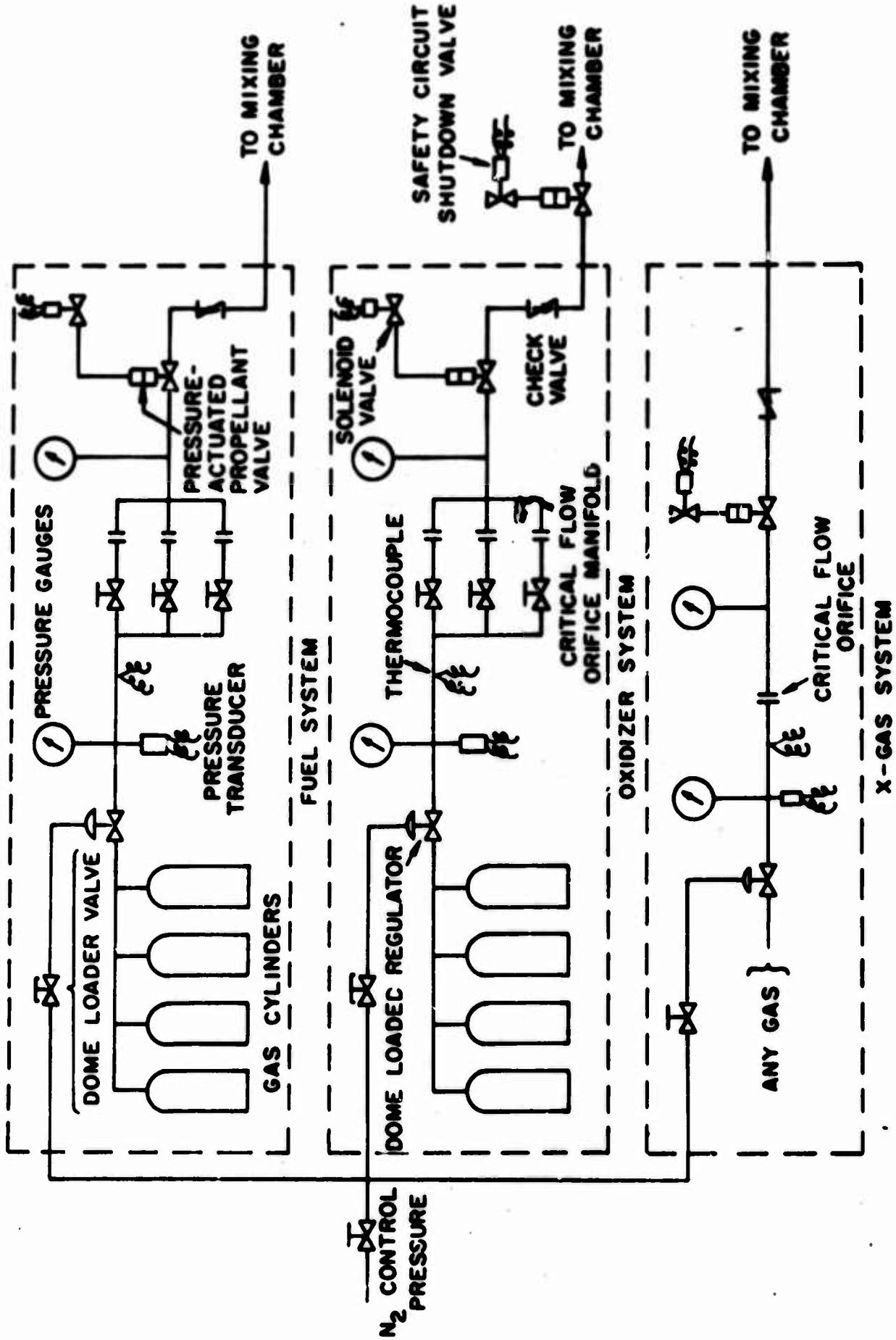
1. Gunder, D. F. and Friant, D. R., "Stability of Flow in a Rocket Motor," Journal of Applied Mechanics, 17, pp. 327-333, 1950.
2. Yachter, M., "A Discussion of Reference 1," Journal of Applied Mechanics, 18, pp. 114-116, 1951.
3. Summerfield, M., "A Theory of Unstable Combustion in Liquid Propellant Rocket Systems," ARS Journal, 21, pp. 108-114, 1951.
4. Crocco, L., "Aspects of Combustion Stability in Liquid Propellant Rocket Motors: Part I," ARS Journal, 21, pp. 163-178, 1951.
5. Crocco, L., "Aspects of Combustion Stability in Liquid Propellant Rocket Motors: Part II," ARS Journal, 22, pp. 7-16, 1952.
6. Tischler, A. O. and Bellman, D. R., "Combustion Instability in an Acid-Heptane Rocket with a Pressurized-Gas Propellant Pumping System," NACA TN 2936, 1953.
7. Barrère, M. and Moutet, A., "Low-Frequency Combustion Instability in Bipropellant Rocket Motors- Experimental Study," Jet Propulsion, 26, pp. 9-19, 1956.
8. Crocco, L. and Cheng, S. I., Theory of Combustion Instability in Liquid Propellant Motors, AGARD Monograph 8, Butterworths Scientific Publications, London, 1956.
9. Berman, K. and Logan, S. E., "Combustion Studies with a Rocket Motor Having a Full-Length Observation Window," ARS Journal, 22, pp. 78-85, 1952.
10. Berman, K. and Cheney, S. H., "Rocket Motor Instability Studies," Jet Propulsion, 25, pp. 513-518, 1955.
11. Ellis, H., Odgers, I., Stosick, A. J., Van de Verg, N. and Wick, R. S., "Experimental Investigation of Combustion Instability in Rocket Motors," Fourth Combustion Symposium, pp. 880-885, 1953.
12. Ross, C. C. and Datner, P. P., "Combustion Instability in Liquid Propellant Rocket Motors- A Survey," AGARD Selected Combustion Problems, Butterworths Scientific Publications, London, 1954.

13. Scala, S. M., "Transverse Wave and Entropy Wave Combustion Instability in Liquid Propellant Rockets," Aero. Eng. Lab. Report No. 380 (Princeton), 1957.
14. Berman, K. and Cheney, S. H., "Combustion Studies in Rocket Motors," ARS Journal, 23, pp. 89-95, 1953.
15. Pass, I. and Tischler, A. O., "Effect of Fuels on Screaming in 200-lb Thrust Liquid-Oxygen-Fuel Rocket Engine," NACA RM E56C10, 1956.
16. Tischler, A. O., Massa, R. V. and Mantler, R. L., "An Investigation of High-Frequency Combustion Oscillations in Liquid-Propellant Rocket Engines," NACA RM E53B27, 1953.
17. Crocco, L., Grey, J. and Harrje, D. T., "Theory of Liquid Propellant Rocket Combustion Instability and Its Experimental Verification," ARS Journal, 30, pp. 159-168, 1960.
18. Crocco, L. and Cheng, S. I., "High-Frequency Combustion Instability in Rockets with Distributed Combustion," Fourth Combustion Symposium, pp. 865-879, 1953.
19. Crocco, L. and Cheng, S. I., "High-Frequency Combustion Instability in Rocket Motor with Concentrated Combustion," ARS Journal, 23, pp. 301-313, 1953.
20. Priem, R. J. and Guentert, D. C., "Combustion Instability Limits Determined by a Nonlinear Theory and a One-Dimensional Model," NASA TN D-1409, 1962.
21. Culick, F. E. C., "Stability of High-Frequency Pressure Oscillations in Rocket Combustion Chambers," AIAA Journal, 1, pp. 1097-1104, 1963.
22. Hart, R. W. and McClure, F. T., "Theory of Acoustic Instability in Solid Propellant Rocket Combustion," Applied Physics Lab. Report TG 335-17. 1964.
23. Sirignano, W. A. and Crocco, L., "A Shock Wave Model of Unstable Rocket Combustors," AIAA Journal, 2, pp. 1285-1296, 1964.
24. Zucrow, M. J., Osborn, J. R. and Bonnell, J. M., "Summary of Experimental Investigations of Combustion Pressure Oscillations in Gaseous Propellant Rocket Motors," Jet Propulsion Center Report No. F-63-2 (Purdue), 1963.

25. Knauer, R. C. and Webb, M. J., "Prevention of Flashback Damage in Combustors," *Astronautics*, 5, p. 84, 1960.
26. Bortzmeyer, H. G. and Crocco, L., "Analysis of Longitudinal High-Frequency Combustion Instability in a Gas Fueled Rocket Motor," Aero. Eng. Lab. Report No. 587 (Princeton), 1961.
27. Pelmas, R., Glassman, I. and Webb, M. J., "An Experimental Investigation of Longitudinal Combustion Instability in a Rocket Motor Using Premixed Gaseous Propellants," Aero. Eng. Lab. Report No. 589 (Princeton), 1961.
28. Bertrand, J., Glassman, I. and Crocco, L., "Theoretical and Experimental Investigations of Longitudinal High-Frequency Combustion Instability in a Gas-Fueled Rocket Motor," Aero. Eng. Lab. Report No. 624 (Princeton), 1962.
29. Schob, W. J., "An Experimental Investigation of Heat Transfer and Pressure Effects on Longitudinal Combustion Instability in a Rocket Motor Using Premixed Gaseous Propellants," M. S. E. Thesis (Princeton University), 1963.
30. Osborn, J. R. and Derr, R. L., "An Experimental Investigation of Longitudinal Combustion Pressure Oscillations," Purdue University Report I-62-8, 1962.
31. Zucrow, M. J. and Osborn, J. R., "An Experimental Study of High-Frequency Combustion Pressure Oscillations," *Jet Propulsion*, 28, pp. 654-659, 1958.
32. Crocco, L., "Comments on the Zucrow-Osborn Paper on Combustion Oscillations," *Jet Propulsion*, 28, pp. 843-844, 1958.
33. Crocco, L., private communication, July, 1965.
34. Tsuji, H. and Takeno, T., "An Experimental Investigation on High-Frequency Combustion Oscillations," Tenth Combustion Symposium, pp. 1327-1335, 1965.
35. Sawyer, R. F., "The Homogenous Gas-Phase Kinetics of Reactions in the Hydrazine-Nitrogen Tetroxide Propellant System," Ph. D. Thesis (Princeton University), 1965.
36. Shtern, V. Y., The Gas-Phase Oxidation of Hydrocarbons, Macmillan Company, New York, p. 435, 1965.

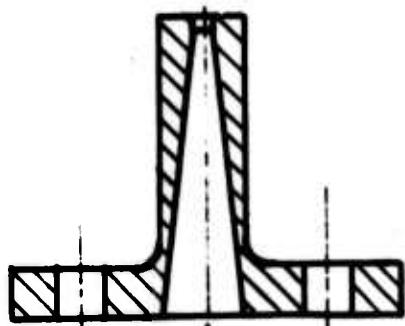
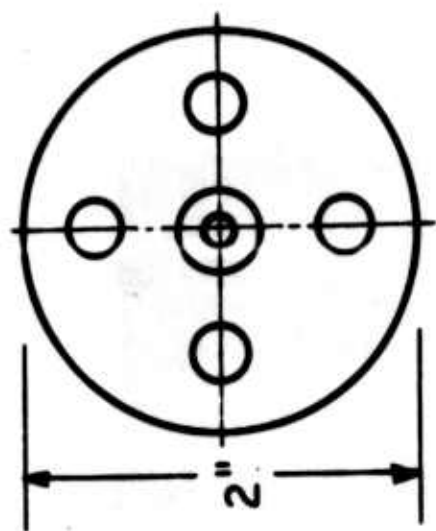
37. Kaskan, W. E. and Browne, W. G., "Kinetics of the  $H_2/CO/O_2$  System," General Electric Space Sciences Lab. Report No. R64SD37, 1964.
38. Friedman, R. and Nugent, R. G., "Flame Structure Studies IV: Premixed Carbon Monoxide Combustion," Project Squid Report No. ARC-3-P, 1958.
39. Lewis, B. and von Elbe, G., Combustion, Flames and Explosions of Gases, Academic Press, New York, pp. 384-385, 1961.
40. Friedman, R. and Cyphers, J. A., "On the Burning Rate of Carbon Monoxide," J. Chem. Phys., 25, pp. 448-457, 1956.
41. Fenimore, C. P. and Jones, G. W., "The Water-Catalyzed Oxidation of Carbon Monoxide at High Temperature," J. Chem. Phys., 61, pp. 651-654, 1957.
42. Damköhler, G., "The Effect of Turbulence on the Flame Velocity in Gas Mixtures," NACA TM 1112, 1947.
43. Karlovitz, B., Denniston, D. W. and Wells, F. E., "Investigation of Turbulent Flames," J. Chem. Phys., 19, pp. 541-547, 1951.
44. Summerfield, M., Reiter, S. H., Kebely, V. and Mascolo, R. W., "The Structure and Propagation Mechanism of Turbulent Flames in High Speed Flow," Jet Propulsion, 25, pp. 377-384, 1955.
45. Williams, F. A., Combustion Theory, Addison-Wesley, Reading, p. 99, 1965.
46. Summerfield, M., "The Liquid Propellant Rocket Engine," Jet Propulsion Engines, Princeton University Press, Princeton, pp. 493-496, 1959.
47. Feiler, C. F., "Reflection of Weak Shock Waves From Nozzles with No Flow and Critical Flow," ARS Journal, 29, pp. 272-275, 1959.
48. Table of Thermal Properties of Gases, NBS Circular 564, 1955.
49. Hardesty, D., private communication, February, 1966.
50. Bowman, C. T., Glassman, I. and Crocco, L., "Combustion Instability in Gas Rockets," AIAA Journal, 3, pp 1981-1982, 1965.

JPI3-4069-65



FLOW SCHEMATIC OF PROPELLANT FEED SYSTEM

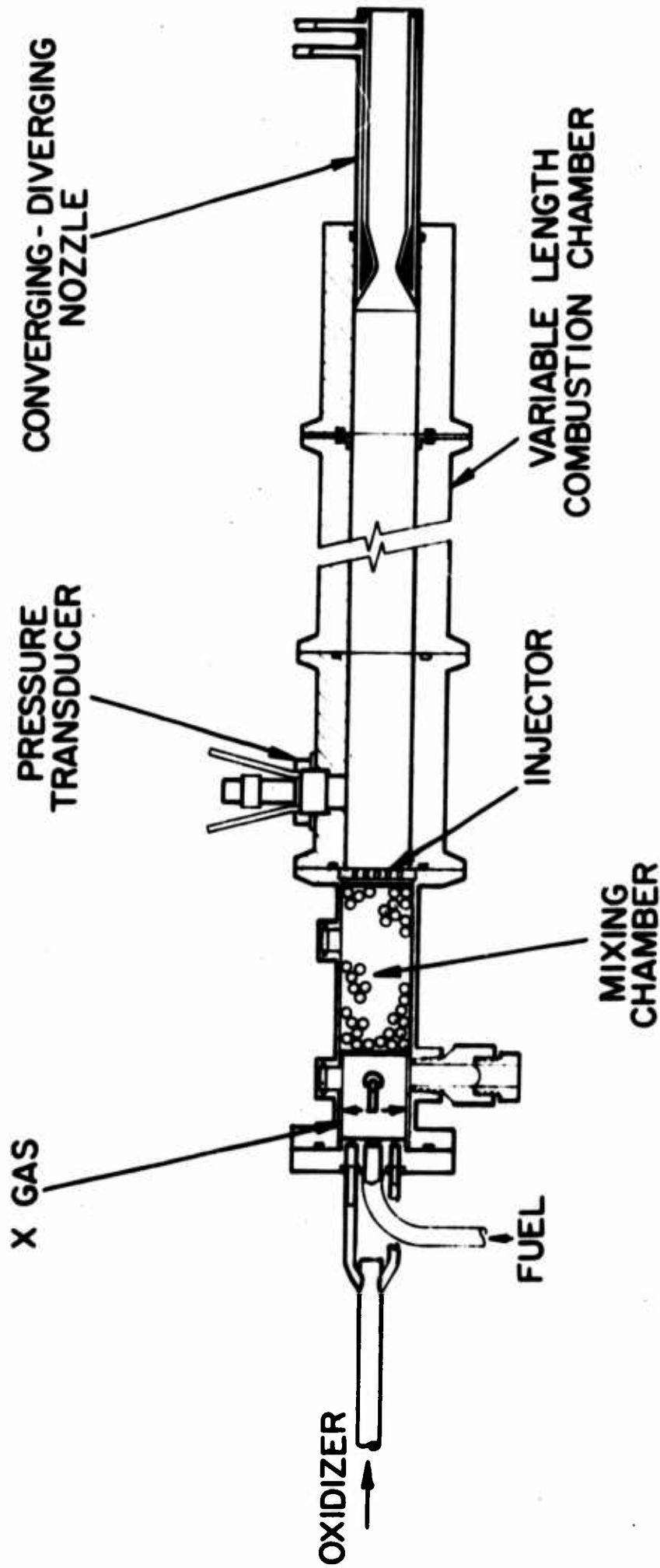
FIGURE 1



FLOW DIRECTION

TYPICAL CRITICAL FLOW ORIFICE

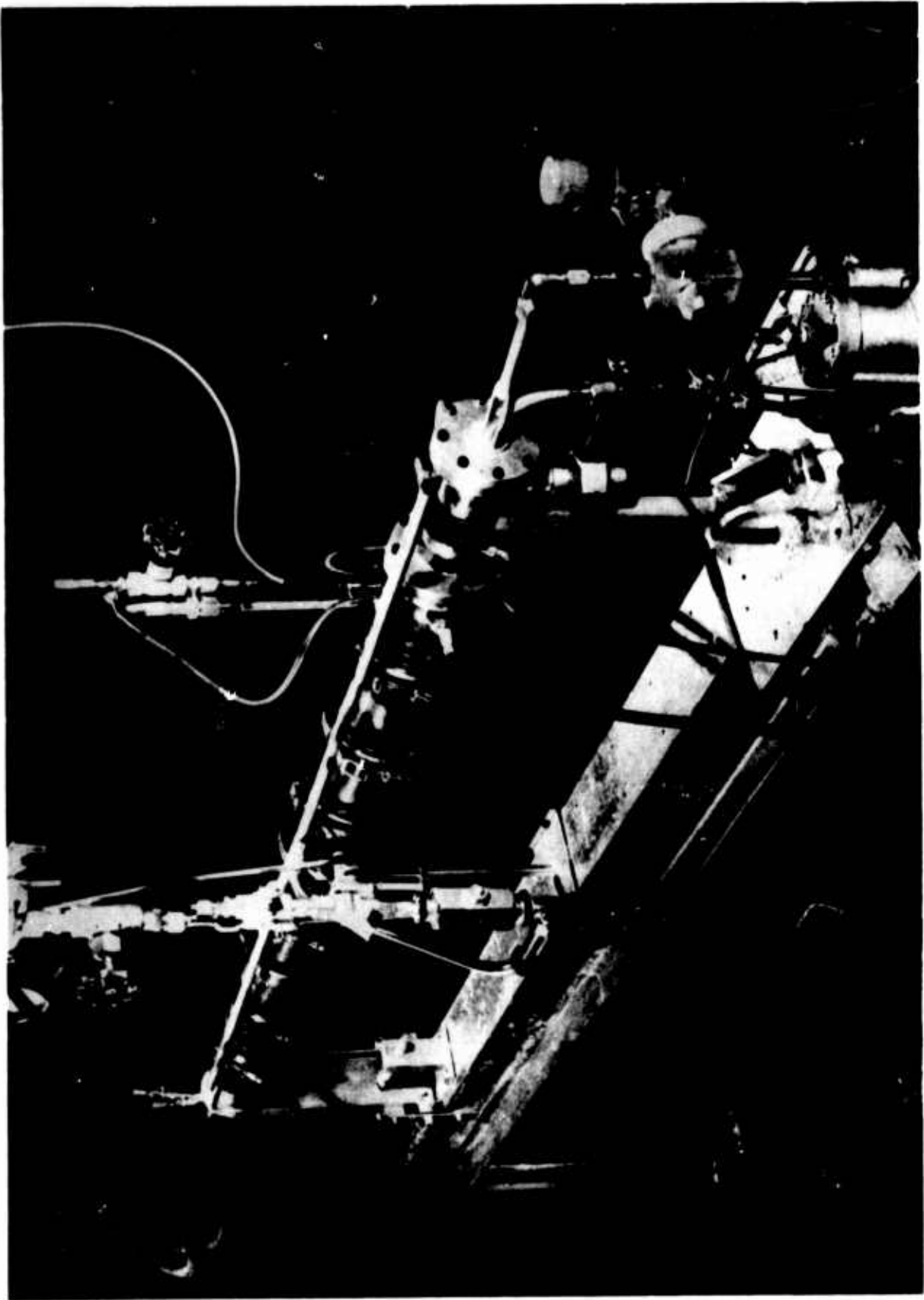
FIGURE 2



SCHEMATIC OF GAS ROCKET (CONVERGING - DIVERGING NOZZLE)

FIGURE 3

JP13 P-28 66



GAS ROCKET MOUNTED ON TEST STAND

FIGURE 4

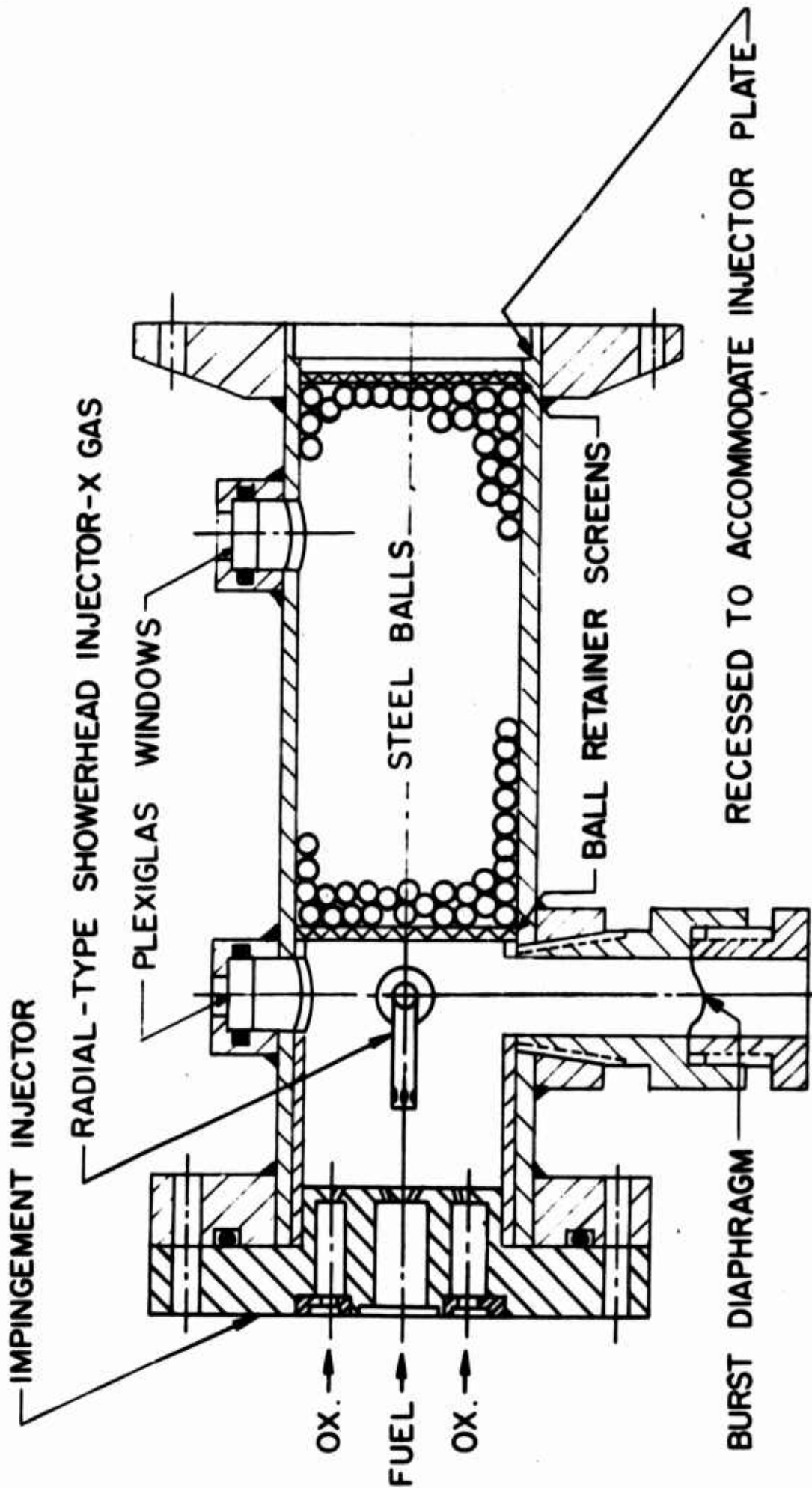
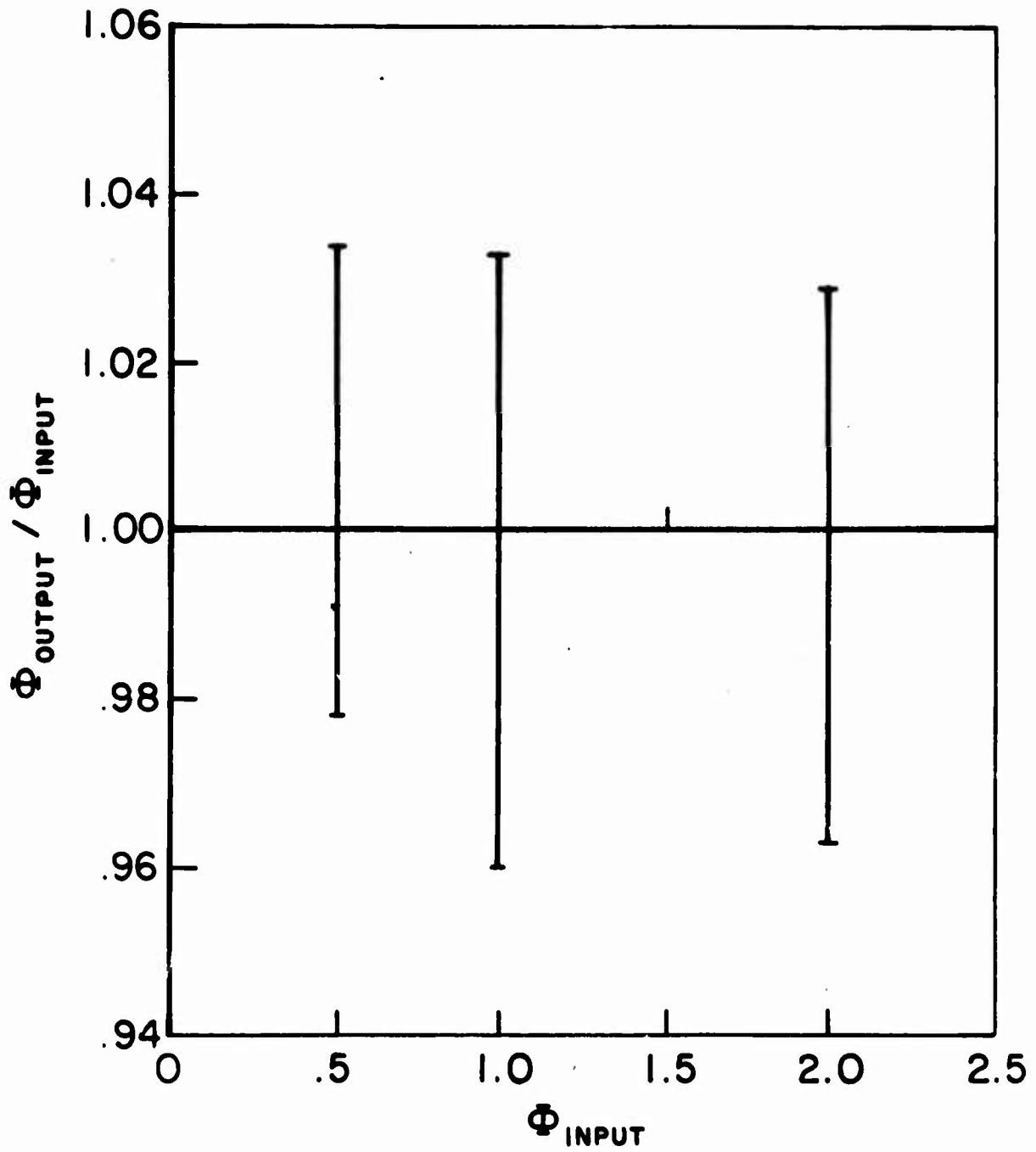


FIGURE 5

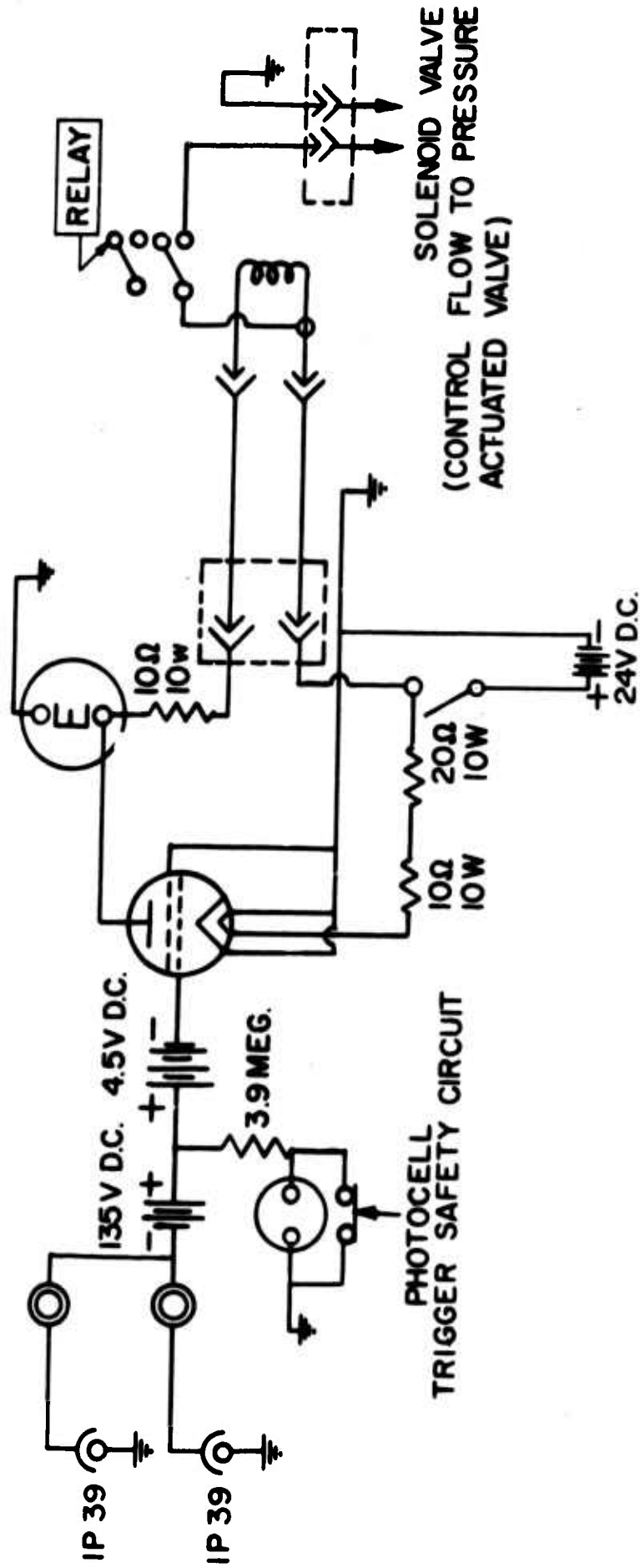
MIXING CHAMBER SECTION



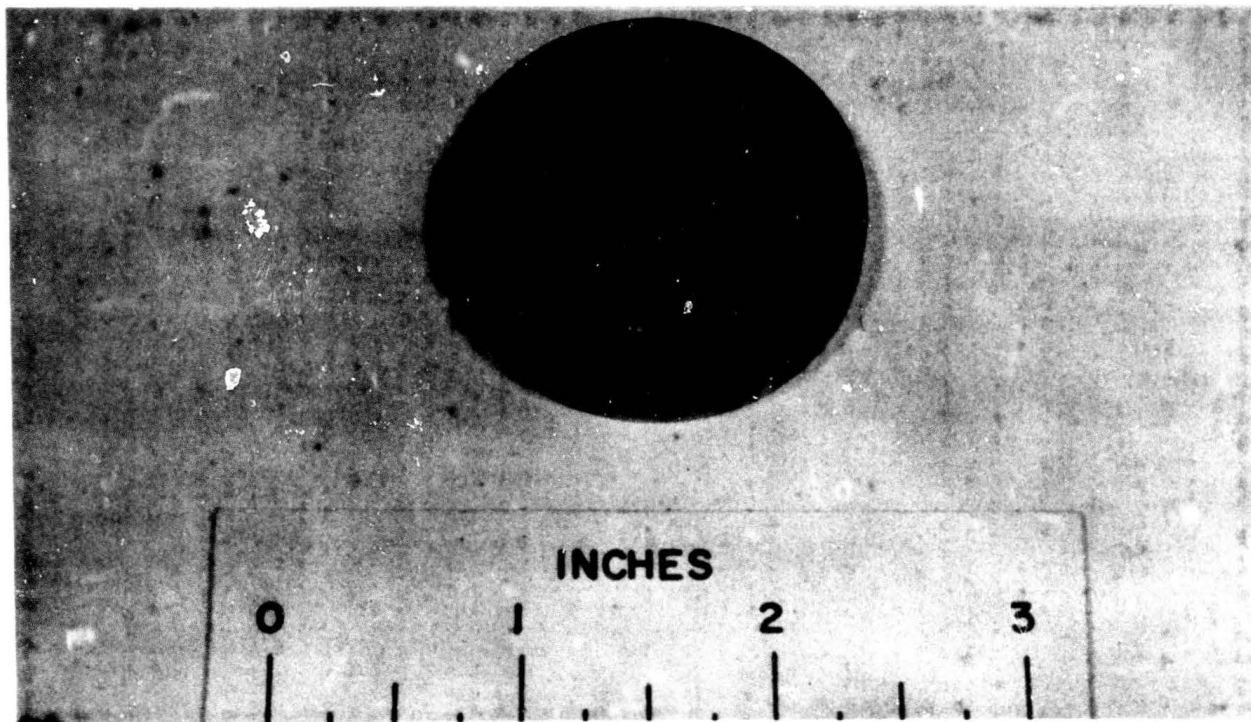
RATIO OF THE EQUIVALENCE RATIO MEASURED  
 DOWNSTREAM FROM MIXING CHAMBER ( $\Phi_{\text{OUTPUT}}$ )  
 TO THE EQUIVALENCE RATIO SUPPLIED TO  
 THE MIXING CHAMBER ( $\Phi_{\text{INPUT}}$ ) FOR SEVERAL  
 VALUES OF  $\Phi_{\text{INPUT}}$ : NO INJECTOR

JP13-4074-65

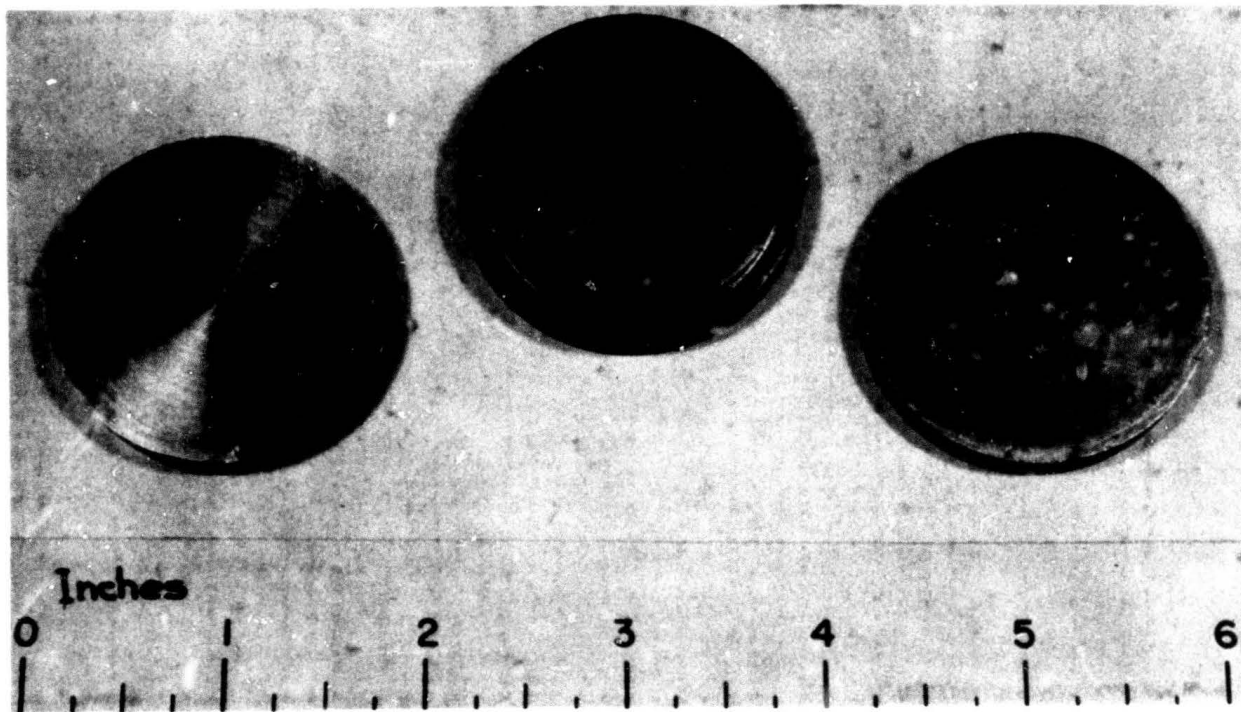
FIGURE 6



FLASHBACK SHUTDOWN SYSTEM  
(WIRING SCHEMATIC)



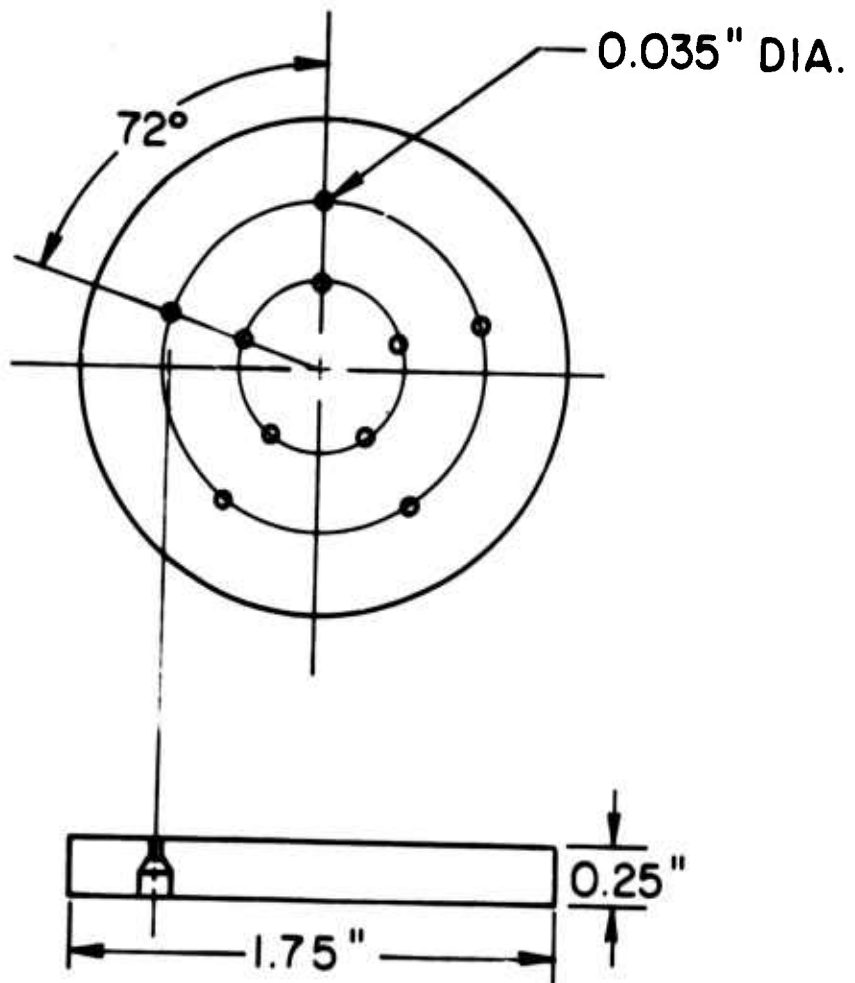
POROUS PLUG INJECTOR



SHOWERHEAD INJECTORS

JP13 P29 66

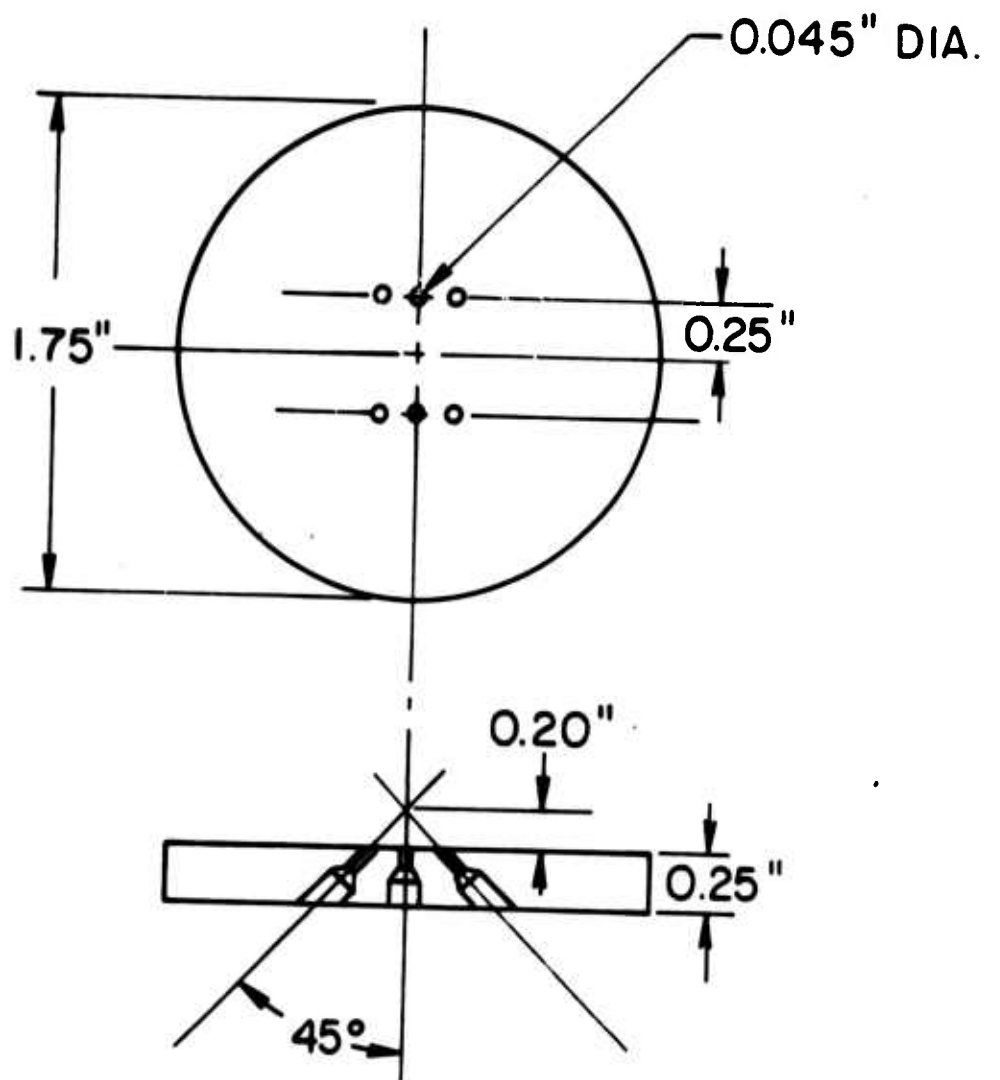
FIGURE 8



SCHEMATIC OF 10-HOLE SHOWERHEAD INJECTOR

JP13-4070-65

FIGURE 9

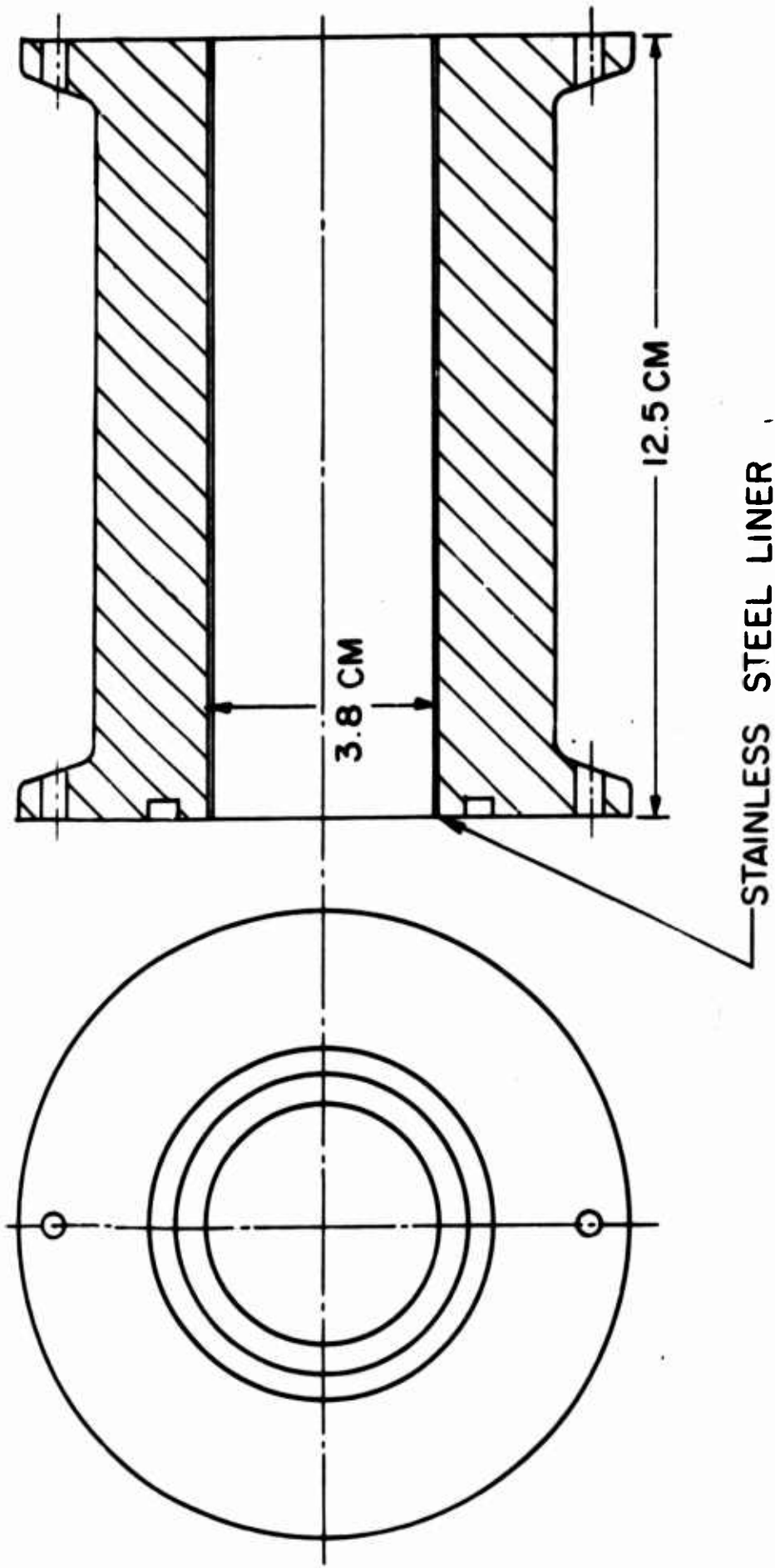


SCHEMATIC OF IMPINGING INJECTOR

JP13-4071-65

FIGURE 10

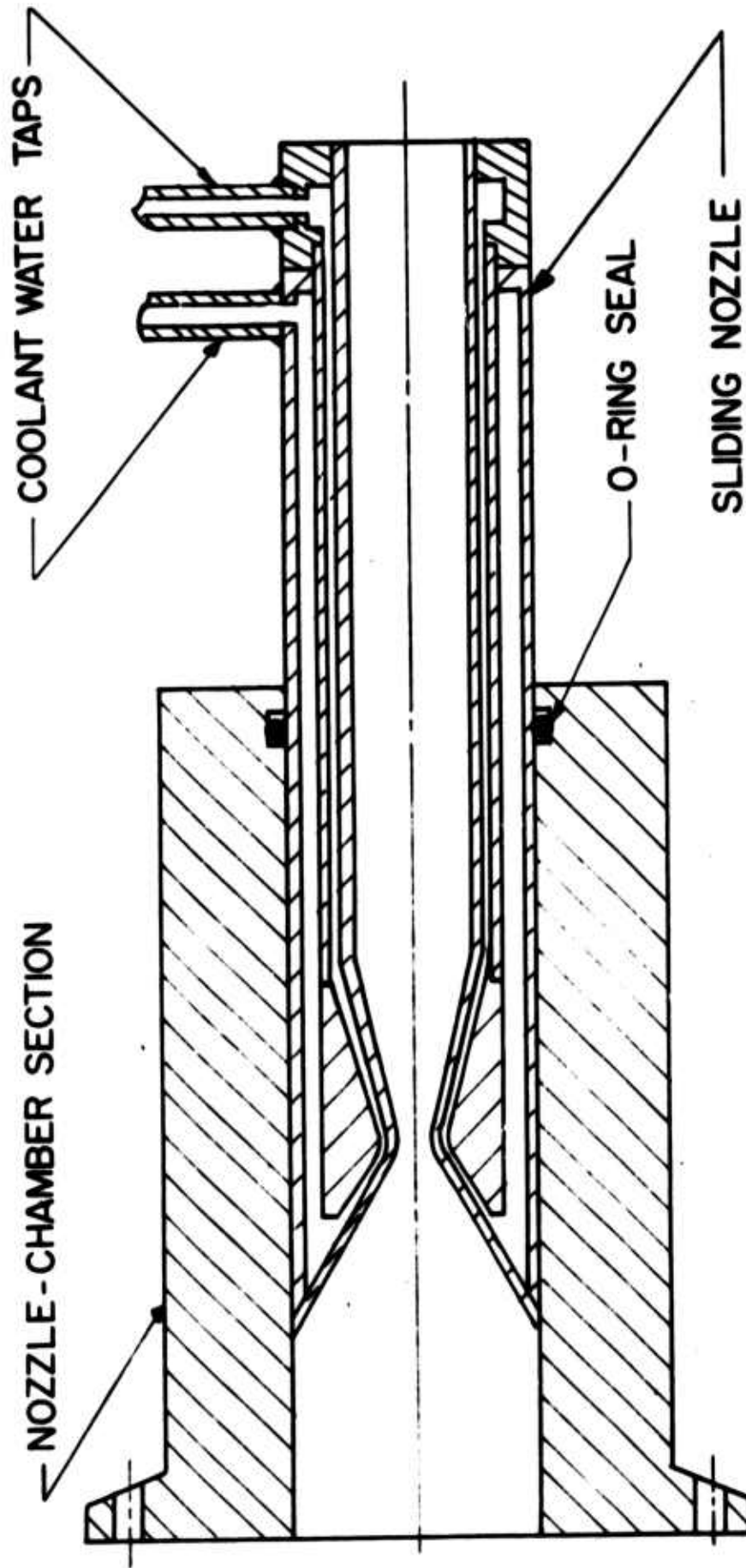
JPR 1088 a



TYPICAL COMBUSTION CHAMBER SECTION

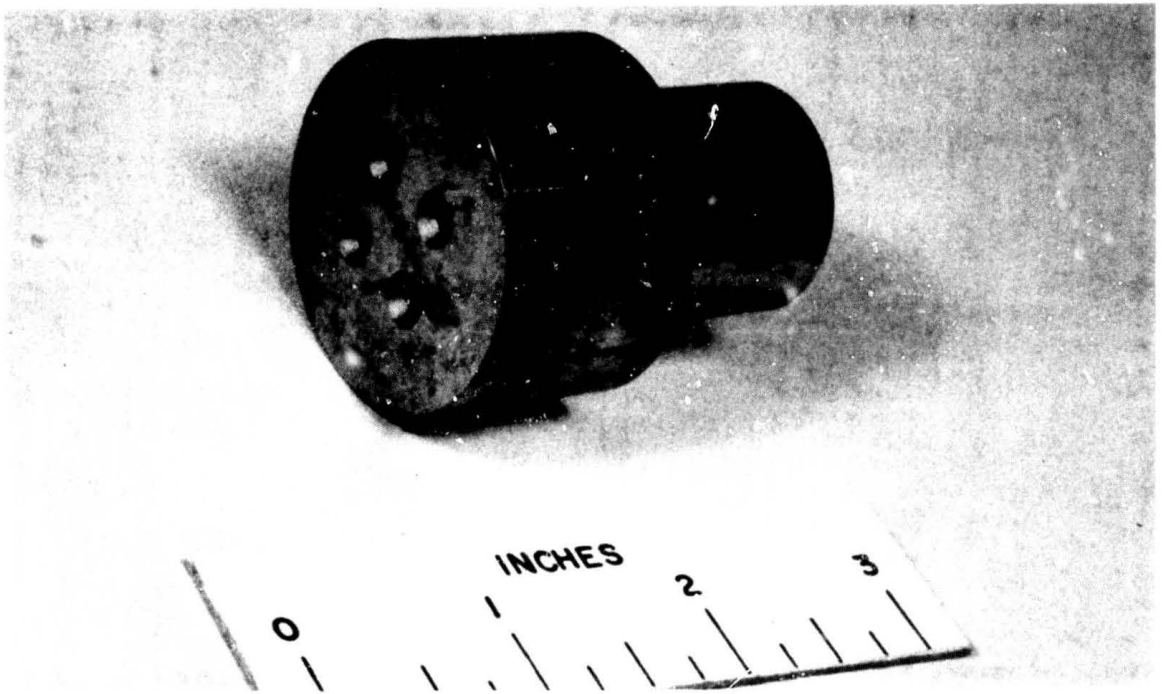
FIGURE 11

JPR 1087 a

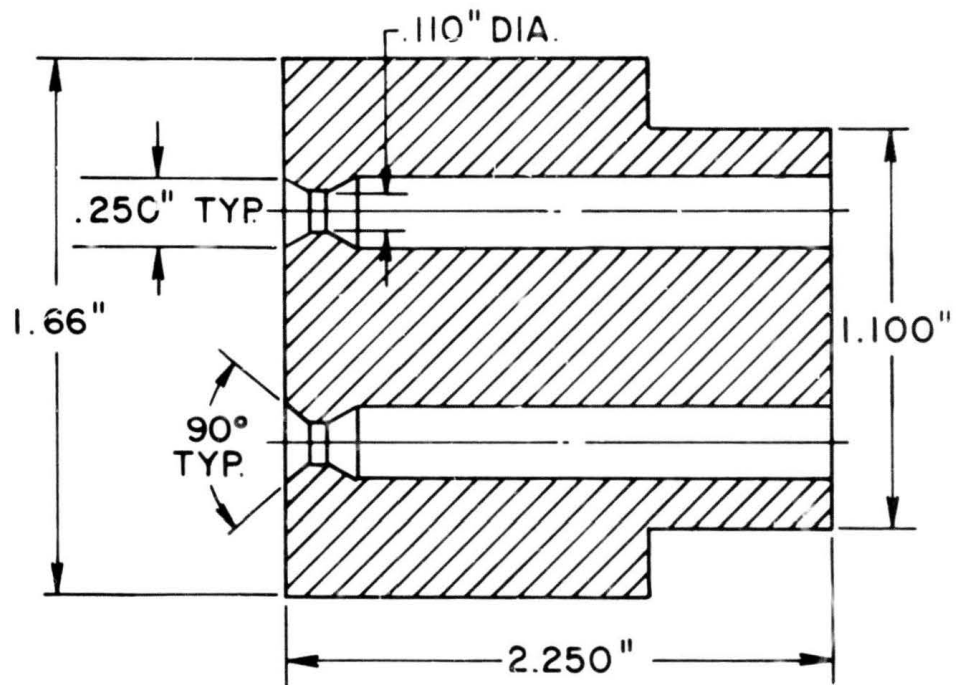


WATER - COOLED CONVERGING - DIVERGING EXHAUST NOZZLE

FIGURE 12



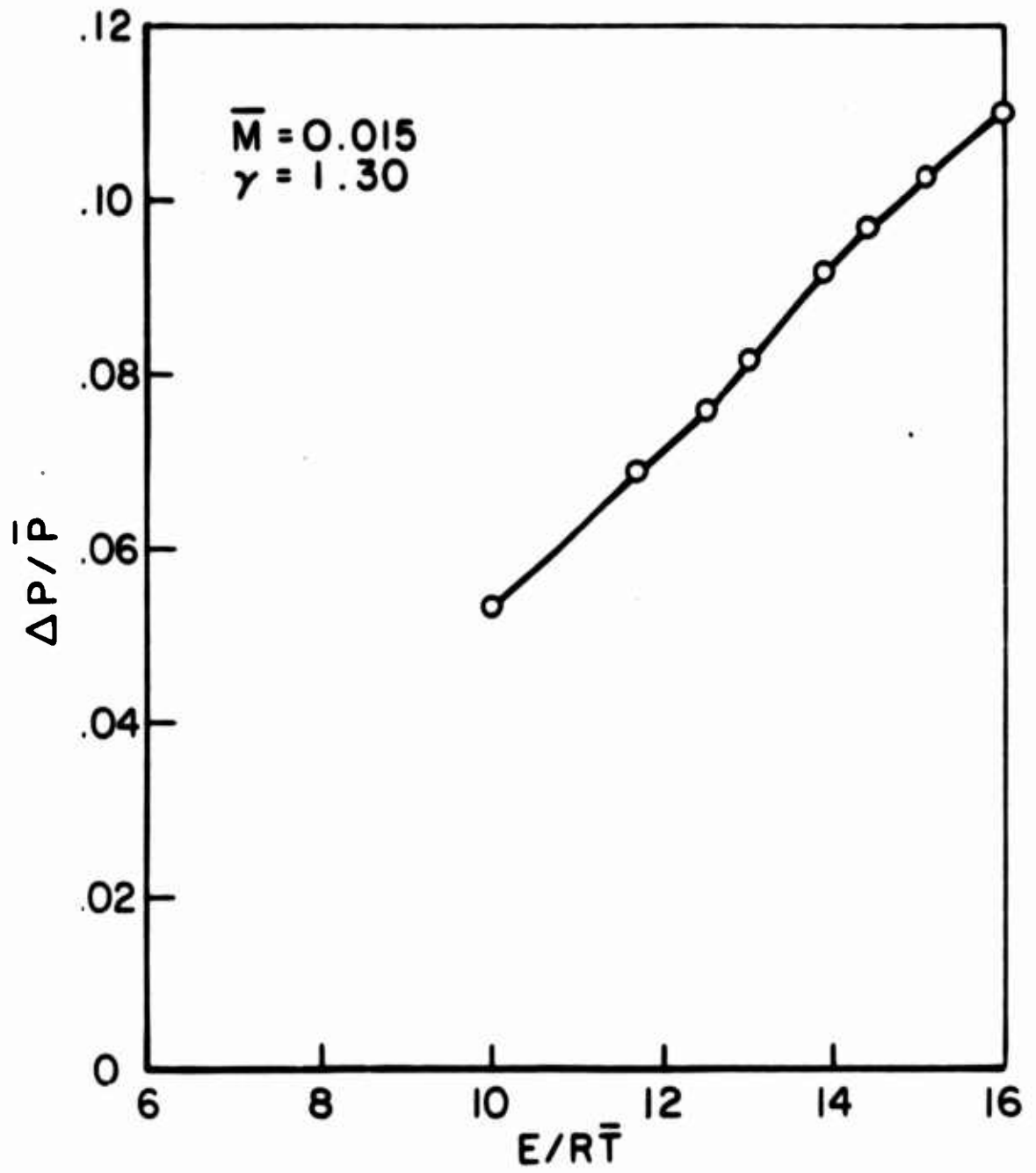
PHOTOGRAPH OF PLUG NOZZLE



SCHEMATIC OF PLUG NOZZLE

JP13 - P15 - 65

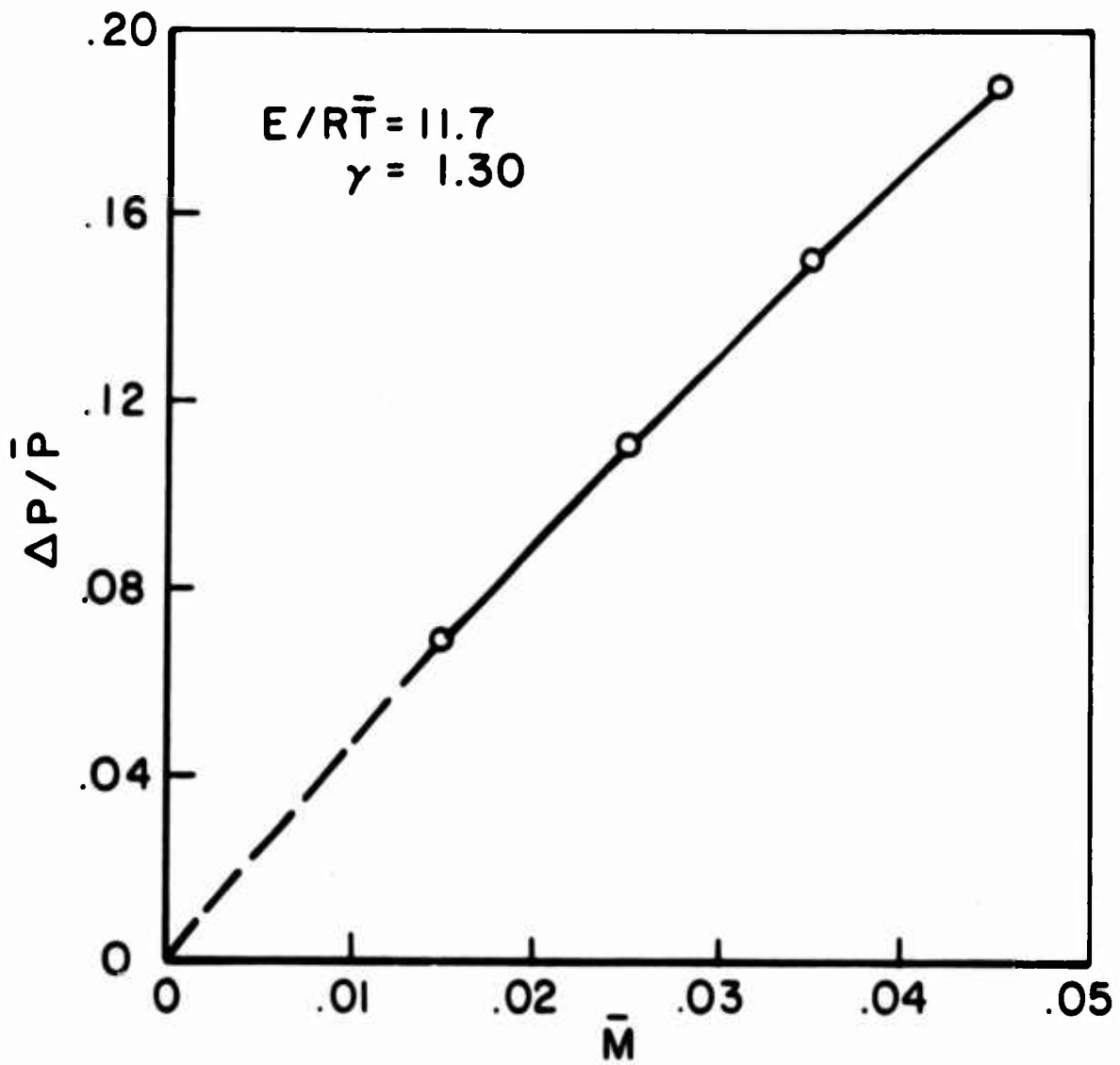
FIGURE 13



THEORETICAL DEPENDENCE OF SHOCK STRENGTH  
ON  $E/R\bar{T}$  FOR CONSTANT  $\bar{M}$

JP13-4073-65

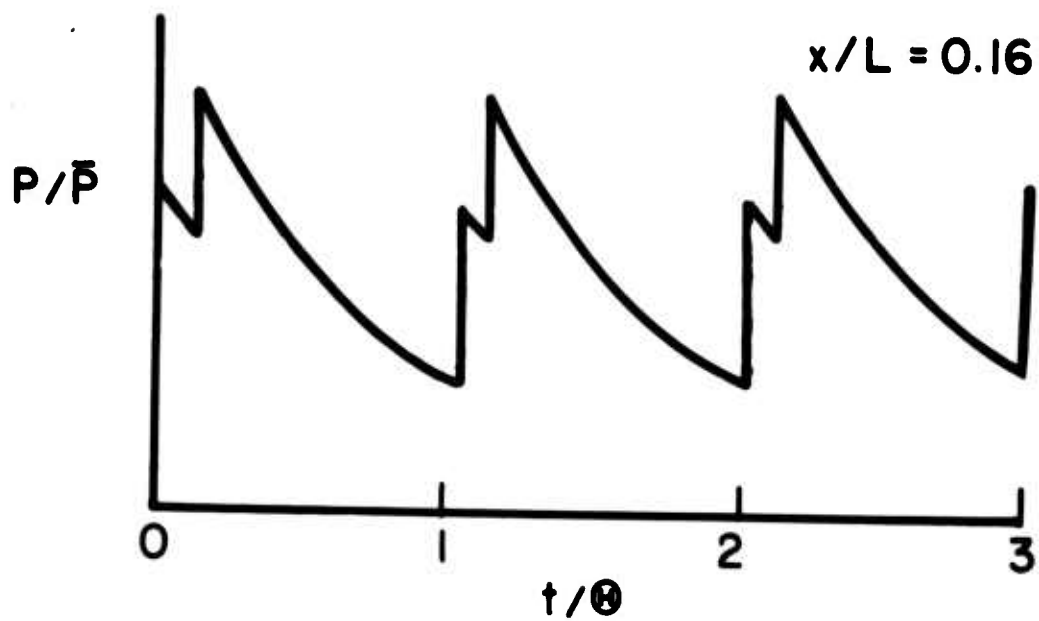
FIGURE 14



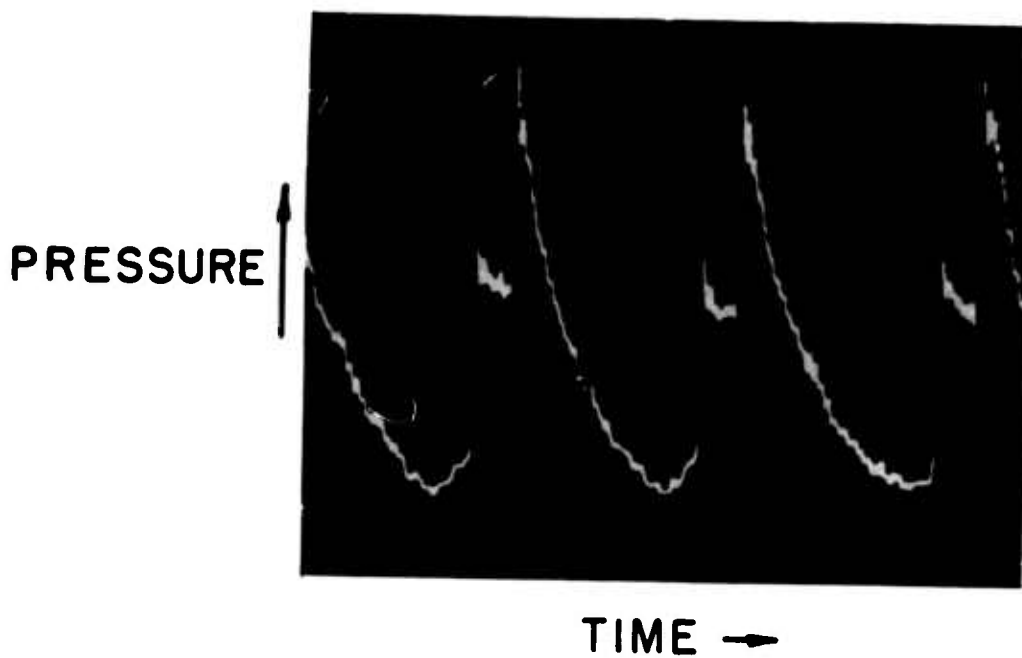
THEORETICAL DEPENDENCE OF SHOCK STRENGTH  
ON  $\bar{M}$  FOR CONSTANT  $E/RT̄$

JP13-4072-65

FIGURE 15



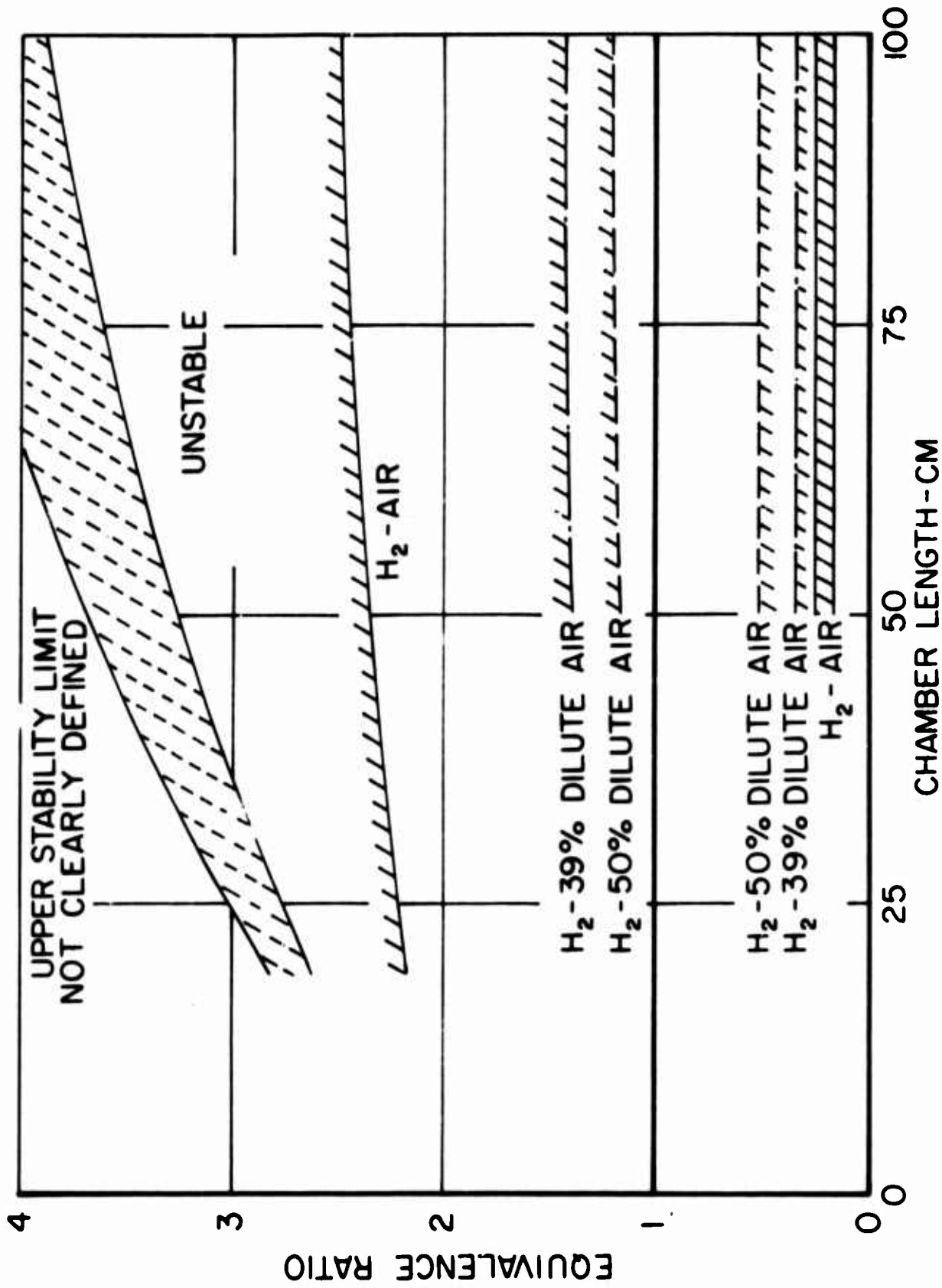
A - TYPICAL THEORETICAL PRESSURE - TIME HISTORY (REFERENCE 23)



B - TYPICAL EXPERIMENTAL PRESSURE - TIME HISTORY: FUNDAMENTAL MODE (x/L = 0.16)

JP3-P21-66

JP13-4085-65



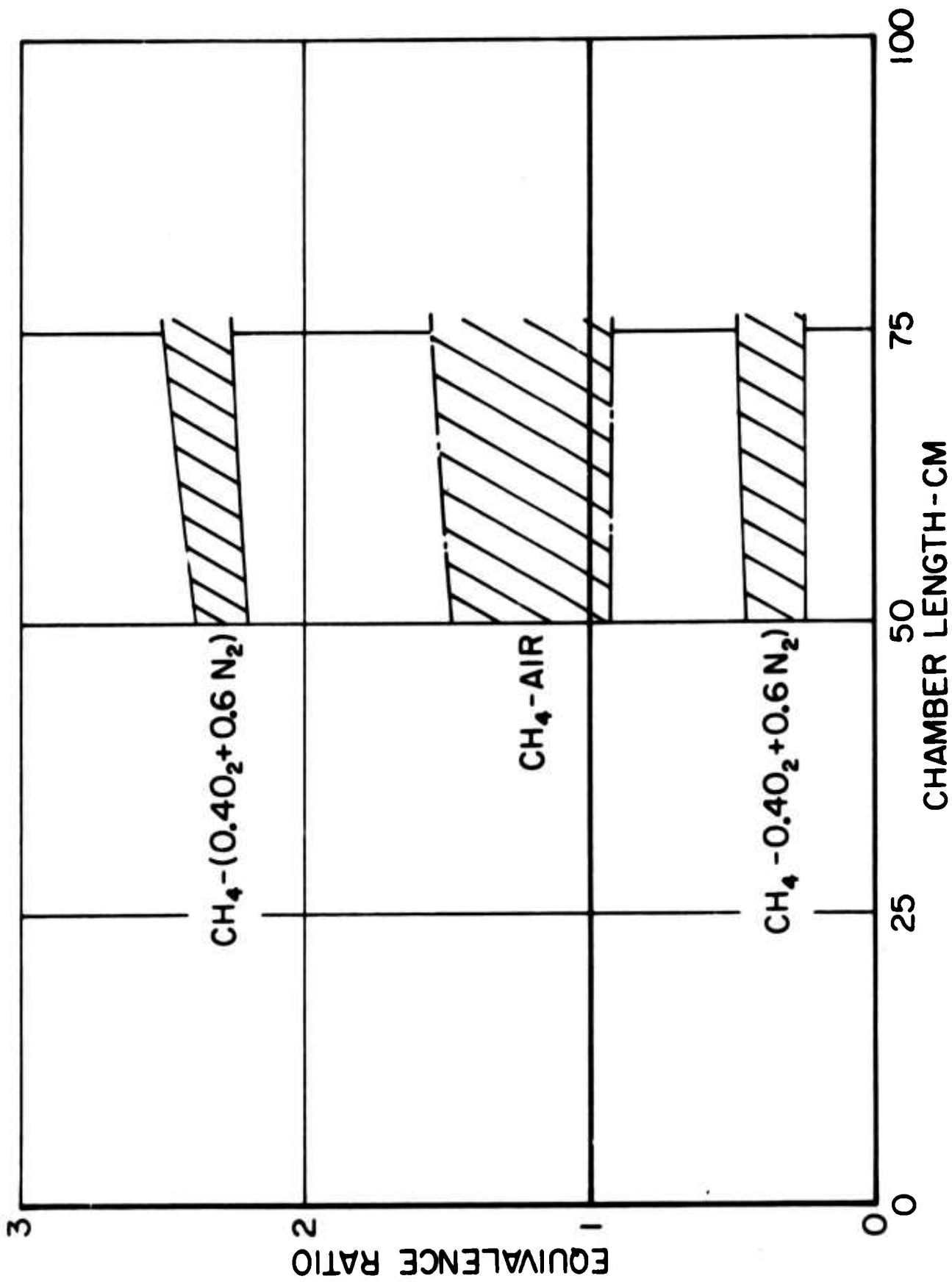
REGIONS OF UNSTABLE COMBUSTION IN THE  $\Phi$ -L PLANE FOR  
H<sub>2</sub>-AIR AND H<sub>2</sub>-DILUTE AIR -  $\bar{P} = 7.8$  ATM

FIGURE 17

CHAMBER LENGTH (CM)	% DILUENT	$\Phi$ LIMIT	$\bar{T}_{\text{AVERAGE}}$ ( $^{\circ}\text{K}$ )	$T_{\text{ADIABATIC}}$ ( $^{\circ}\text{K}$ )
104	0	2.47	1405 $\pm$ 25	2422
104	39	1.46	1413	1838
104	50	1.22	1416	1641
104	0	0.25	1398 $\pm$ 15	2422
104	39	0.32	1382	1838
104	50	0.52	1385	1641
53	0	2.35	1466	2422
53	39	1.40	1457	1838
53	0	0.26	1435 $\pm$ 40	2422
53	39	0.34	1410	1838

MEAN COMBUSTION TEMPERATURE AT THE STABILITY LIMITS FOR HYDROGEN-AIR AND  
HYDROGEN-DILUTE AIR:  $P = 7.8$  ATM, 31-HOLE SHOWERHEAD INJECTOR

JP13-4084-65



REGIONS OF UNSTABLE COMBUSTION IN THE  $\Phi$ -L PLANE FOR  
CH<sub>4</sub> - DILUTE OXYGEN AND CH<sub>4</sub> - AIR -  $\bar{P} = 7.8$  ATM

FIGURE 19

CHAMBER LENGTH (CM)	OXIDIZER	$\Phi$ LIMIT	$\bar{T}_{\text{AVERAGE}}$ ( $^{\circ}\text{K}$ )	$\bar{T}_{\text{ADIABATIC}}$ ( $^{\circ}\text{K}$ )
76	$0.4\text{O}_2 + 0.6\text{N}_2$	2.25	$2050 \pm 35$	2854
76	$0.4\text{O}_2 + 0.6\text{N}_2$	0.55	2076	2854
53	$0.4\text{O}_2 + 0.6\text{N}_2$	2.20	$2060 \pm 20$	2854
53	$0.4\text{O}_2 + 0.6\text{N}_2$	0.55	2072	2854
76	AIR	-	2102	2239

MEAN COMBUSTION TEMPERATURE AT THE STABILITY LIMITS FOR METHANE-DILUTE OXYGEN AND METHANE-AIR: P= 7.8 ATM, 49-HOLE SHOWERHEAD INJECTOR

FIGURE 20

PROP.	$\bar{T}_{AV}$ ( $^{\circ}K$ )	$(E/RT)_{LIMIT}$	$E_{LIM}$ (KCAL/MOLE)	EQUATION	$E_{ACT}$ (KCAL/MOLE)	SOURCE
H <sub>2</sub> -AIR	1459	4.95	14.2	(3-4)	37.8	(35)
		9.90	28.4	(4-6)		
H <sub>2</sub> -39% DIL. AIR	1436	4.95	14.1	(3-4)	37.8	(35)
		9.90	28.2	(4-6)		
CH <sub>4</sub> -O <sub>2</sub> -N <sub>2</sub>	2050	5.85	23.6	(3-4)	44.46	(36)
		11.70	47.2	(4-6)		

COMPARISON OF  $E_{LIMIT}$  WITH  $E_{ACT}$  FOR VARIOUS PROPELLANT COMBINATIONS

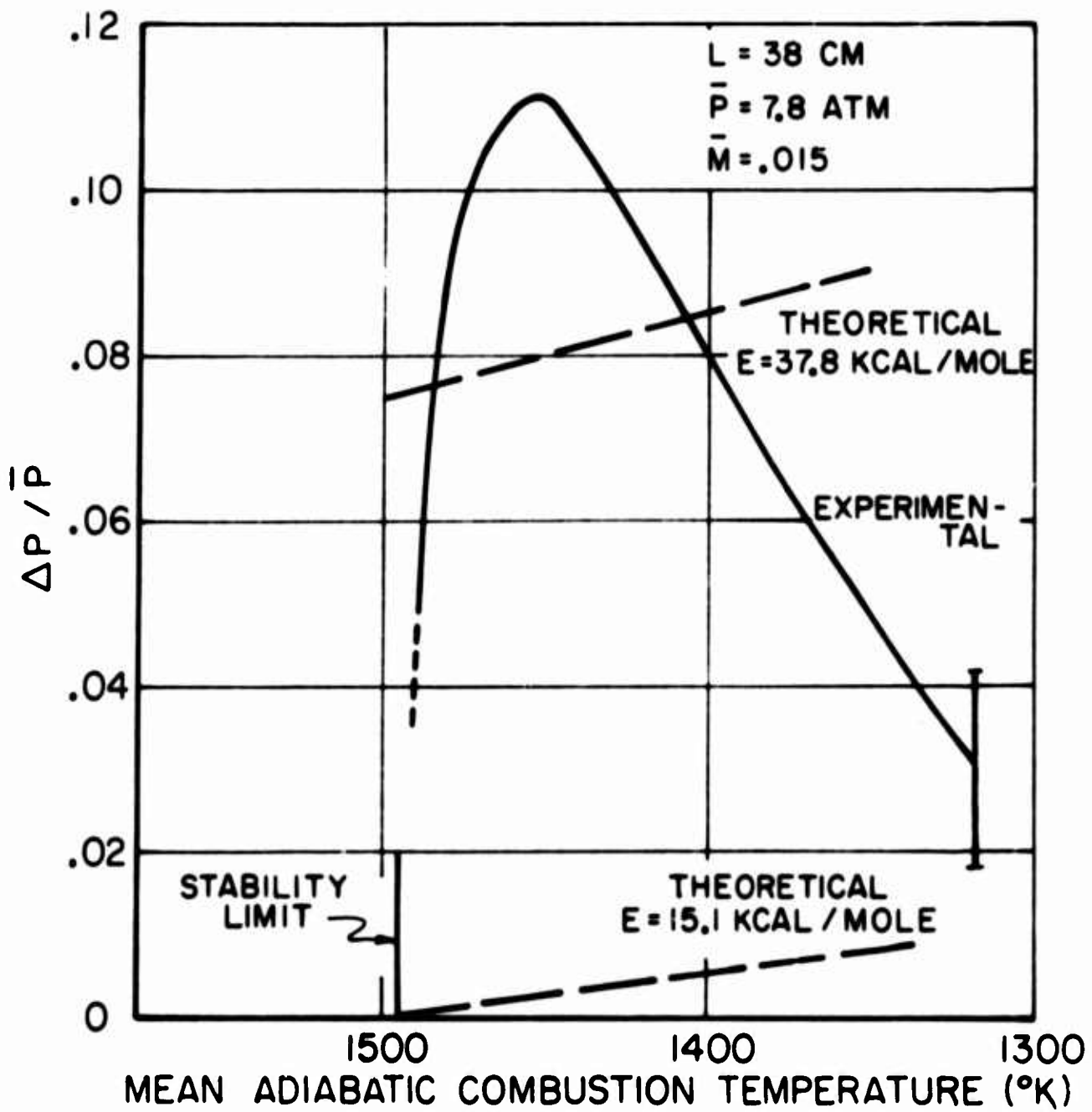
REACTION	$\Phi$ LIMIT	$\bar{T}_{CRIT}$ ( $^{\circ}K$ )	$E_{LIMIT}$ (KCAL/MOL)	EQN.	$E_{ACT}$ (KCAL/MO)	SOURCE
CO/AIR	2.35 $\pm$ .05	1173 $\pm$ 20	11.2 $\pm$ 0.2	(3-4)	20	(40)
			22.4 $\pm$ 0.2	(4-6)		24
CO/AIR/H <sub>2</sub>	2.90 $\pm$ .05	1012 $\pm$ 13	9.5 $\pm$ 0.1	(3-4)	-	-
			19.0 $\pm$ 0.1	(4-6)		

A. STABILITY LIMITS FOR CO(H<sub>2</sub>O)-AIR AND CO(H<sub>2</sub>O)-AIR-H<sub>2</sub> FOR  $\bar{P} = 7.8$  ATM,  
L = 104 CM, 49-HOLE SHOWERHEAD INJECTOR

SOURCE	THEORY + INSTAR. DATA	(4-17a) + FLAME DATA (39)	(4-17b) + RATE DATA (40)	(4-17b) + RATE DATA (40)	(4-17a) + FLAME DATA (40)
$\bar{r}_1/\bar{r}_2$ or $\bar{r}_{T1}/\bar{r}_{T2}$	0.61 $\pm$ 0.06	0.59 $\pm$ 0.09	(COMP) 0.32	(TEMP) 0.57	0.41

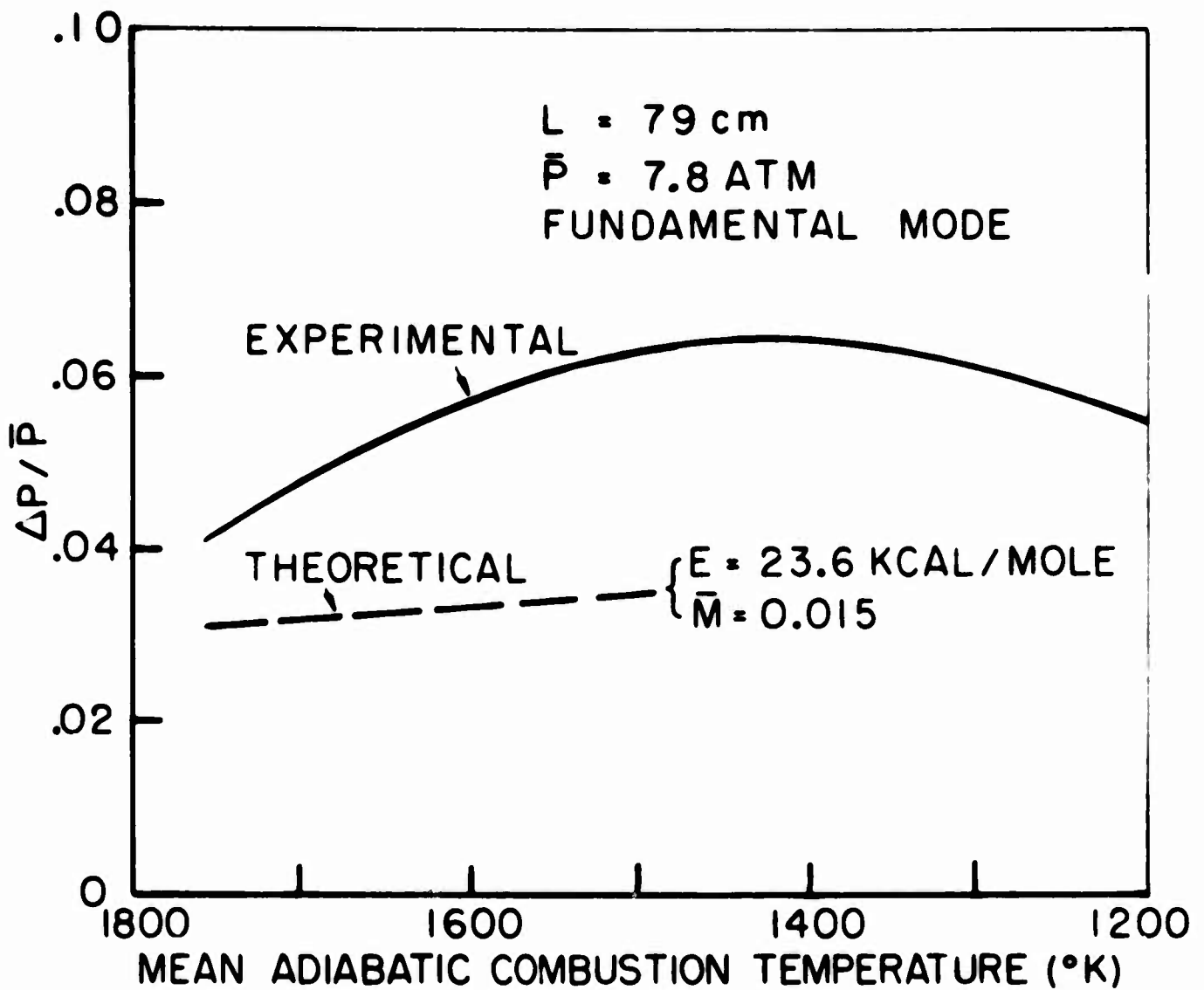
B. COMPARISON OF RESULTS OF THE SIRIGNANO-CROCCO THEORY WITH CHEMICAL  
KINETICS DATA

JP13-4089-65



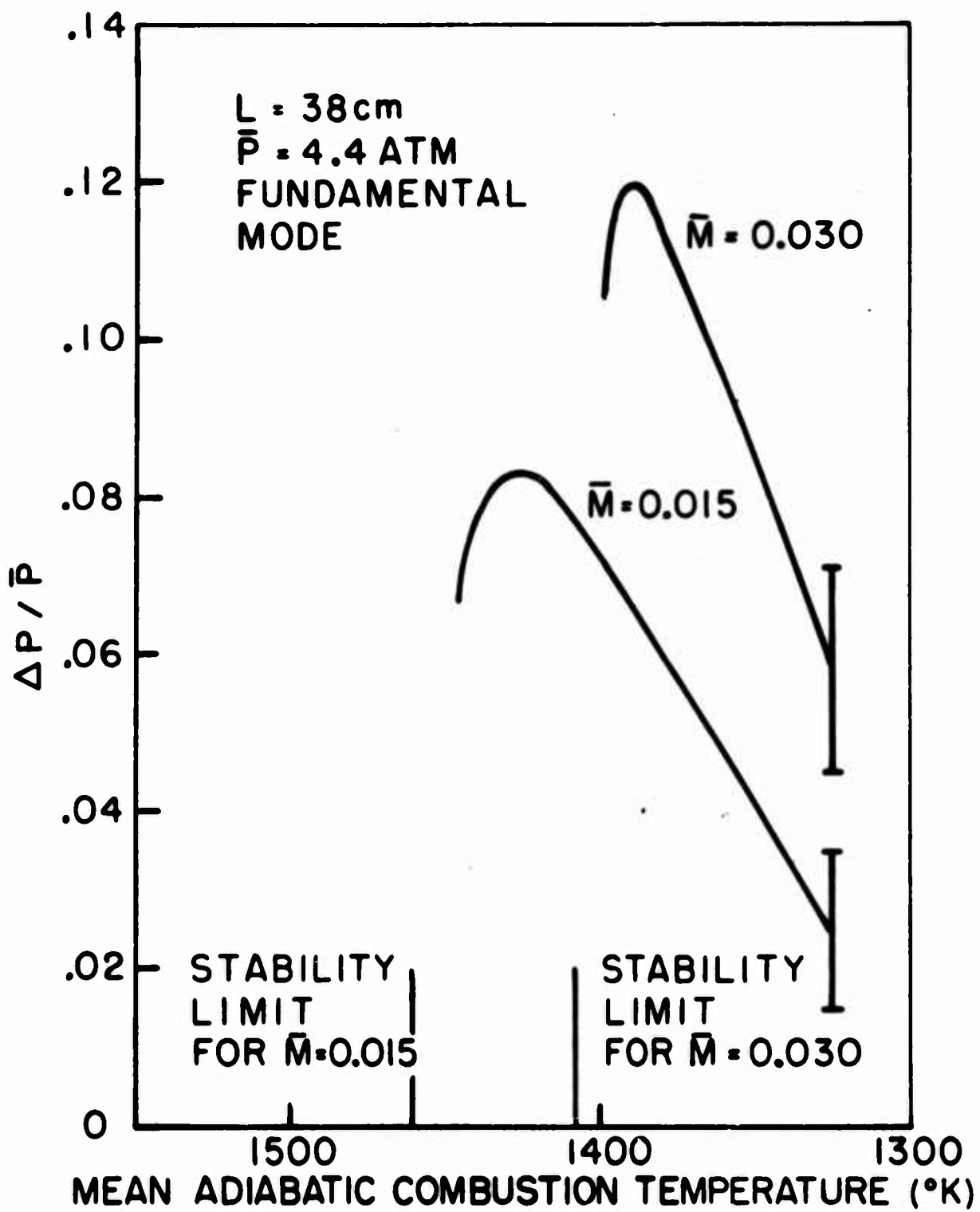
VARIATION OF  $\Delta P / \bar{P}$  WITH COMBUSTION TEMPERATURE FOR  $H_2$  -AIR

FIGURE 23



VARIATION OF  $\Delta P / \bar{P}$  WITH COMBUSTION TEMPERATURE  
 $\text{CH}_4 - (0.4\text{O}_2 + 0.6\text{N}_2)$ : DATA FROM REFERENCE 27

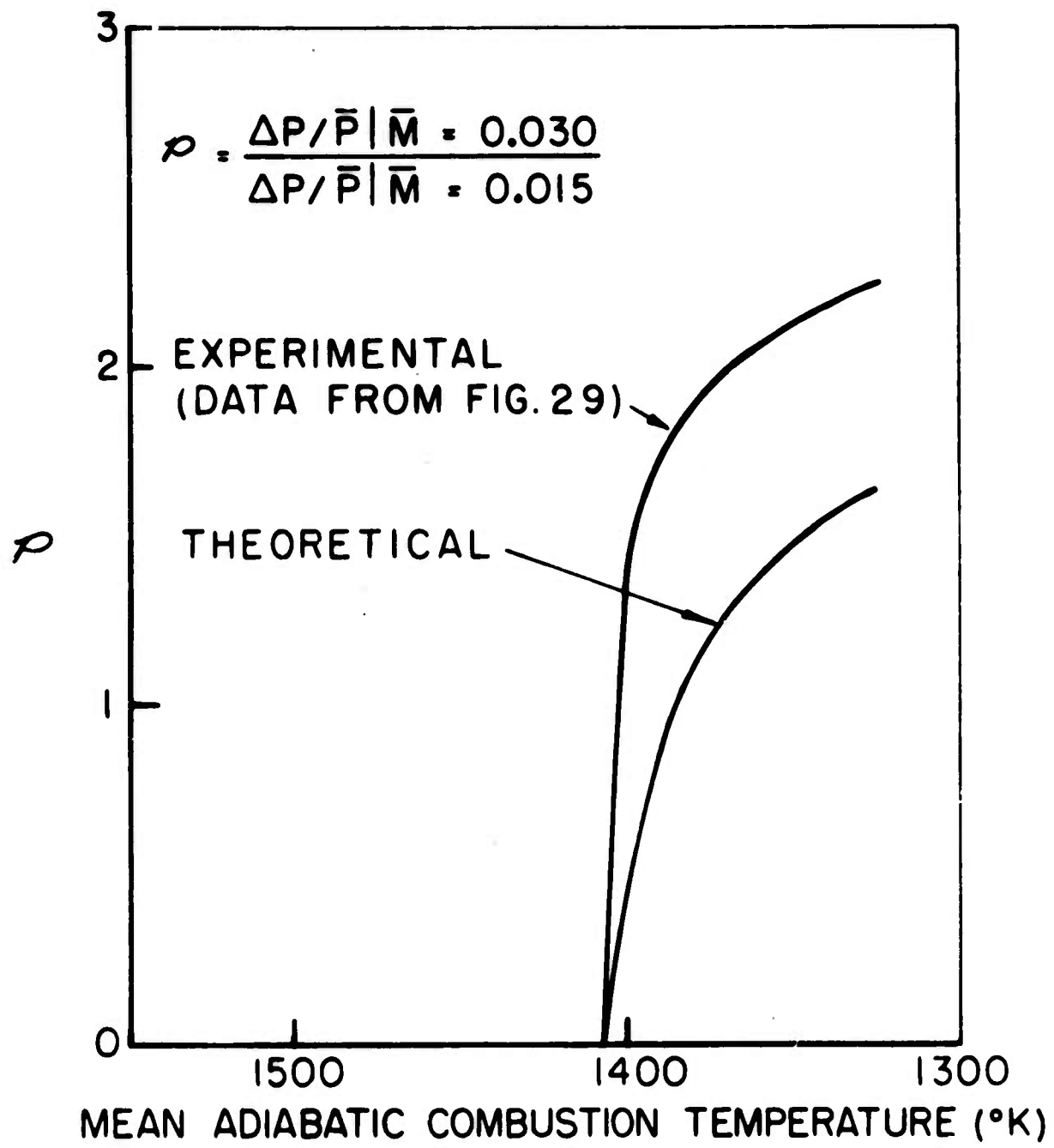
JP13-R4094-66



JPL-RES-66-66

VARIATION OF  $\Delta P / \bar{P}$  WITH COMBUSTION TEMPERATURE  
 FOR  $H_2$ -AIR AND TWO VALUES OF  $\bar{M}$

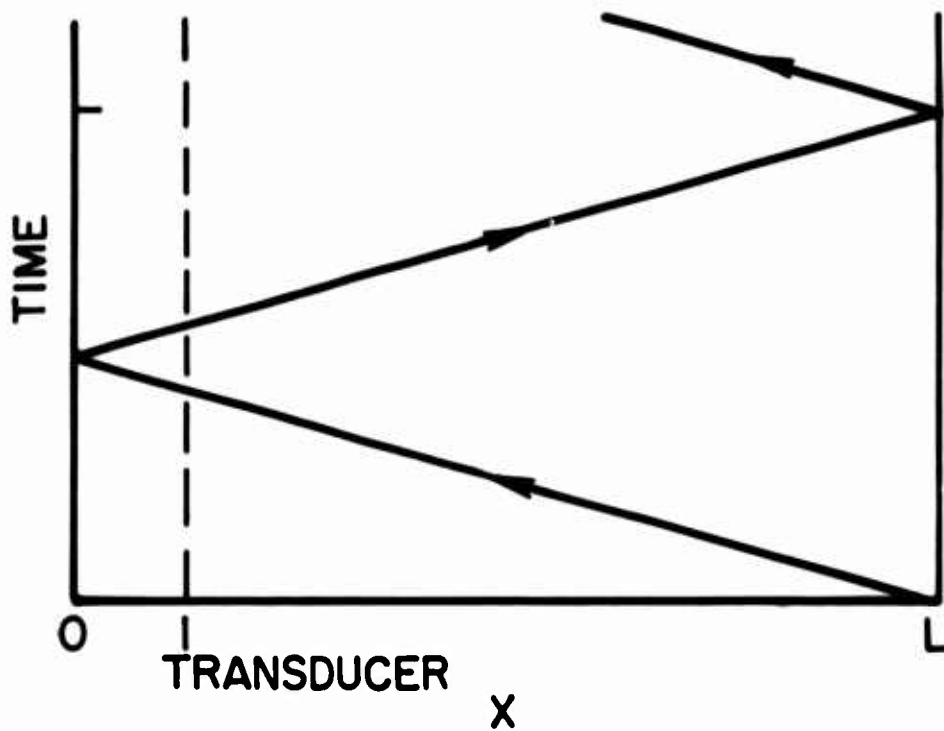
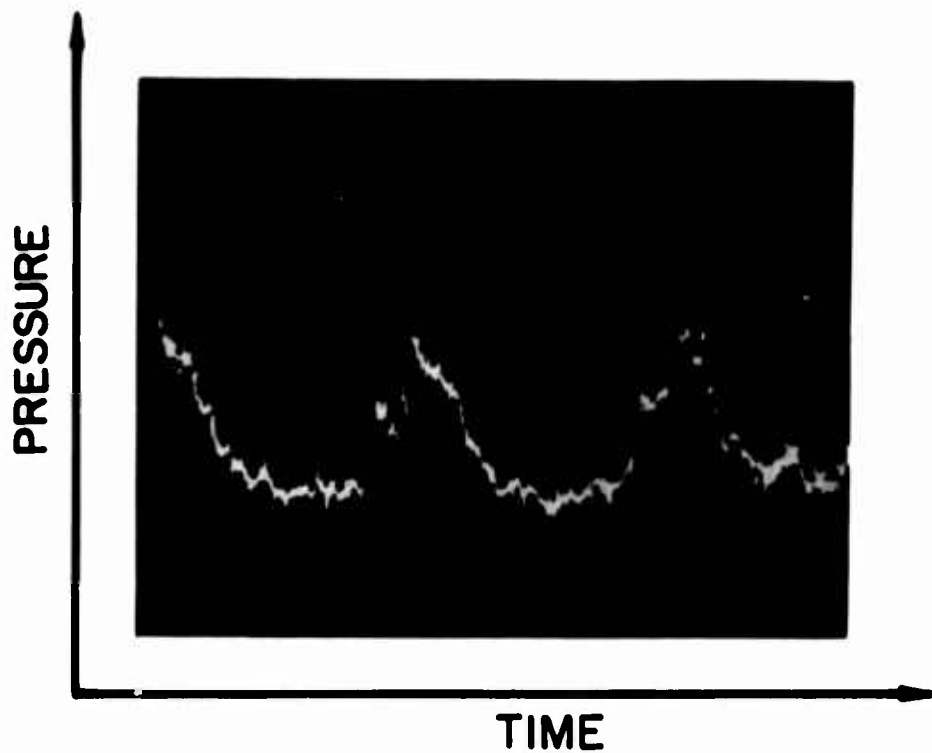
FIGURE 25



VARIATION OF THEORETICAL AND  
 EXPERIMENTAL  $\rho$  WITH COMBUSTION  
 TEMPERATURE FOR H<sub>2</sub>-AIR

FIGURE 26

JP13-R 4098-66

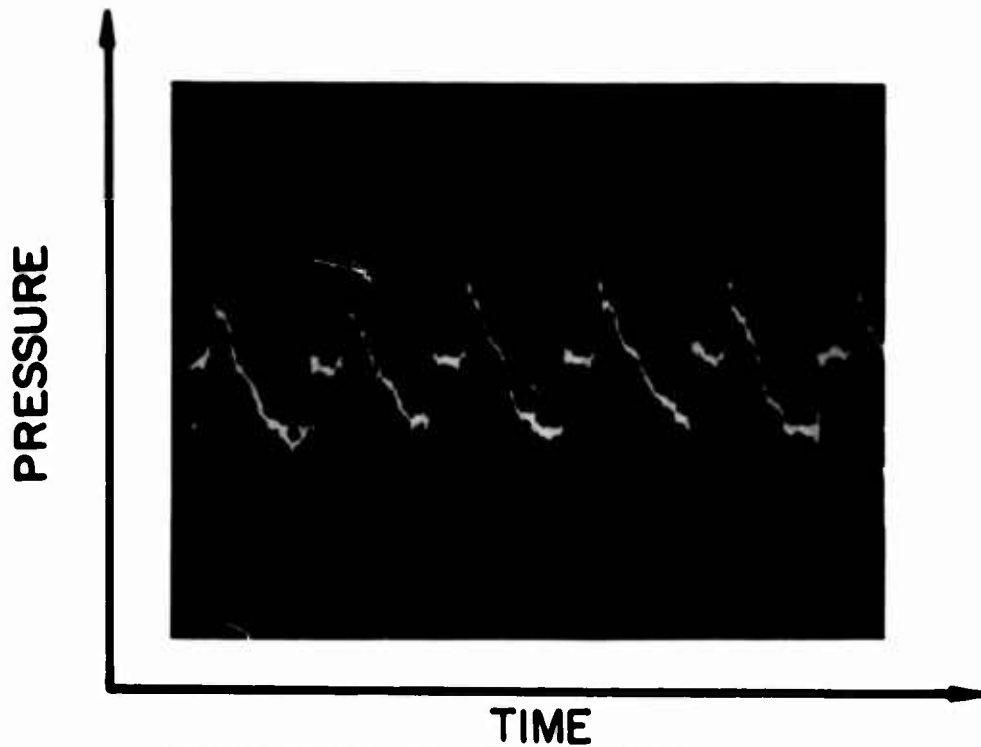


B. X-t DIAGRAM

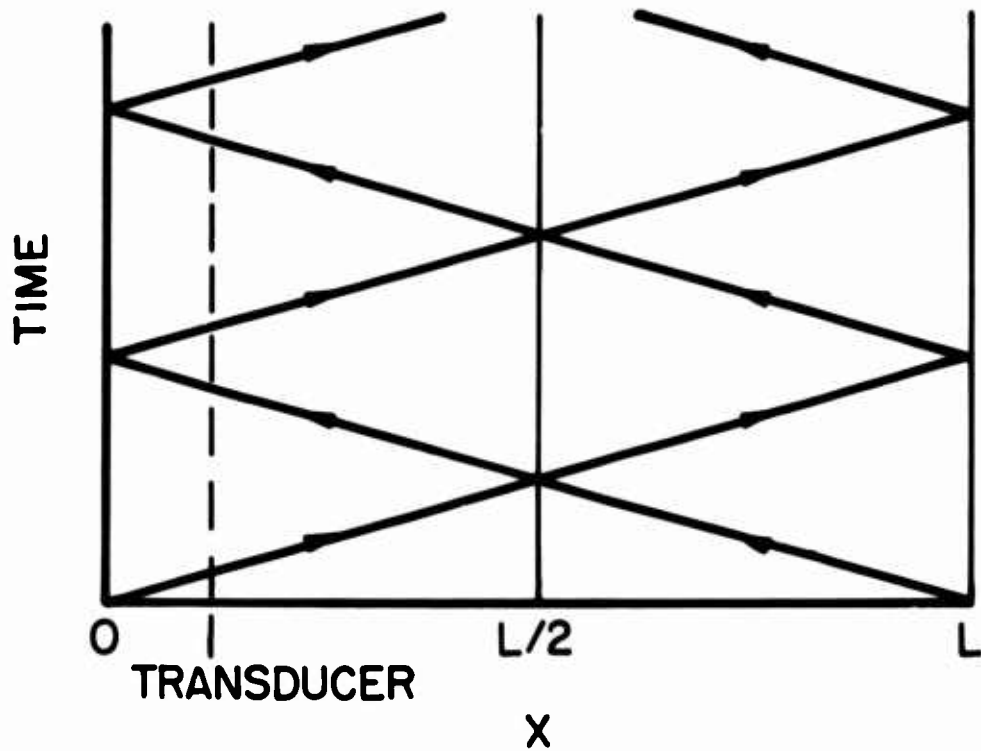
PRESSURE-TIME HISTORY AND X-t DIAGRAM FOR ONE SHOCK WAVE ( $n=1$ )

FIGURE 27

JP13-P22-66



A. PRESSURE-TIME HISTORY



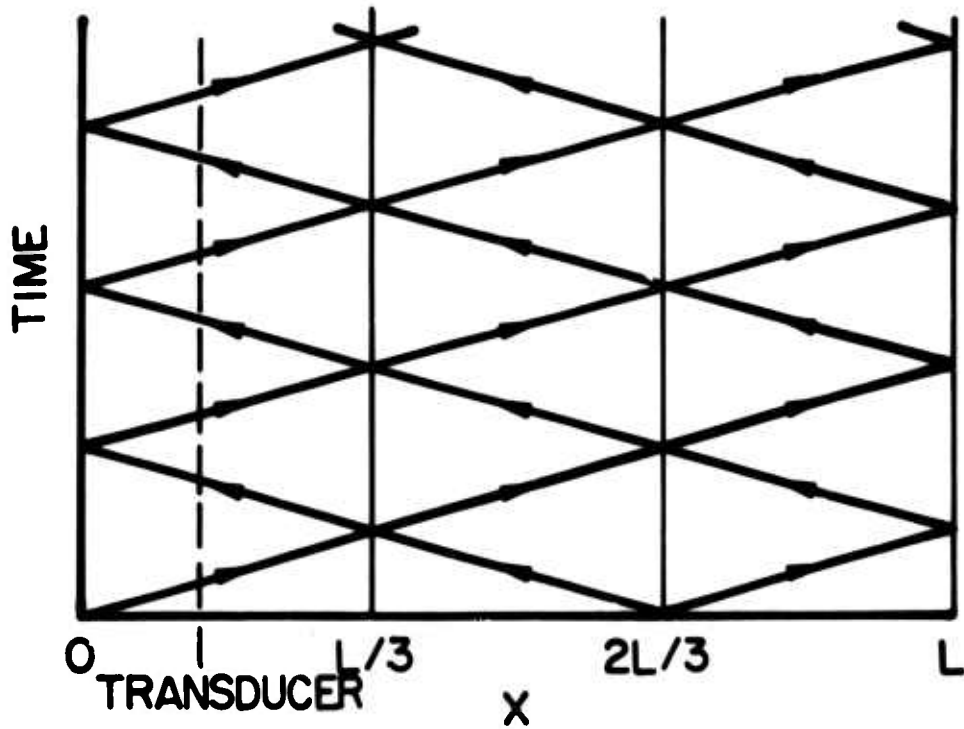
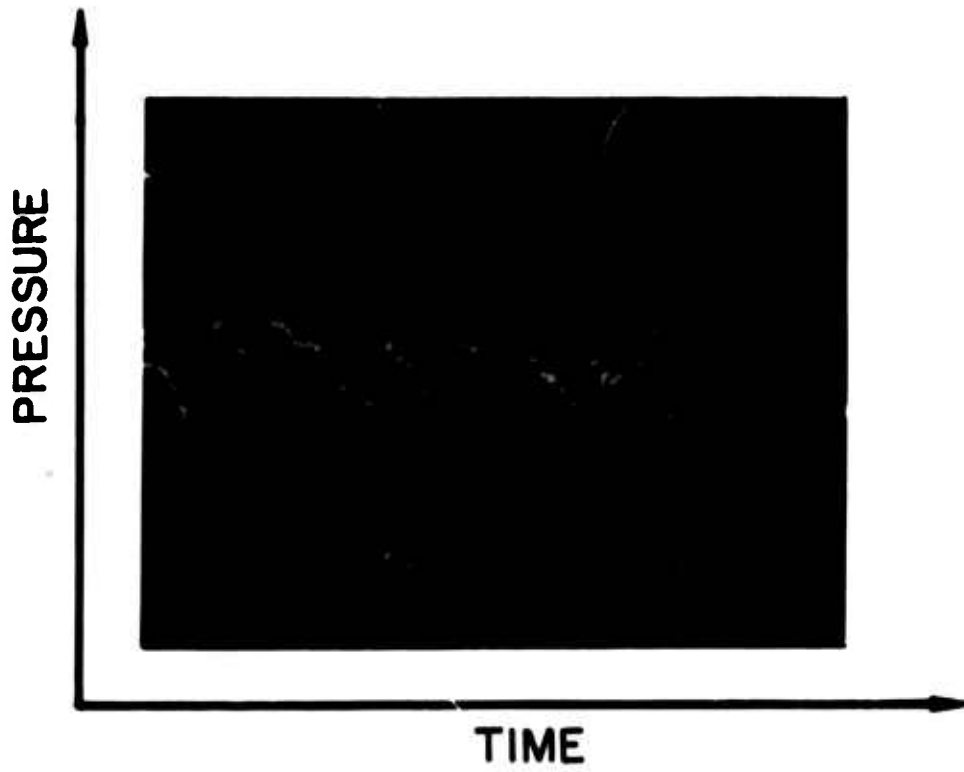
B. X-t DIAGRAM

PRESSURE-TIME HISTORY AND X-t DIAGRAM FOR TWO SHOCK WAVES ( $n=2$ )

FIGURE 28

JPI3-P23-66

1013 P-4-66



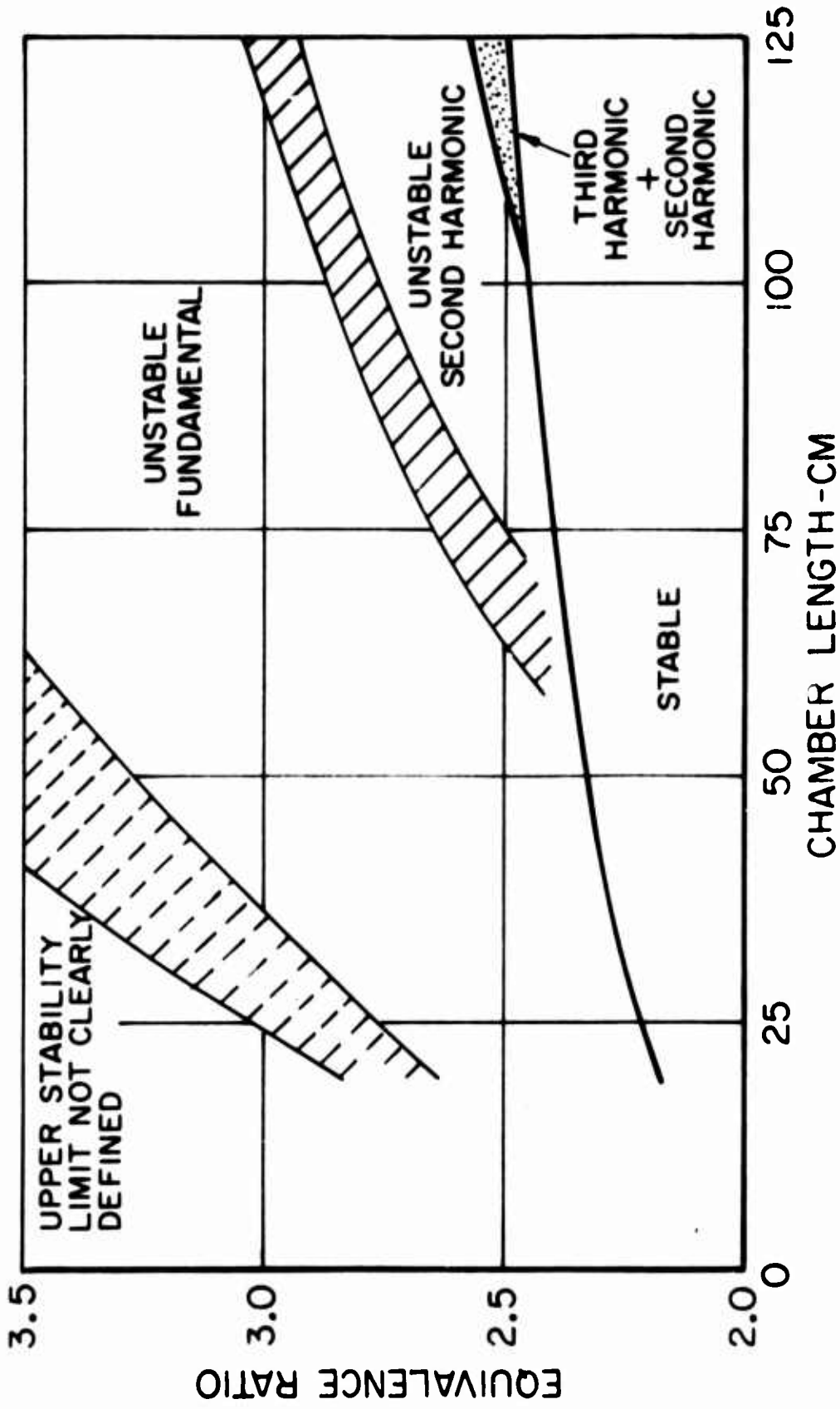
B. X-t DIAGRAM

PRESSURE-TIME HISTORY AND X-t DIAGRAM FOR THREE SHOCK WAVES ( $n=3$ )

FIGURE 29

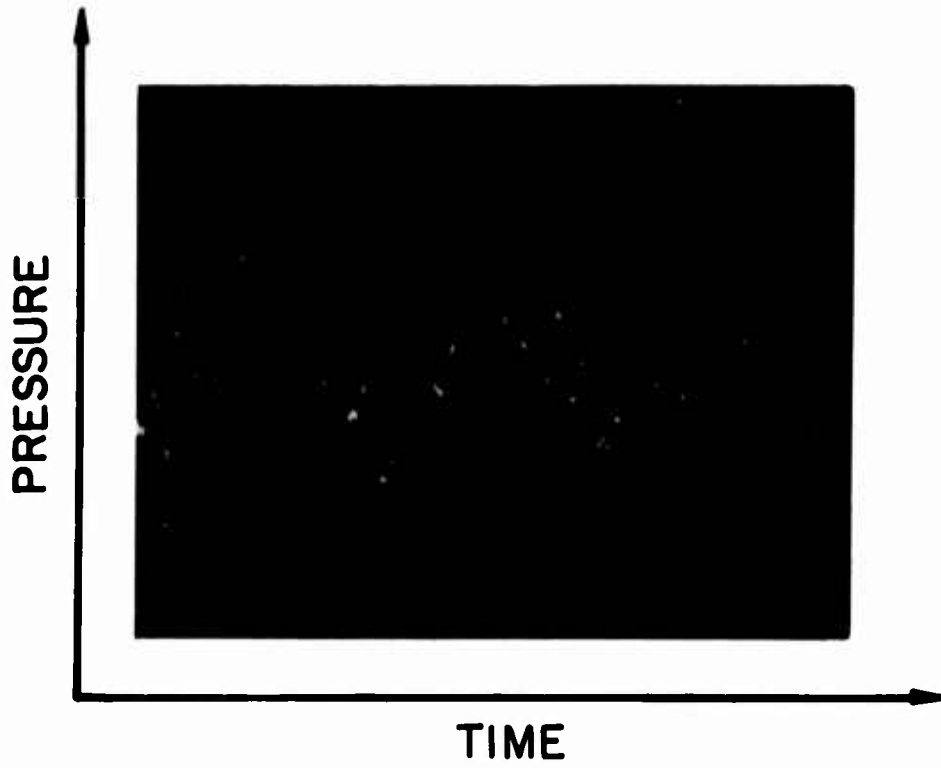
JP13-P24-66

JP13-4100-66



REGIONS OF HARMONIC MODE INSTABILITY IN THE  $\Phi$ -L PLANE FOR  $H_2$  - AIR:  
 $\bar{P}=7.8$  ATM, 31-HOLE SHOWERHEAD INJECTOR

FIGURE 30

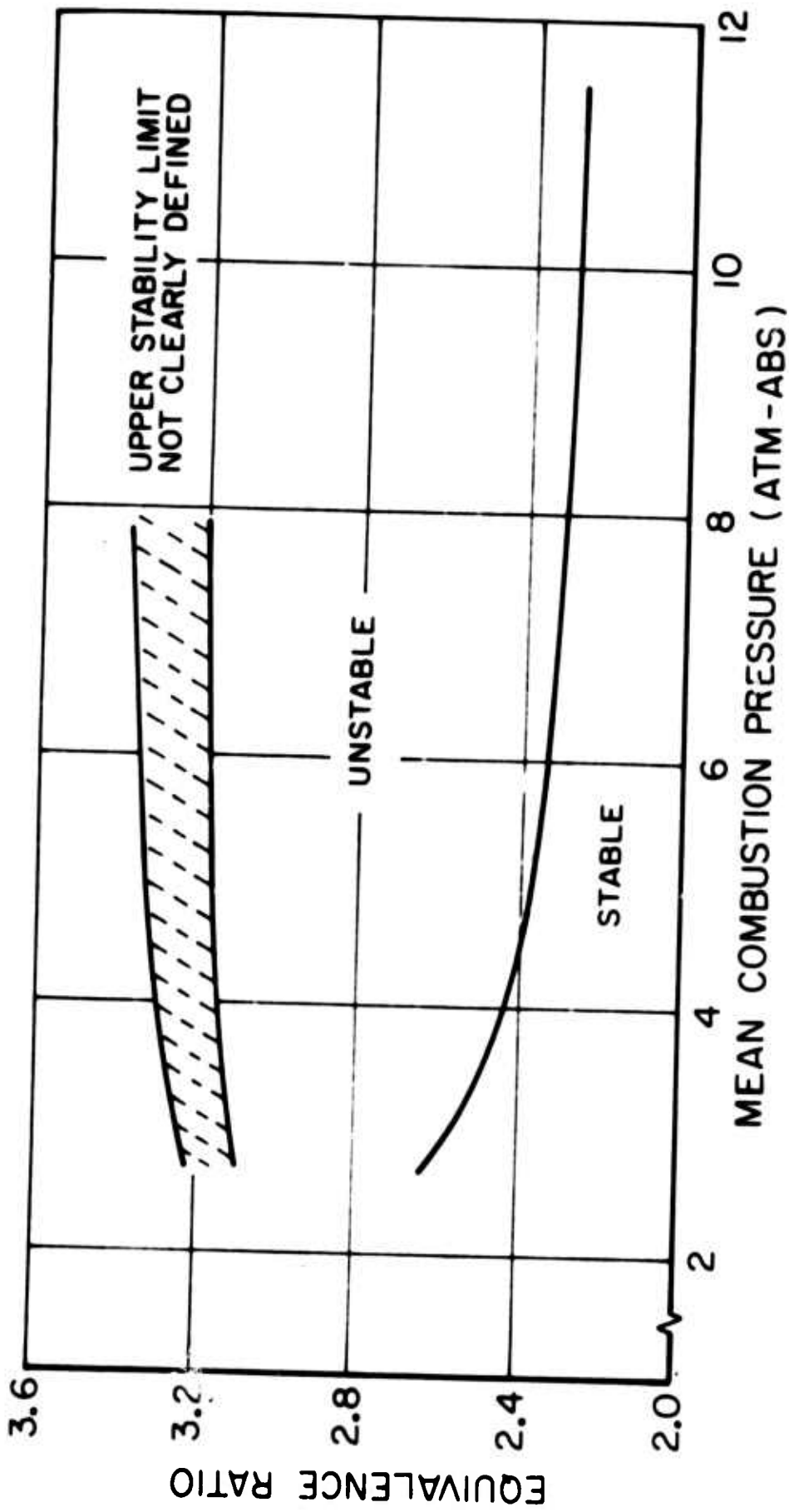


PRESSURE-TIME HISTORY SHOWING SUPERPOSITION OF  
FIRST TANGENTIAL AND LONGITUDINAL MODES

JP13-P25-66

FIGURE 31

JP13-4093-65

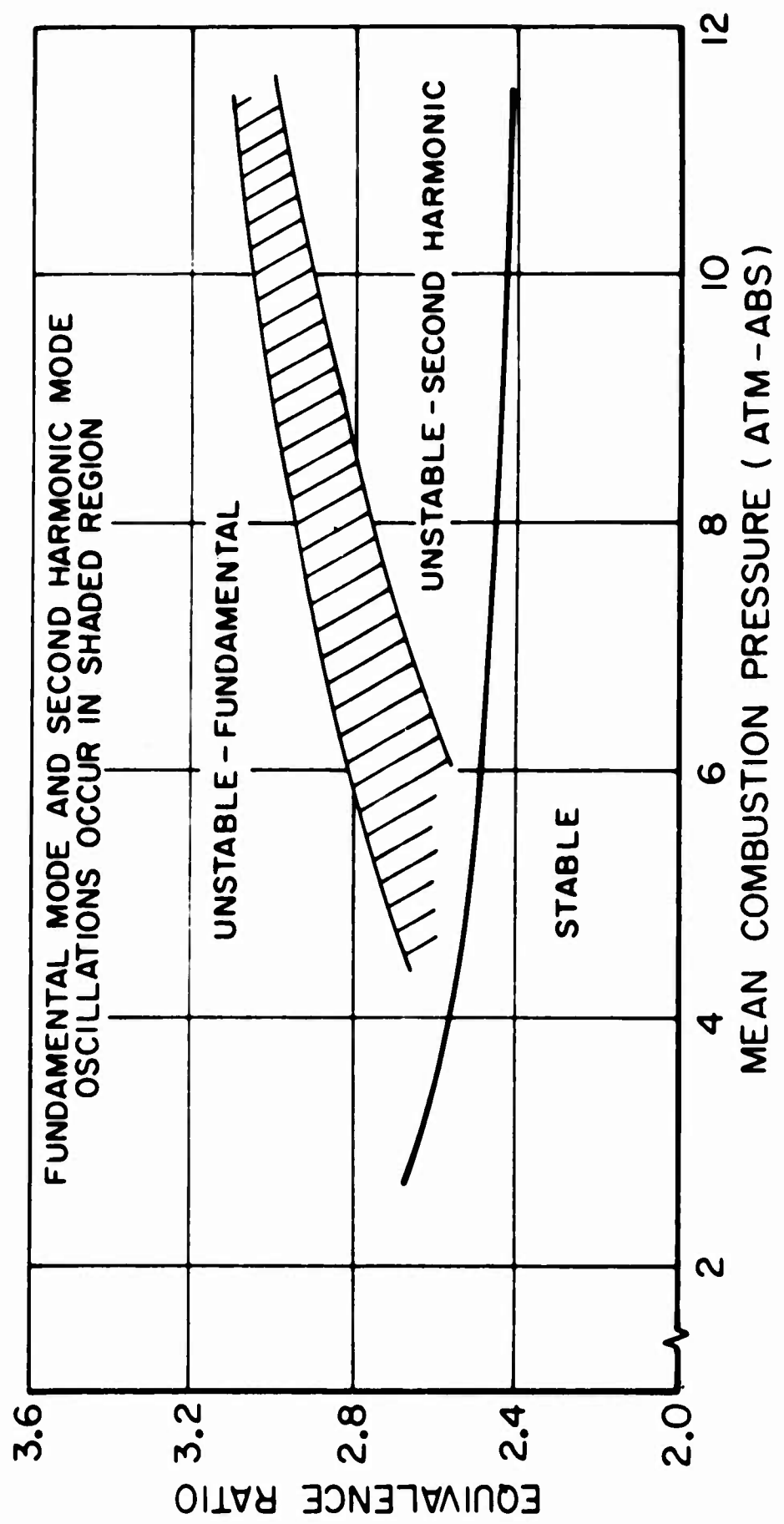


REGIONS OF UNSTABLE COMBUSTION IN THE  $\Phi - \bar{P}$  PLANE FOR  $H_2$ -AIR -  $L=38$  CM

FIGURE 32

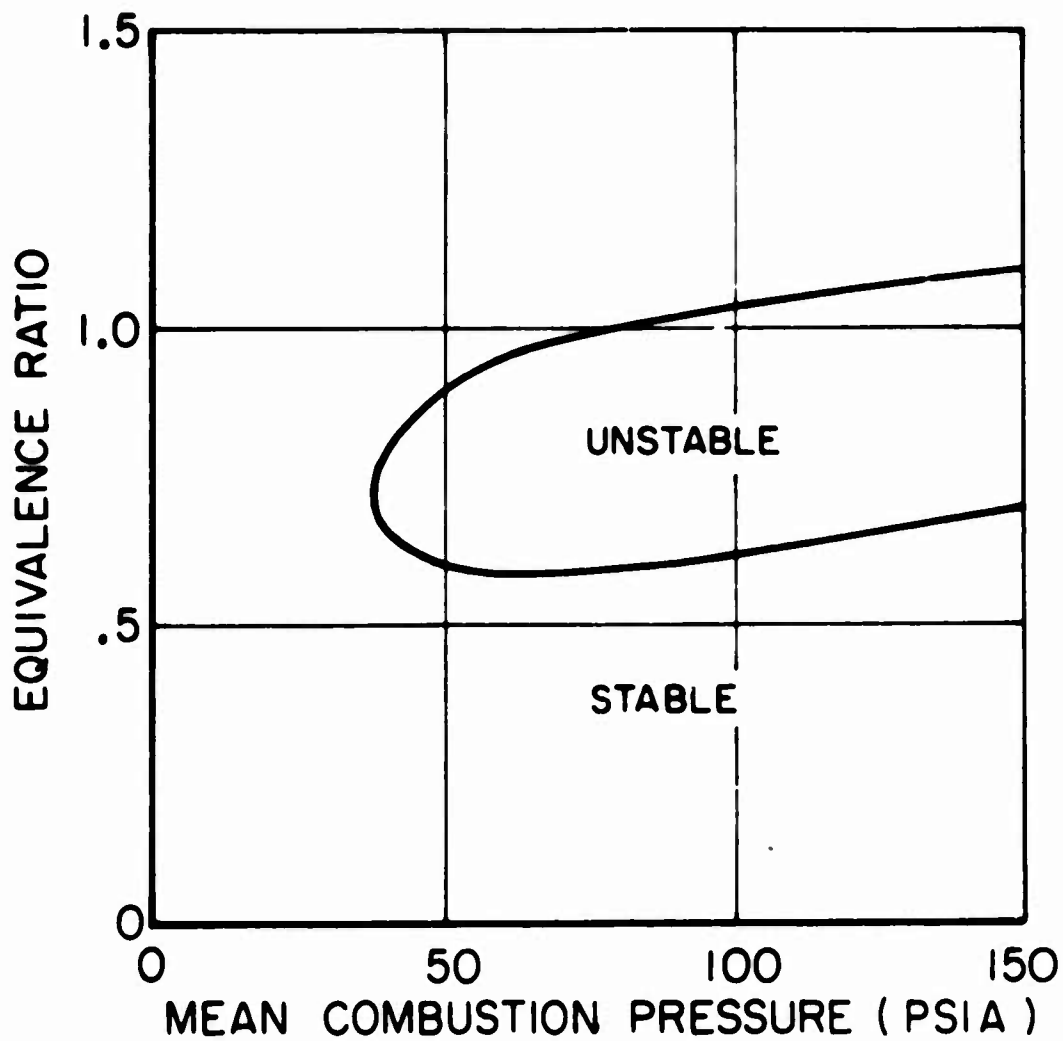
JP13-4093-65

JPI3-4092-65



REGIONS OF UNSTABLE COMBUSTION IN THE  $\Phi - \bar{P}$  PLANE FOR  $H_2$  - AIR -  $L=104$  CM

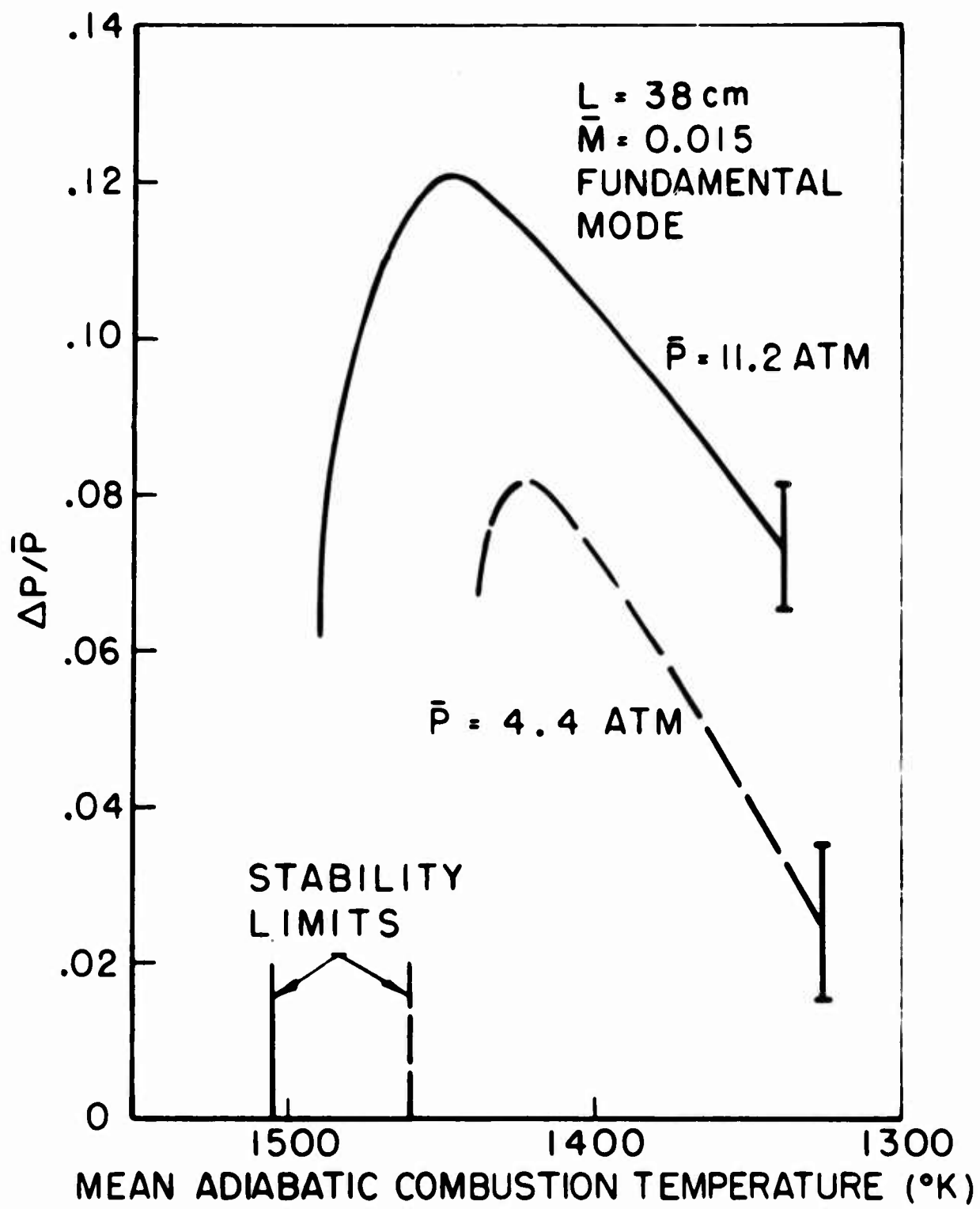
FIGURE 33



REGIONS OF UNSTABLE COMBUSTION IN THE  $\Phi$ - $\bar{P}$  PLANE FOR CH<sub>4</sub>-AIR: CHAMBER LENGTH NOT SPECIFIED (DATA FROM REFERENCE 31)

FIGURE 34

JP13-4091-65

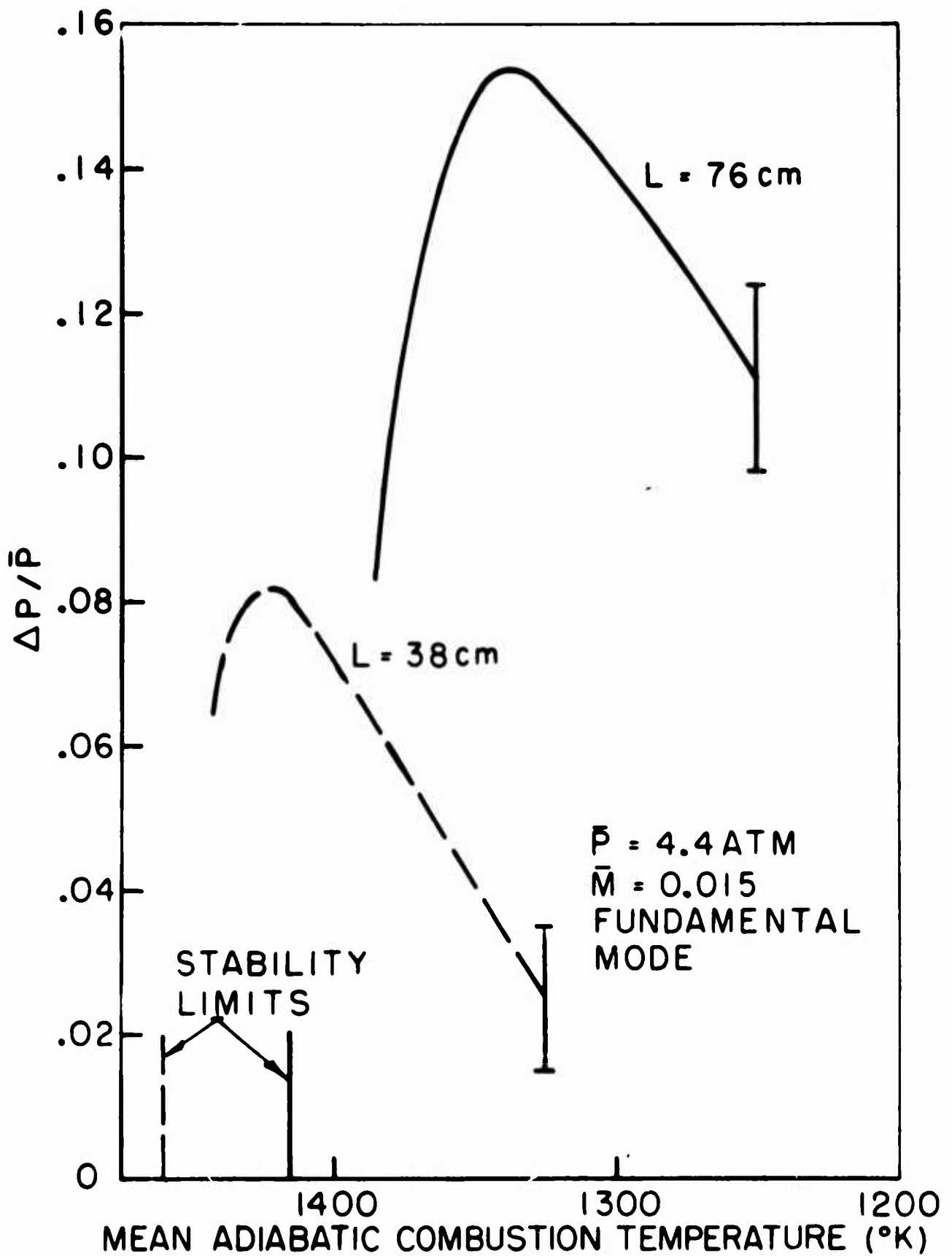


VARIATION OF  $\Delta P / \bar{P}$  WITH COMBUSTION TEMPERATURE FOR  $\text{H}_2$ -AIR AND TWO COMBUSTION PRESSURES

FIGURE 35

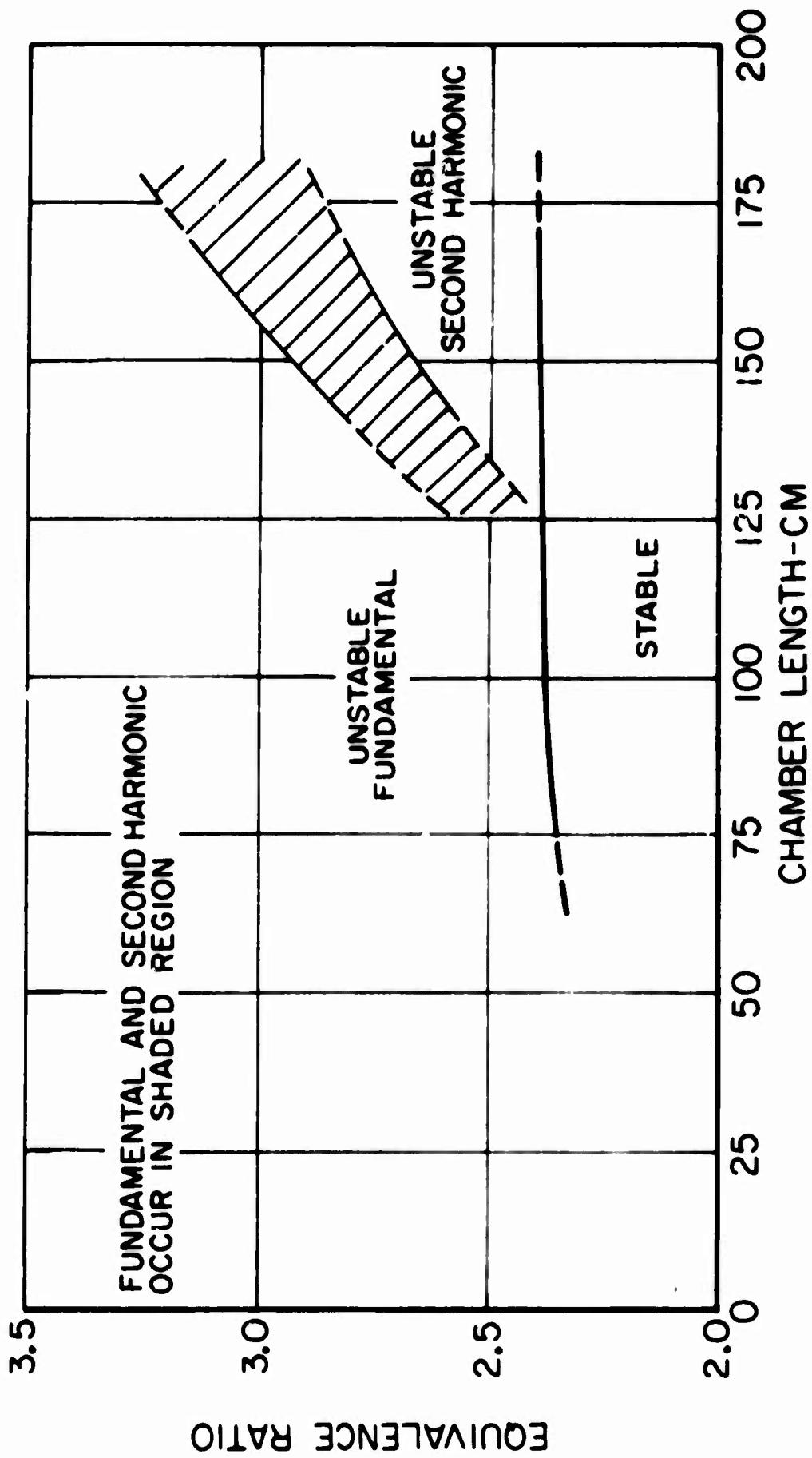
JP13-R4096-66

JP13-R 4097-66



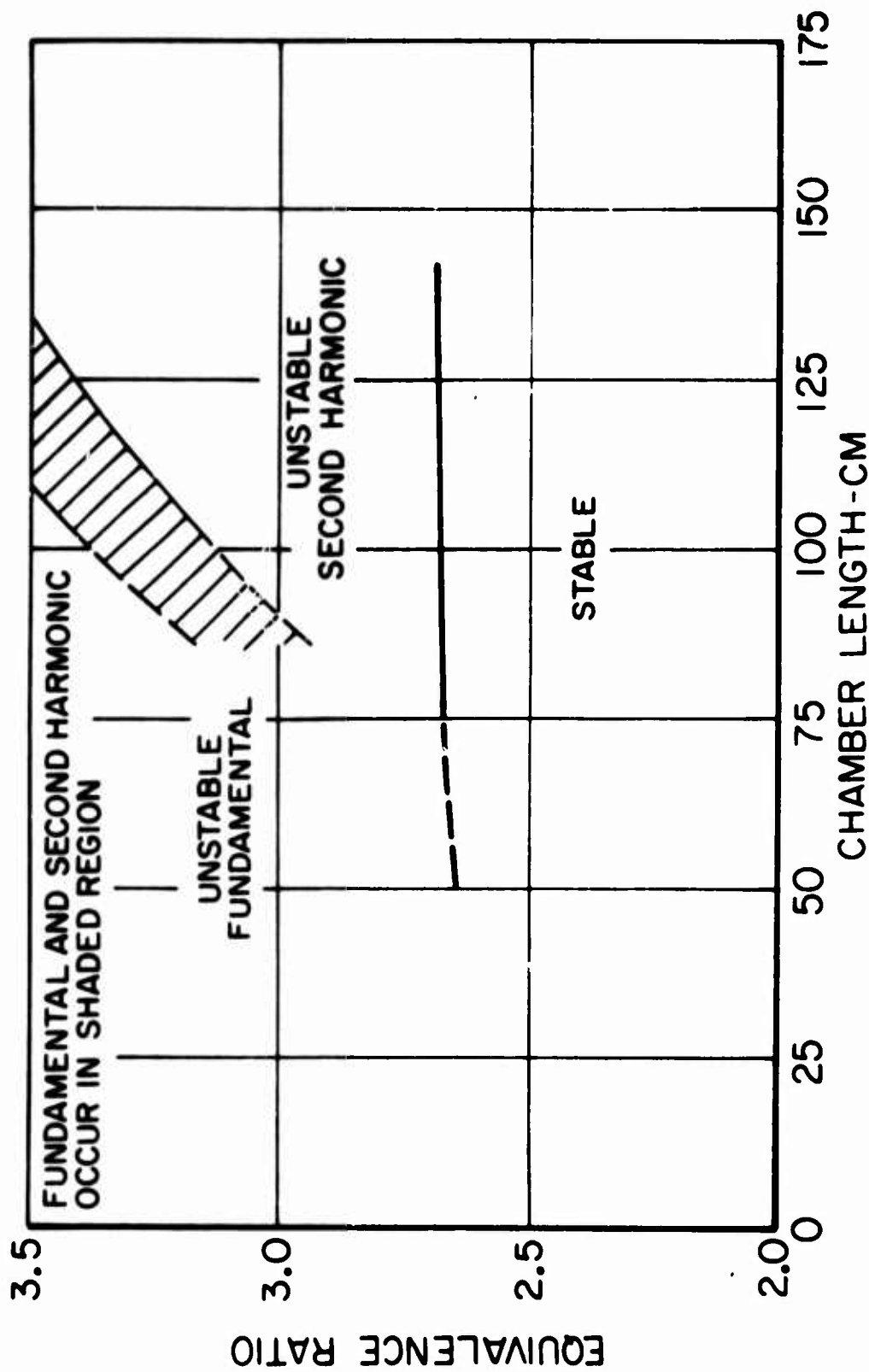
VARIATION OF  $\Delta P / \bar{P}$  WITH COMBUSTION TEMPERATURE FOR  $\text{H}_2$ -AIR AND TWO CHAMBER LENGTHS

JP13-4101-66



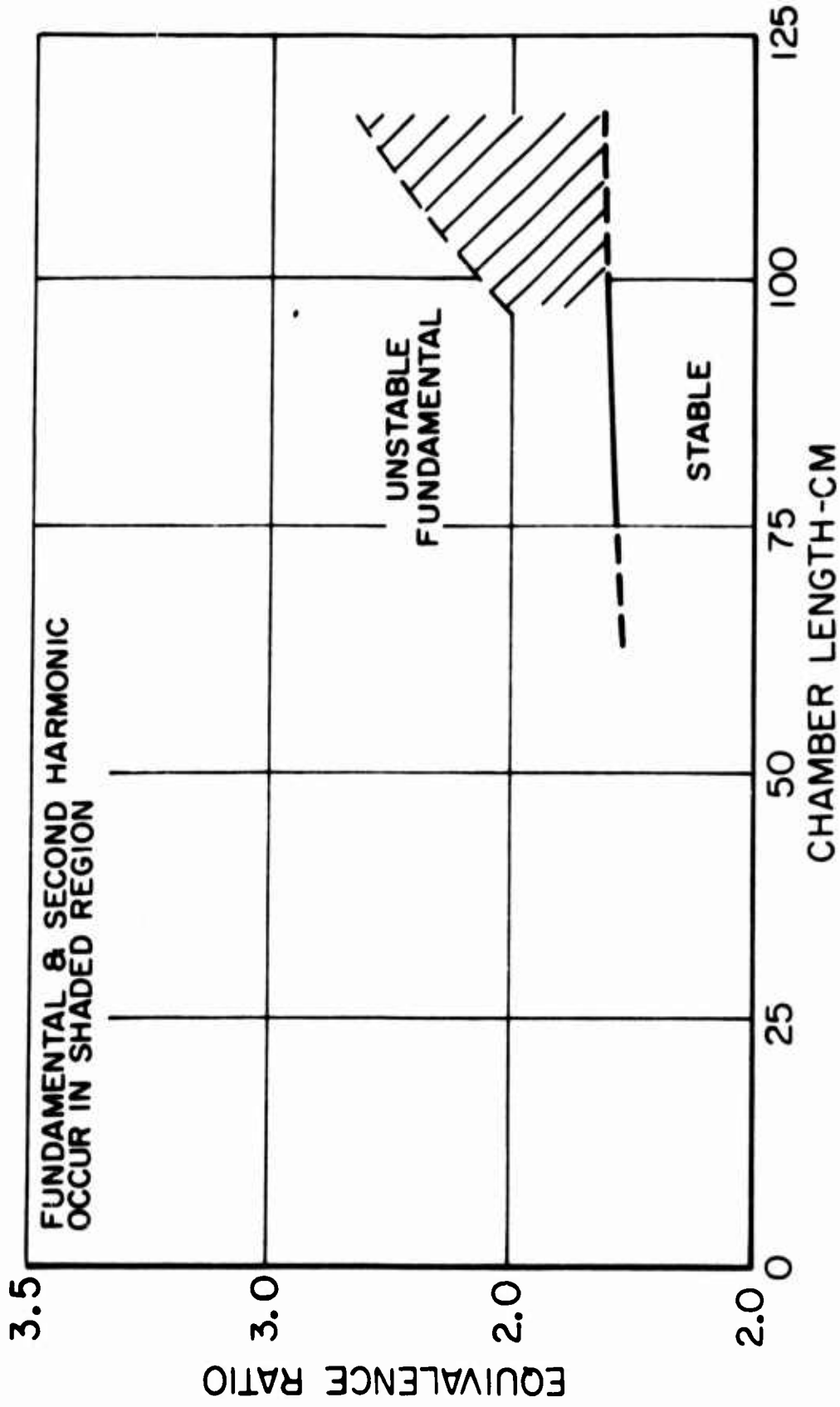
REGIONS OF UNSTABLE COMBUSTION IN THE  $\Phi$ -L PLANE FOR  $H_2$ -AIR:  
 $\bar{P} = 7.8$  ATM, 10-HOLE SHOWERHEAD INJECTOR

FIGURE 37



REGIONS OF UNSTABLE COMBUSTION IN THE  $\Phi$ -L PLANE FOR  $H_2$ -AIR:  
 $\bar{P} = 7.8$  ATM, 49-HOLE SHOWERHEAD INJECTOR

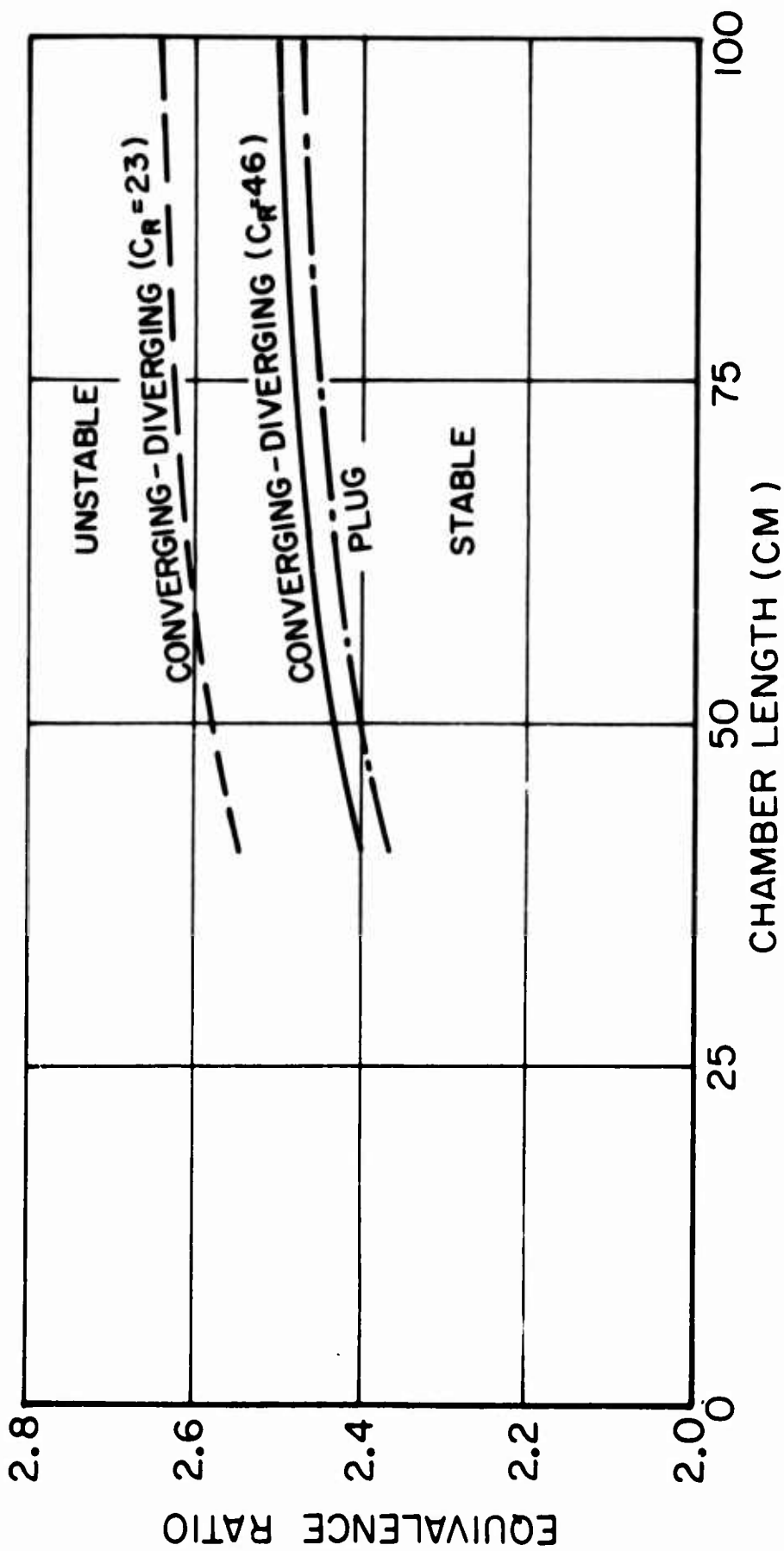
FIGURE 38



REGIONS OF UNSTABLE COMBUSTION IN THE  $\Phi$ -L PLANE FOR  $H_2$ -AIR:  
 $\bar{P} = 7.8$  ATM, IMPINGING INJECTOR

FIGURE 39

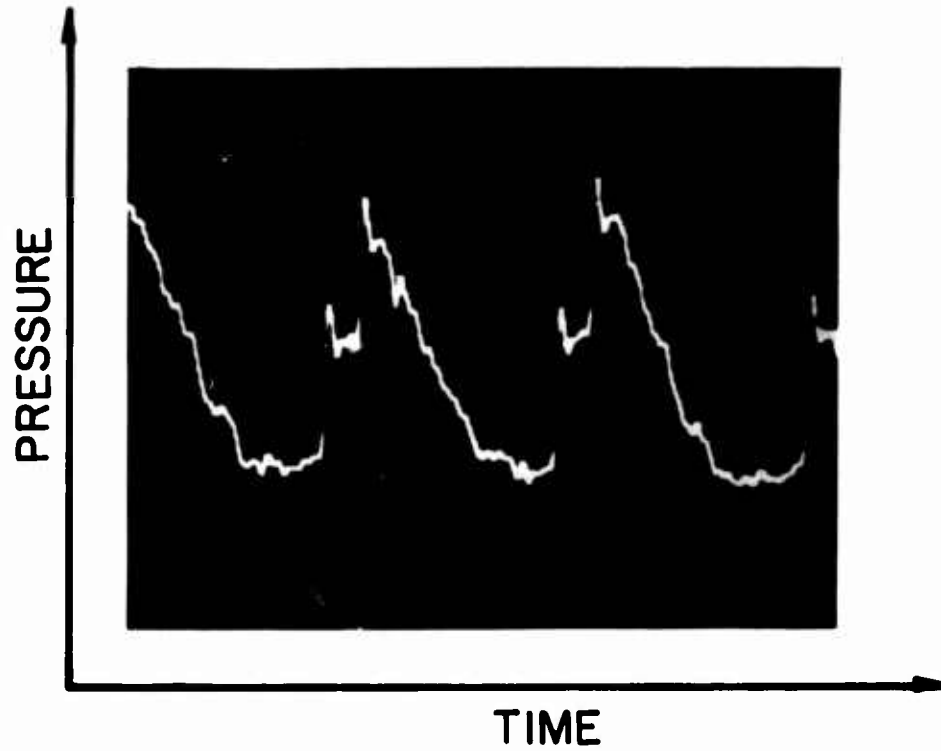
JPI13-4090-65



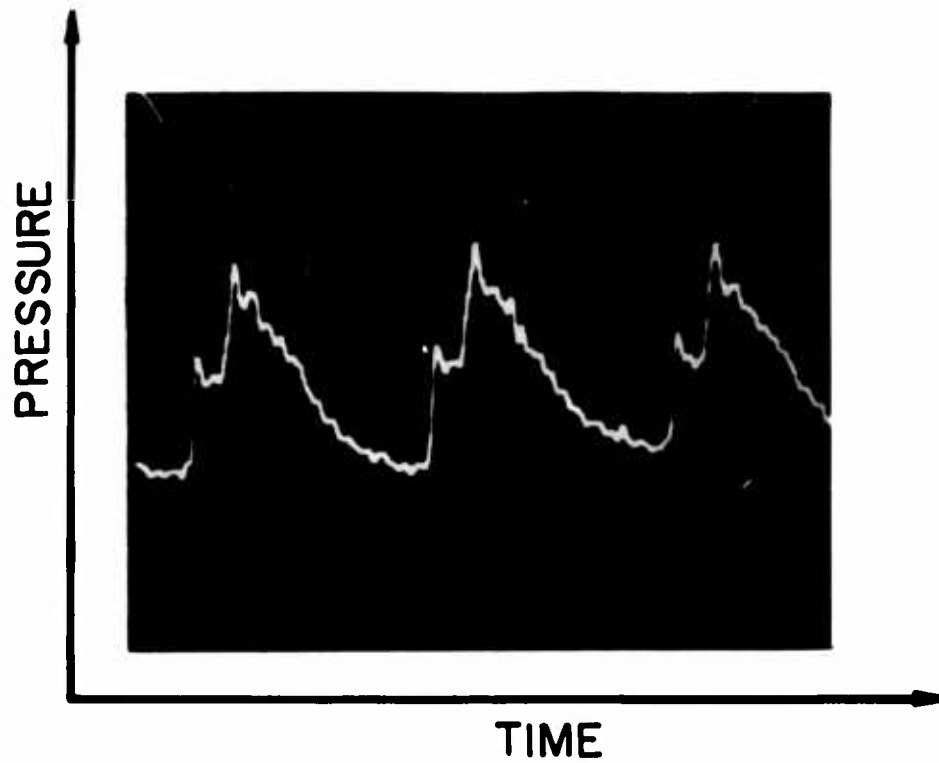
REGIONS OF UNSTABLE COMBUSTION IN THE  $\Phi$ -L PLANE FOR  $H_2$ -AIR AND VARIOUS EXHAUST NOZZLES -  $\bar{P} = 4.4$  ATM

FIGURE 40

1013-P97-66



A. PLUG NOZZLE

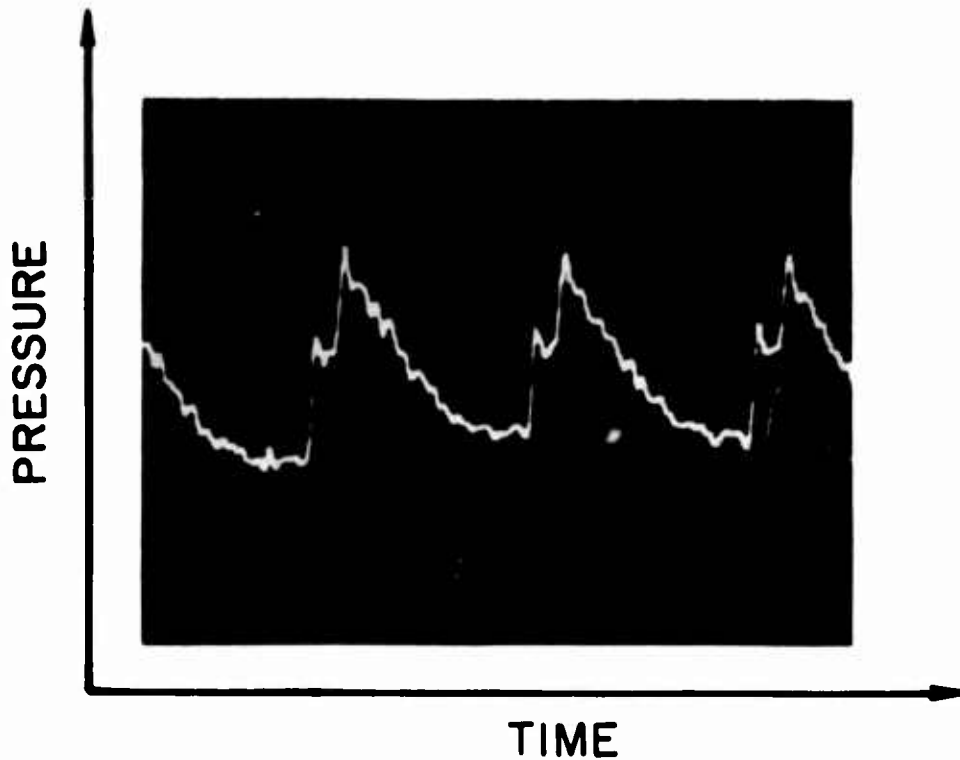


B. CONVERGING-DIVERGING NOZZLE ( $C_R = 46$ )

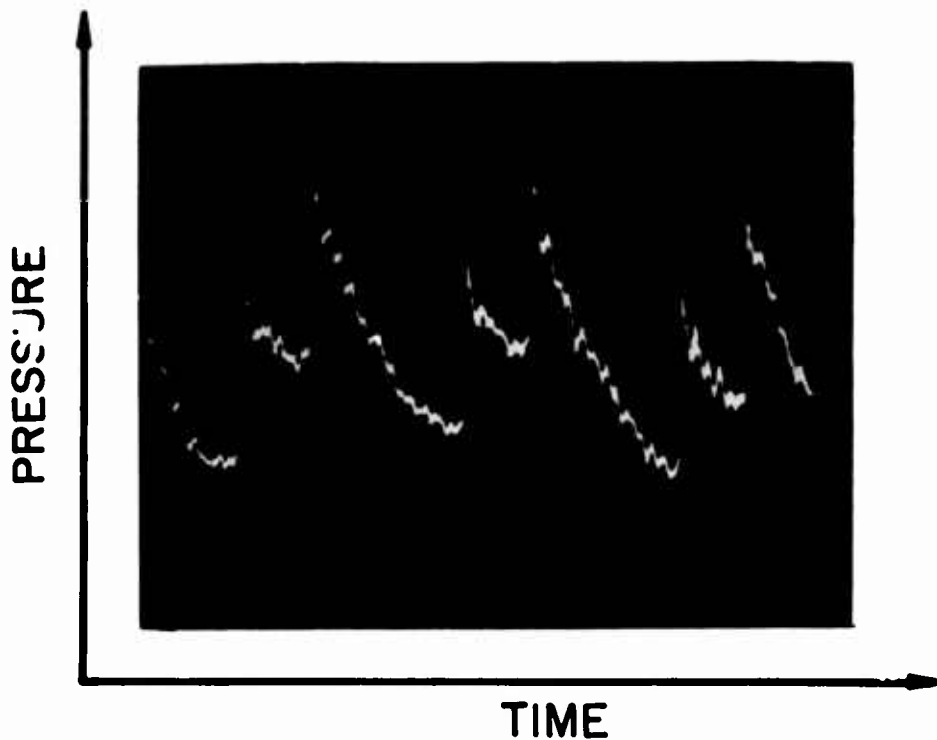
TYPICAL PRESSURE-TIME HISTORIES FOR VARIOUS EXHAUST NOZZLE: SECOND HARMONIC ( $X/L = 0.95$ )

FIGURE 41

JP13-P27-66



A. CONVERGING-DIVERGING NOZZLE ( $C_R=23$ )



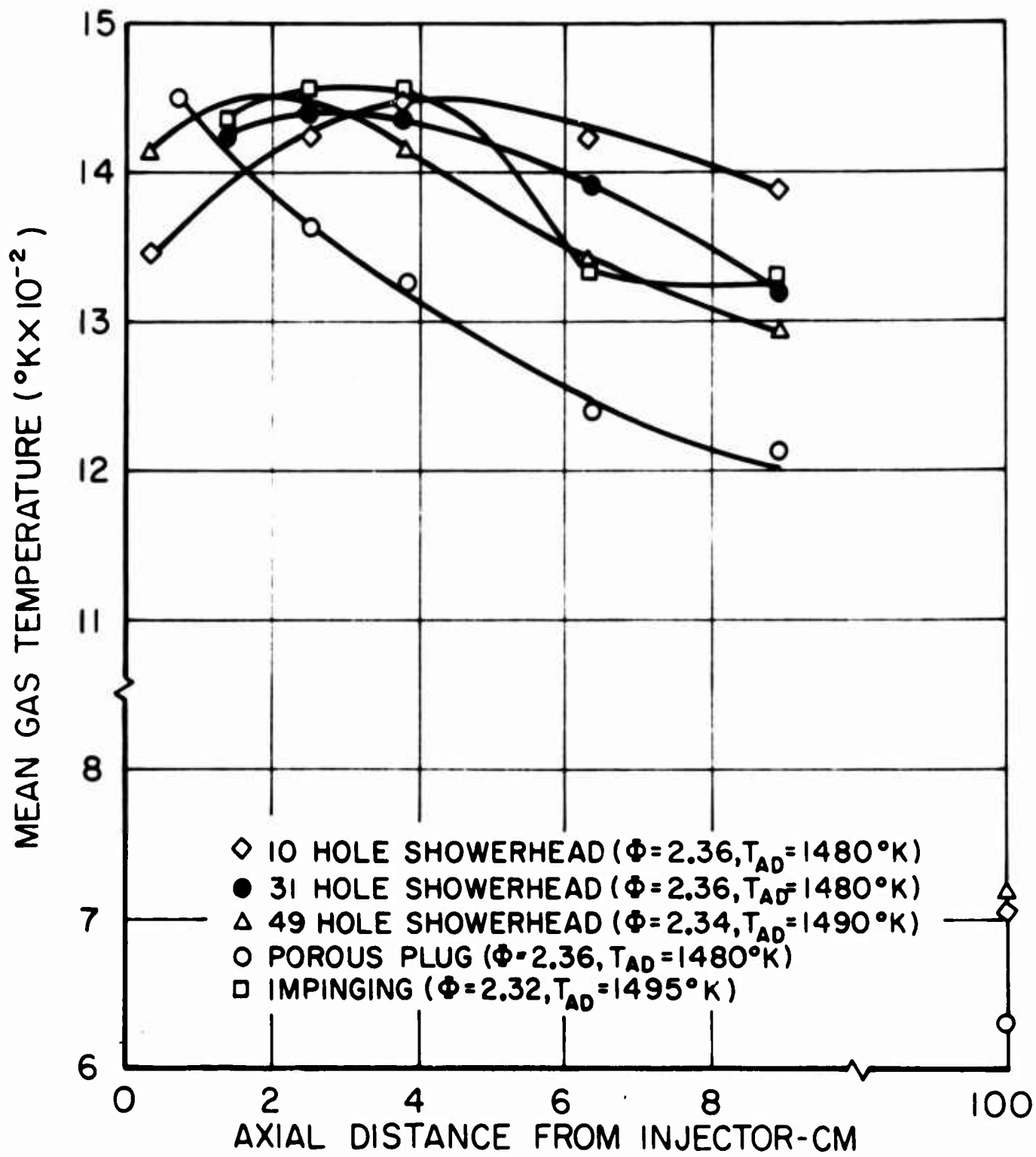
B. CONVERGING-DIVERGING NOZZLE ( $C_R=46$ )

TYPICAL PRESSURE-TIME HISTORIES FOR VARIOUS  
EXHAUST NOZZLE: SECOND HARMONIC

FIGURE 42

JP13-P26-66

JP13-4103-66



TYPICAL AXIAL TEMPERATURE PROFILES FOR VARIOUS INJECTORS:  $\text{H}_2$ -AIR,  $\bar{P}=7.8$  ATM

FIGURE 43

Security Classification

DOCUMENT CONTROL DATA - R & D

(Security classification of title, body of abstract and indexing annotation must be entered when the overall report is classified)

1. ORIGINATING ACTIVITY (Corporate author) <b>Princeton University Department of Aerospace and Mechanical Sciences Princeton, New Jersey 08540</b>		2a. REPORT SECURITY CLASSIFICATION <b>UNCLASSIFIED</b>	
		2b. GROUP	
3. REPORT TITLE <b>EXPERIMENTAL INVESTIGATION OF HIGH-FREQUENCY LONGITUDINAL COMBUSTION INSTABILITY IN GASEOUS PROPELLANT ROCKET MOTORS</b>			
4. DESCRIPTIVE NOTES (Type of report and inclusive dates) <b>Scientific Interim</b>			
5. AUTHOR(S) (First name, middle initial, last name) <b>Craig Thomas Bowman</b>			
6. REPORT DATE	7a. TOTAL NO. OF PAGES <b>173</b>	7b. NO. OF REFS <b>50</b>	
8a. CONTRACT OR GRANT NO. <b>AF 49(638)1268</b>	9a. ORIGINATOR'S REPORT NUMBER(S) <b>TR 784</b>		
b. PROJECT NO. <b>9711-01</b>	9b. OTHER REPORT NO(S) (Any other numbers that may be assigned this report) <b>AFOSR 66-2725</b>		
c. <b>61445014</b>			
d. <b>681308</b>			
10. DISTRIBUTION STATEMENT <b>1. Distribution of this document is unlimited</b>			
11. SUPPLEMENTARY NOTES		12. SPONSORING MILITARY ACTIVITY <b>AF Office of Scientific Research (SREP) 1400 Wilson Boulevard Arlington, Virginia 22209</b>	
13. ABSTRACT <p>The properties of the longitudinal mode of high-frequency combustion instability in a rocket motor burning premixed gaseous propellants have been determined experimentally. The experimental observations have been compared with the results of a non-linear instability theory based on a chemical kinetic driving mechanism. It has been shown that the theory gives the correct waveform for longitudinal instability. In addition the theory gives the correct qualitative dependence of the stability limits on the mean combustion temperature and activation energy. The theory also gives the correct qualitative dependence of the instability strength on the mean combustion temperature and mean Mach number of the combustion gases. Harmonic mode longitudinal instabilities have been observed, and a criterion for their appearance, consistent with a chemical kinetic driving mechanism, has been suggested. The dependence of the stability limits and instability strength on the mean combustion pressure, combustion chamber length, injector and exhaust nozzle have been determined experimentally. These effects are not included in the instability theory. Plausible explanations for the above effects, consistent with the theoretical model, have been suggested. Based on the general agreement between the experimental observations and theoretical results it is concluded that the appropriate driving mechanism for high-frequency longitudinal gas phase combustion instability is chemical kinetics.</p>			

DD FORM 1473  
1 NOV 65

Security Classification

14 KEY WORDS	LINK A		LINK B		LINK C	
	ROLE	WT	ROLE	WT	ROLE	WT
Combustion Instability Gaseous Rocket Motor Gaseous Propellants Activation Energies in Combustion Longitudinal Combustion Instability Harmonics in Combustion Instability Hydrogen-oxygen-nitrogen Propellants Methane-oxygen-nitrogen Propellants Carbon Monoxide-oxygen-nitrogen Propellants						